Tampere University

Antti Nurminen

NOVEL CORNEA-SPECIFIC BIOINK FOR 3D BIOPRINTING

Faculty of Medicine and Health Technology
Master's thesis
April 2022

ABSTRACT

Antti Nurminen: Novel cornea-specific bioink for 3D bioprinting
Master's thesis
Tampere University
Master's Programme in Biomedical Technology
Supervisors: PhD Anni Mörö and PhD candidate Paula Puistola
Examiners: Professor Vesa Hytönen and PhD Anni Mörö
April 2022

Background and aims: Healthy cornea is transparent which is crucial for its role in light transmission and refraction. The corneal stroma (CS) constitutes a significant portion of cornea and its complex architecture, playing a major role in corneal transparency. The CS is populated by corneal keratocytes (CKs), which maintain the CS. As the cornea is the most anterior part of the eye it is susceptible to injuries and diseases, which disrupt the native corneal organization. This is associated with a decrease in corneal transparency and vision, referred to as corneal blindness. Currently, the choice of treatment for corneal blindness patients is corneal transplantation. However, there is a global shortage of donor corneas, thus only a fraction of patients can benefit from this treatment. Keratoprostheses (KPros) can be used instead, however these come with significant limitations. Previously, conventional corneal tissue engineering (TE) methods have been used to address this problem. However, it is not possible to mimic the corneal structure with these methods. Three-dimensional (3D) bioprinting has recently gained attention as a novel approach to generate transplantable corneal equivalents. The aim of this thesis was to develop a cornea-specific bioink for extrusion-based bioprinting (EBB) and to study the printability and biocompatibility of the bioink.

Materials and methods: Human adipose tissue stem cells (hASCs) were differentiated towards CKs (hASC-CKs), which were used to produce cornea-specific cell-derived matrix (Co-CDM). The presence of corneal extracellular matrix proteins (ECM) in the Co-CDM was studied with immunofluorescence staining. Macromolecular crowding (MMC) conditions were used to study if the amount of produced Co-CDM can be increased. In order to incorporate the Co-CDM into the bioink it was decellularized, hence the name Co-dCDM, and processed. In this thesis the characteristics of Co-dCDM bioink were compared to a bioink which had similar composition, containing collagen I (Col I) instead of Co-dCDM. Then, the bioink compositions and printing parameters were optimized. Characterized bioink properties were printability, shape fidelity, swelling behavior and viscosity. In the final step of the thesis Co-dCDM bioink was printed with hASCs and biocompatibility was studied by measuring cell viability and proliferation.

Results and conclusions: The immunofluorescence stainings of hASC-CKs showed expression of CK specific marker proteins in the Co-CDM. The studied MMC culture conditions did not increase the amount of produced Co-CDM, since it led to cell detachment. Decellularization of the produced Co-CDM resulted in a clear decrease in the DNA content, although the inclusion of DNase 1 did not improve decellularization efficacy compared to decellularization without DNase 1. The Co-dCDM bioink showed good printability and shape fidelity post-printing. Transparency of Co-dCDM was excellent, although it was greater for Col I bioink. In viscosity measurements Co-dCDM demonstrated the desirable shear-thinning property for EBB. The biocompatibility of Co-dCDM was excellent since hASCs were viable and proliferative in the bioink. Similarly, immunofluorescence staining's showed expression of proliferation marker Ki-67 and elongated morphology of hASCs. This is the first study where a cornea-specific bioink, incorporating Co-dCDM instead of decellularized cornea, is developed and characterized. The Co-dCDM demonstrated beneficial properties and thus it should be studied more closely in the future to evaluate its potential for corneal 3D bioprinting applications.

Keywords: cornea, corneal tissue engineering, 3D bioprinting, bioink, human adipose tissue stem cell, cell-derived matrix

TIIVISTELMÄ

Antti Nurminen: Uudenlainen sarveiskalvospesifinen biomuste 3D biotulostukseen
Pro Gradu
Tampereen yliopisto
Bioteknologian ja biolääketieteen tekniikan maisteriohjelma
Ohjaajat: Tutkijatohtori Anni Mörö ja väitöskirjatutkija Paula Puistola
Tarkastajat: Professori Vesa Hytönen ja tutkijatohtori Anni Mörö
Huhtikuu 2022

Tausta ja tavoitteet: Terve sarveiskalvo on läpinäkyvä, mikä on välttämätöntä sarveiskalvon roolille valon läpäisevyydessä ja taitossa. Sarveiskalvon strooma käsittää merkittävän osan sarveiskalvosta ja sen monimutkaisesta rakenteesta. Sarveiskalvon keratosyytit ylläpitävät tätä ja ovat merkittävässä roolissa sarveiskalvon läpinäkyvyyden ylläpitämisessä. Sarveiskalvo on altis vaurioille ja taudeille, koska se on silmän etummaisin osa. Nämä tuhoavat sarveiskalvon luontaisen rakenteen, mihin liittyy sarveiskalvon läpinäkyvyyden vähentyminen ja sokeutuminen. Sarveiskalvon siirto on yleisin hoitokeino potilaille, jotka kärsivät sarveiskalvon vaurioitumisesta aiheutuvasta sokeutumisesta. Kuitenkin maailmanlaajuisesta sarveiskalvosiirteiden pulasta johtuen vain pieni osa potilaista voidaan hoitaa. Keratoproteesit ovat vaihtoehtoinen hoitokeino sarveiskalvon siirrolle, mutta niihin liittyy merkittäviä rajoitteita. Aiemmin perinteisiä kudosteknologian menetelmiä on käytetty sarveiskalvopulan ratkaisemiseksi. Näillä menetelmillä ei kuitenkaan ole mahdollista jäljitellä sarveiskalvon luontaista rakennetta. Viime aikoina kolmiulotteinen (3D) biotulostus on saanut huomiota uudenlaisena lähestymistapana tuottaa sarveiskalvon kaltaisia siirrännäisiä. Tämän työn tavoite oli kehittää sarveiskalvospesifinen extruusio 3D biotulostettava biomuste ja tutkia sen tulostettavuutta ja bioyhteensopivuutta.

Materiaalit ja menetelmät: Ihmisen rasvakudoksen kantasolut (human adipose tissue stem cells, hASCs) erilaistettiin keratosyyttien kaltaisiksi soluiksi, joita käytettiin sarveiskalvospesifisen soluperäisen matriisin (cornea-specific cell-derived matrix, Co-CDM) tuottamiseen. Immunofluoresenssi värjäyksillä tutkittiin sarveiskalvon soluväliaineen proteiinien olemassaoloa Co-CDM:sta. Makromolekulaarisella täytöllä (Macromolecular crowding, MMC) tutkittiin vaikutusta tuotetun Co-CDM määrään. Ennen Co-CDM:n sekoittamista biomusteeseen, se desellularisoitiin, josta tuli nimi Co-dCDM. Tässä työssä vertailtiin kahden biomusteen ominaisuuksia, joilla oli muuten sama koostumus, paitsi yksi sisälsi Co-dCDM:ta ja toinen kollageeni I:ta. Sitten biomusteiden koostumukset ja tulostusolosuhteet optimoitiin. Biomusteista tutkitut ominaisuudet olivat tulostettavuus, filamenttien muodon pysyvyyttä, turpoaminen ja leikkausohenevuus. Lopuksi työssä tulostettiin hASCs-soluja Co-dCDM-biomusteen kanssa. Biomusteen bioyhteensopivuutta tutkittiin mittaamalla solujen elinkelpoisuutta ja proliferaatiota.

Tulokset ja päätelmät: Immunofluoresenssi värjäyksissä havaittiin, että hASC-CKs-solujen tuottamassa Co-CDM:ssa expressoitui keratosyyttispesifisiä proteiinimarkereita. Lisäksi MMC-olosuhteet eivät lisänneet tuotetun Co-CDM:n määrää, koska se johti solujen irtoamiseen. Desellularisaatio vähensi Co-CDM:n sisältämän DNA:n määrää, mutta DNase 1:n lisäys ei parantanut desellularisaatiota. Co-dCDM-biomusteen tulostettavuus ja filamenttien muodon pysyvyys tulostamisen jälkeen olivat hyvät. Lisäksi biomusteen läpinäkyvyys oli erinomainen, vaikkakin se oli matalampi kuin Col I-biomusteella. Viskositeettimittauksissa havaittiin, että Co-dCDM-biomuste oli leikkausohenevaa. Tämä on haluttu ominaisuus extruusio 3D biotulostuksessa käytettäville biomusteille. Myös Co-dCDM-biomusteen bioyhteensopivuus oli erinomainen, sillä hASCs olivat elinkelpoisia ja proliferatiivisia biomusteessa. Tämän lisäksi tulostettujen rakenteiden immunofluoresenssivärjäyksissä havaittiin proliferaatiomarkkerin Ki-67 expressio ja hASCs-solujen pitkänomainen morphologia. Tämä on ensimmäinen tutkimus, missä sarveiskalvospesifinen biomuste on kehitetty käyttämättä desellularisoituja sarveiskalvoja. Tutkitulla Co-dCDM-biomusteella oli lupaavia ominaisuuksia ja sitä tulisi tutkia lisää, jotta saadaan enemmän tietoa sen koostumuksesta ja potentiaalista 3D-biotulostuksessa.

Avainsanat: sarveiskalvo, kudosteknologia, 3D biotulostus, biomuste, ihmisen rasvakudoksen kantasolut, soluperäinen matriksi

PREFACE

This Master of Science thesis was conducted in the Eye group at the Faculty of Medicine and Health Technology at Tampere University, Finland. I would like to thank the leader of Eye Group Professor Heli Skottman for giving me the opportunity to do my thesis in this interesting project involving 3D bioprinting. I want to show my gratitude my supervisor PhD Anni Mörö for excellent teaching, guidance and supervision throughout this project. I would also like to thank my co-supervisor Paula Puistola for guidance and assistance in the rheology measurements.

Lastly, I want to thank my friends and family, who have always believed in me and supported me throughout my studies.

Tampere, 24 April 2022

Antti Nurminen

CONTENTS

LIST OF SYMBOLS AND ABBREVIATIONS

‘ene’	Carbon double bond
2D	Two-dimensional
3D	Three-dimensional
ALDH1A1	Aldehyde dehydrogenase 1A1
ALDH1A3	Aldehyde dehydrogenase 1A3
AM	Amniotic membrane
A2P	Ascorbic acid-2-phosphate
BPL	Borland Package Library
BSA	Bovine serum albumin
$CaCl_2$	Calcium chloride
CAD	Computer-aided design
$CaSO_4$	Calcium sulfate
CDM	Cell-derived matrix
CE	Corneal epithelium
CIJ	Continuous inkjet
CMC	Carboxymethylcellulose
Co-CDM	Cornea-specific cell-derived matrix
Co-dCDM	Cornea-specific decellularized cell-derived matrix
Co-dECM	Cornea-derived extracellular matrix
Col I	Collagen Type I
Col III	Collagen Type III
Col V	Collagen Type V
Col VI	Collagen Type VI
COO^-	Carboxylic acid group
CS	Corneal stroma
CT	Computed tomography
DALK	Deep anterior lamellar keratoplasty
dECM	Decellularized ECM
DLP	Digital light processing
DMEK	Descemet’s membrane endothelial keratoplasty
DOD	Drop-on-demand
DSEK	Descemet’s stripping endothelial keratoplasty
DTT	Dithioretinol
EBB	Extrusion based bioprinting
ECM	Extracellular matrix
EDC	1-Ethyl-3-(3-dimethylaminopropyl)carbodiimide
ESCs	Embryonic stem cells
FECD	Fuchs’ endothelial corneal dystrophy
FGF2	Fibroblast growth factor 2
GAG	Glycosaminoglycan
GelMA	Gelatin methacryloyl
hASCs	Human adipose tissue stem cells
hCEnCs	Human corneal endothelial cells
hCEpCs	Human corneal epithelial cells
hCESCs	Human corneal epithelial stem cells
hCFs	Human corneal fibroblasts
hiPSCs	Human induced pluripotent stem cells
hCKs	Human corneal keratocytes
hCSSCs	Human corneal stromal stem cells
hTMSCs	Human turbinate-tissue derived mesenchymal stromal cells
HA	Hyaluronic acid
HUVECs	Human umbilical vein endothelial cells

KDM	Keratocyte differentiation medium
KPros	Keratoprostheses
LAB	Laser-assisted bioprinting
LAP	Lithium phenyl-2,4,6-trimethylbenzoylphosphinate
LBB	Lithography-based bioprinting
LESCs	Limbal epithelial stem cells
LGDW	Laser guidance direct writing
LIFT	Laser induced forward transfer
LSCD	Limbal stem cell deficiency
IL-1	Interleukin-1
Irgacure 2959	2-hydroxy-l-[4-(hydroxyethoxy)phenyl]-2-methyl-1-propanone
MMC	Macromolecule crowding
MOOKP	Modified osteo-odonto-keratoprosthesis
MPC	2-methacryloyloxyethyl phosphorylcholine
MRI	Magnetic resonance imaging
MSCs	Mesenchymal stem cells
MUSE	Multilineage-differentiating stress-enduring
PA	Peptide amphiphile
PBS	Phosphate-buffered saline
PDGF	Platelet-derived growth factor
PDMS	Polydimethylsiloxane
PEG	Poly(ethylene glycol)
PEGDA	Poly(ethylene glycol)-diacrylate
PKP	Penetrating keratoplasty
PMMA	Poly(methyl methacrylate)
POV	Palisades of Vogt
PRs	Photoreceptor cells
PUK	Peripheral ulcerative keratitis
RA	Retinoic acid
RGD	Arginine-glycine-aspartic acid
RPE	Retinal pigment epithelium
SD	Sodium deoxycholate
SLA	Stereolithography
SLRP	Small leucine rich proteoglycans
TACs	Transient amplifying cells
TDCs	Terminal differentiated cells
TE	Tissue engineering
TGF-β	Transforming growth factor beta
UV	Ultraviolet

1. INTRODUCTION

The transparent cornea is the most anterior part of the eye, which is crucial for eyesight as it transmits light and is the main source of eye's refractive power (Espana & Birk, 2020; Meek & Knupp, 2015; Sridhar, 2018). Corneal stroma (CS) is the largest corneal structural layer and its organization is essential for corneal transparency and mechanical strength (Meek & Knupp, 2015; Sridhar, 2018). The CS is synthetized and maintained by human corneal keratocytes (hCKs) that are mitotically quiescent in healthy cornea (Meek & Knupp, 2015; Sridhar, 2018). However, damage to the cornea induces hCKs proliferation and abnormal extracellular matrix (ECM) deposition, disrupting the native CS organization (Yam et al., 2020). This decreases corneal transparency, leading to corneal blindness (Yam et al., 2020). In 2016, it was estimated that corneal blindness was the third cause of blindness worldwide and that 10 million people suffered from bilateral corneal blindness (Gain et al., 2016).

The current gold standard treatment for patients suffering from corneal blindness is corneal transplantation (Singh et al., 2019; Wong et al., 2017). However, the surgery requires donor corneas, which availability is limited and in 2016 it was estimated that 12.7 million people were waiting for corneal transplantation (Gain et al., 2016). Although synthetic corneas called keratoprostheses (KPros) can be used instead of donor corneas, these are uncomfortable and have high risk of complications (Holland et al., 2021; Matthyssen et al., 2018). Therefore, there is a vast need for novel approaches such as corneal tissue engineering (TE) which aims to generate engineered corneas (Ahearne et al., 2020).

In corneal TE the key requirements are that the used biomaterials need to be transparent and have similar viscoelastic and mechanical strengths as *in vivo* cornea (Ahearne et al., 2020; Matthyssen et al., 2018). Conventional TE has the limitation that it is not possible to mimic the *in vivo* architecture of tissues as cells are cultured in a 2D environment (Mahdavi, Abdekhodaie, Mashayekhan, et al., 2020; B. Zhang, Xue, Li, et al., 2019). Although layered biosynthetic corneas have been generated, it is time consuming and the control over structural organization is limited (Ruiz-alonso et al., 2021; B. Zhang, Xue, Li, et al., 2019). To overcome this, 3D bioprinting can be used, which enables precise control of bioprinted structure architecture (Ruiz-alonso et al., 2021; B. Zhang, Xue, Li, et al., 2019). In addition, different biomaterial and cell types can be incorporated into the bioprinted structures, increasing the resemblance to native tissues (Ruiz-alonso et al., 2021; Vijayavenkataraman et al., 2018; B. Zhang, Xue, Li, et al., 2019). In the field

of ophthalmology several studies have demonstrated that it is possible to bioprinting different corneal layers and even corneal equivalents. Thus, the potential of 3D bioprinting is huge and bioprintable corneal equivalents could alleviate the severe donor cornea shortage (Ruiz-alonso et al., 2021; Sommer & Blumenthal, 2019).

In this thesis, the aim was to develop and characterize a cornea-specific bioink, suitable for extrusion-based bioprinting (EBB). The first step in this thesis was to differentiate human adipose tissue stem cells (hASCs) towards CKs. The CKs were used to produce cornea-specific cell-derived matrix (Co-CDM), which was decellularized and called cornea-specific cell-derived matrix (Co-dCDM). The Co-dCDM was incorporated into the bioink, making the bioink cornea-specific. The second step was to optimize the bioink composition and printing parameters to achieve satisfactory printability. The third step was bioink characterization, which was done by studying the bioink transmittance and viscosity. Finally, the biocompatibility of the bioink was studied by printing it with hASCs.

This thesis begins with a literature review of human cornea structure and provides information about common injuries and diseases affecting cornea. Then current treatments are discussed together with corneal TE. Subsequently, various 3D bioprinting technologies, bioink biomaterials and crosslinking methods are introduced. The literature review is concluded with a discussion on previous studies on corneal 3D bioprinting. In the experimental part of the thesis, the used materials and methods are described in detail. Finally, the results of the performed study are presented which are then discussed and concluded.

2. LITERATURE REVIEW

2.1 Human cornea

The cornea is the most anterior part of the eye, providing mechanical stability and a refractive surface for the eye (Espana & Birk, 2020; Meek & Knupp, 2015). It also functions as a protective layer against the external environment such as microbes and trauma (DelMonte & Kim, 2011; Espana & Birk, 2020; Meek & Knupp, 2015; Sridhar, 2018). The cornea is an avascular and immunologically privileged tissue with a thickness of 500 µm that increases at the corneal periphery (Espana & Birk, 2020; Sridhar, 2018; B. Zhang, Xue, Li, et al., 2019). In addition, the shape of the cornea is curved, which increases towards the posterior part of cornea (B. Zhang, Xue, Li, et al., 2019). Moreover, the cornea is transparent with transmittance values of 86–94% in the range of wavelengths 450–600 nm and more than 95% in the range of 600–1000 nm (Beems & Van Best, 1990).

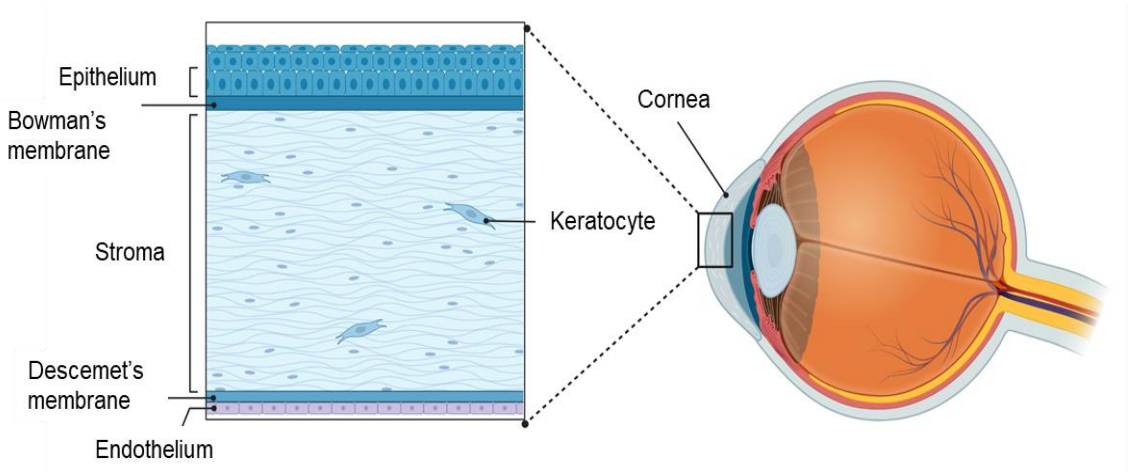

Figure 1: *Illustration of the human cornea structure. Corneal epithelium (CE) covered with tear film is the most anterior layer. Beneath is the Bowmans's membrane that separates the epithelium from the CS. The CS is occupied and maintained by human corneal keratocytes (hCKs). Descemet's membrane lies between CS and endothelium. Endothelium is the most posterior layer of cornea. Created with BioRender.com. Modified from Zhang et al., (2019).*

The normal function of cornea is highly dependent on its composition and organization (Espana & Birk, 2020; Meek & Knupp, 2015). The structure of human cornea contains both acellular layers, Bowman's and Descemet's membrane and cellular layers, epithelium, stroma and endothelium (DelMonte & Kim, 2011; Espana & Birk, 2020; Gibney et al., 2017) (Figure 1). The corneal epithelium (CE) is the most anterior part of cornea with a thickness of 50 µm, consisting of 5–7 layers of highly proliferative non-keratinizing

stratified squamous epithelial cells, that are renewed every 7–10 days (DelMonte & Kim, 2011; Sridhar, 2018). These epithelial cells have a high intracellular concentration of crystalline enzymes, which might be involved in transparency maintenance as in lens epithelial cells (Sridhar, 2018). The CE has three distinct cell types which are superficial, wing and basal cells (Sridhar, 2018). Superficial cells form tight junctions via desmosomes with each other, preventing the entrance of microbes and toxins to the cornea (DelMonte & Kim, 2011; Sridhar, 2018). In addition, superficial cells have microvilli on their apical domain, which increases their surface area, improving adhesion with the tear film. Wing cells lie beneath the superficial cells and have wing shape appearance. The superficial and wing cells are derived from the underlying basal cells that are attached to the basement membrane via hemidesmosomes, attaching the CE to other corneal layers (DelMonte & Kim, 2011; Sridhar, 2018).

Bowman's membrane is a 15–18 µm thick acellular layer separating the CE and CS (DelMonte & Kim, 2011; Espana & Birk, 2020). It consists of proteoglycans and networks of small type collagen I, III, V and VI fibrils (Col I, Col III, Col V and Col VI) (Bukowiecki et al., 2017; Espana & Birk, 2020; Sridhar, 2018). The bowman's membrane is believed to participate in corneal shape maintenance by providing mechanical strength (DelMonte & Kim, 2011; Espana & Birk, 2020). Yet, there is no definite proof of this or other possible functions of bowman's membrane, thus the exact purpose of the membrane is still largely unknown (Wilson, 2020). The membrane lacks regenerative ability and it is lost after an insult (Espana & Birk, 2020; Sridhar, 2018). However, the loss of Bowman's membrane does not appear to adversely affect normal function of cornea (Espana & Birk, 2020).

The CS is the thickest layer of the cornea and it accounts 80–90% of the whole corneal thickness (DelMonte & Kim, 2011; Espana & Birk, 2020; Sridhar, 2018). The structure of CS contributes to important properties in eye function including transparency and mechanical stability (Espana & Birk, 2020; Sridhar, 2018). In addition, it is responsible for corneal shape maintenance and is the main source of corneal refractive power (Bukowiecki et al., 2017; Sridhar, 2018). The CS is populated with hCKs that synthesize, maintain and organize stromal ECM (Espana & Birk, 2020; Gibney et al., 2017; Sridhar, 2018). The ECM is mainly composed of Col I that form heterodimeric complexes with Col V, necessary for fibril assembly initiation (DelMonte & Kim, 2011; Espana & Birk, 2020). Moreover, Col V is required to achieve the small diameter of collagen fibrils in CS (Espana & Birk, 2020). These fibrils are then organized into fibers that are organized into layered lamellar structures that are positioned about 90° from the adjacent lamellae (Espana & Birk, 2020; Sridhar, 2018; Yam et al., 2020). In addition, collagen types VI and XII are found in lesser amounts in CS (Sridhar, 2018). The precise control over the

organization of the ECM is essential for corneal transparency (DelMonte & Kim, 2011; Espana & Birk, 2020; Meek & Knupp, 2015). Distortion to the organization increases light scattering which in turn leads to decrease in transparency (Espana & Birk, 2020; Gibney et al., 2017; Meek & Knupp, 2015).

Furthermore, the CS contains various glycosaminoglycan (GAG) attached to small leucine rich proteoglycans (SLRP), synthesized by hCKs, that regulate collagen fibril formation (Espana & Birk, 2020; Sridhar, 2018). In CS class I, II and III SLRPs are expressed (Espana & Birk, 2020). Decorin and biglycan are class I SLRPs that are attached to chondroitin or dermatan sulfate (Espana & Birk, 2020; Meek & Knupp, 2015). Keratocan, lumican and fibromodulin belong to class II and are attached to keratan sulfate. Osteoglycin is a class III SLRP that is attached also to keratan sulfate, whose exact function is not known (Espana & Birk, 2020; Meek & Knupp, 2015). These SLRPs are involved in tissue homeostasis and participate in cell signaling pathways by regulating hormone and growth factor availability (Espana & Birk, 2020). Class I and II SLRPs are vital for CS structure as their deletion distrust fibril organization (Espana & Birk, 2020; Meek & Knupp, 2015). Additionally, class II SLRPs are crucial for corneal transparency as their absence causes corneal opacity (Espana & Birk, 2020).

Consisting from laminin and collagen types VIII, IV and XII, Descemet's membrane lies between CS and endothelium (Espana & Birk, 2020; Sridhar, 2018). It is synthesized by the endothelial cells and the membrane's main function is to integrate the two layers together (Espana & Birk, 2020; Sridhar, 2018). Notably the current understanding of Descemet's membrane is limited as it has not been characterized in the literature (Espana & Birk, 2020). However, it's likely that the membrane has some distinct structural properties that are responsible for its function. It has been observed that endothelial cells form processes that penetrate the Descemet's membrane and enter the CS. A recent study discovered that there is crosstalk between hCKs and endothelial cells, mediated by the processes (Espana & Birk, 2020).

The corneal endothelium is formed by a monolayer of endothelial cells (Sridhar, 2018). Apart from synthesizing the Descemet's membrane the endothelial cells also maintain corneal transparency (Yokoi et al., 2012). This is achieved with transmembrane Na^+/K^+-ATPase's and carbonic anhydrase pathway that together cause ion influx from stroma into the aqueous humor (DelMonte & Kim, 2011; Yokoi et al., 2012). This leads to water transport from stroma to the aqueous humor (DelMonte & Kim, 2011). The number of endothelial cells gradually decreases throughout life as the cells are mitotically inactive (DelMonte & Kim, 2011). Damage to the corneal endothelium causes increase in corneal swelling, leading to a decrease in transparency (Yokoi et al., 2012).

The human cornea is surrounded by the limbal zone, called limbus and conjunctiva (Osei-Bempong et al., 2013). The limbus is a thin tissue that prevents the ingrowth of blood vessels from conjunctiva into the cornea (Osei-Bempong et al., 2013). In addition, the limbus contains the limbal epithelial stem cells (LESCs) niche, which is necessary for CE regeneration (Gonzalez et al., 2018). Around these structures is the sclera, protecting the eye and maintaining its shape (Osei-Bempong et al., 2013).

2.2 Corneal cell types

The human cornea contains multiple cell types such as epithelial, endothelial and hCKs cells (Sridhar, 2018). In addition, there are at least two stem cell populations in the cornea which are human corneal stromal stem cells (hCSSCs) and LESCs (Nurković et al., 2020). Next, the characteristics and functions of hCKs, hCSSCs and LESCs are discussed in more detail.

2.2.1 Human corneal keratocytes

hCKs are the most abundant cell type found in the CS, responsible for corneal homeostasis and transparency (Espana & Birk, 2020; Yam et al., 2020). hCKs are derived from neural crest cells that migrate to the developing cornea during development (Espana & Birk, 2020; Yam et al., 2020). First the neural crest cells differentiate into keratoblasts, active keratocytes, that proliferate rapidly and synthesize the CS specific collagens and proteoglycans (Espana & Birk, 2020; West-Mays & Dwivedi, 2006). After development hCKs become mitotically inactive and they adapt a dendritic morphology (Espana & Birk, 2020; Jester, 2008). The hCKs have compact cell bodies with distinct nuclei, located between lamellae, minimizing light scattering (Espana & Birk, 2020; Jester, 2008; Yam et al., 2020). Adjacent hCKs form interconnected processes with gap junctions which enables communication between cells (Espana & Birk, 2020; West-Mays & Dwivedi, 2006; Yam et al., 2020). Beside synthesizing the ECM of CS and maintaining it, hCKs release maspin, a cell migration inhibitor and cell-ECM contact simulator and are phagocytically active (Yam et al., 2020).

Specific markers for hCKs phenotype identification are lumican, keratocan and crystallins such as aldehyde dehydrogenase 1A1 and 1A3 (ALDH1A1 and ALDH1A3, respectively) (Espana & Birk, 2020; Yam et al., 2020). In addition, the cells express various integrins such as α2β1 and α5β1 that are collagen binding integrins and necessary in ECM organization (Yam et al., 2020). Moreover, the hCKs are negative for fibronectin, tenascin and αSMA (Yam et al., 2020).

hCKs contain high intracellular concentrations of crystallins which are believed to be important for CS transparency (Espana & Birk, 2020; Jester, 2008; Yam et al., 2020). This is supported by the evidence that crystallins absorb ultraviolet (UV) light and this is speculated to minimize light scattering (Espana & Birk, 2020; Jester, 2008). Previous studies have identified that ALDH3A1 crystallin is highly conserved between mammalian species (Espana & Birk, 2020). This could indicate that ALDH3A1 crystallin is critical for normal corneal function although animal studies with deficient mice have not confirmed this (Espana & Birk, 2020).

2.2.2 Corneal Stromal Stem Cells

hCSSCs reside in the limbal region of stroma adjacent to the LESCs niche (Funderburgh et al., 2016; Yam et al., 2020). These cells have similar properties compared to mesenchymal stem cells (MSCs) such as clonal growth, differentiation potential and expression of stem cell-specific markers (Funderburgh et al., 2016; Yam et al., 2020). Moreover, hCSSC express Six2–3 and Notch1 neural ectoderm marker proteins, indicating that they originate from the neural crest cells (Nurković et al., 2020; Yam et al., 2020).

When hCSSCs are co-cultured with LESCs, the proliferation and survival of LESCs is enhanced, suggesting that hCSSCs regulate LESCs cellular functions (Yam et al., 2020). In addition, with appropriate culture conditions hCSSCs can be differentiated into chondrocytes and neural cells (Funderburgh et al., 2016; Yam et al., 2020). However, it seems that the default differentiation of hCSSCs is into CKs as cells injected to corneal stroma differentiate into hCKs (Yam et al., 2020). Furthermore, *in vivo* corneal wound healing studies have indicated hCSSCs involvement in immune responses and stromal regeneration initiation (Funderburgh et al., 2016).

2.2.3 Limbal Epithelial Stem Cells

LESCs are highly proliferative cells, which reside in the limbal niche called palisades of Vogt (POV), having important functions in CE homeostasis and maintaining corneal transparency (Gonzalez et al., 2018; Vattulainen et al., 2019; Yazdanpanah et al., 2017). The niche regulates the proliferation and differentiation of LESC, achieved by the unique composition of the niche ECM (Yazdanpanah et al., 2017). In addition, LESCs communicate with CSSC via processes which are necessary to maintain LESCs stemness (Seyed-Safi & Daniels, 2020; Yazdanpanah et al., 2017). Moreover, the niche is known to contain other cell types such as melanocytes, immune cells and nerve cells (Gonzalez et al., 2018; Yazdanpanah et al., 2017).

The exact mechanism of how CE regeneration is carried out by LESCs is unclear and to date the most recognized hypothesis is that this is achieved by LESCs residing in limbal epithelial crypts of POV (Yazdanpanah et al., 2017). Firstly, the LESCs divide centripetally and form transient amplifying cells (TACs) at the basal epithelial layer. Secondly, the TACs are proposed to proliferate and differentiate while migrating toward the corneal surface (Yazdanpanah et al., 2017). Eventually, these cells form terminal differentiated cells (TDCs), which are then shedded from the corneal surface (Yazdanpanah et al., 2017).

2.3 Corneal blindness

Globally 10 million people suffer from bilateral corneal blindness caused by injuries and diseases, making it the third cause of blindness after cataract and glaucoma (Gain et al., 2016). Furthermore, it has been estimated that 12.7 million people are waiting for corneal transplantation. The majority of these cases are in developing countries such as China (2 million) and India (7 million) (Gain et al., 2016). In addition, corneal blindness is a major global socio-economic burden as it decreases life quality and reduces life expectancy and employment opportunities (Oliva et al., 2012; Tran et al., 2020). Here, the pathophysiology of corneal injuries and the most common diseases leading to corneal blindness are discussed first, before discussing the current corneal treatments.

2.3.1 Corneal injuries

Since the cornea is the most anterior part of the eye, it is susceptible to different types of injuries such as physical lesions and chemical burns (Bukowiecki et al., 2017; Ljubimov & Saghizadeh, 2015). The healing of damaged cornea normally takes 7–14 days (Vaidyanathan et al., 2019). Depending on the injury type different corneal layers can be affected (Khosravimelal et al., 2021). When the CE is injured, its healing occurs in two phases, laten and closure phase (Bukowiecki et al., 2017; Ljubimov & Saghizadeh, 2015). During the laten phase adjacent epithelial cells migrate onto the injured site and slowly cover the defect (Bukowiecki et al., 2017; Ljubimov & Saghizadeh, 2015). In the closure phase basal cells migrate to the injury site, begin to proliferate and differentiate to restore the stratified epithelium (Ljubimov & Saghizadeh, 2015). Furthermore, basal cells form new hemidesmosome connections to restore attachment to the epithelial basement membrane (Bukowiecki et al., 2017).

Severe corneal injuries or infections cause epithelial basement membrane disruption, damaging the CS (Wilson, 2020). In normal state, CKs are inactive, however, upon damage CKs apoptosis is induced in the affected area (Bukowiecki et al., 2017; Ljubimov & Saghizadeh, 2015). The adjacent CKs lose their native morphology and differentiate into fibroblasts, associated by down-regulation of CKs specific markers (Bukowiecki et al., 2017; Espana & Birk, 2020; Yam et al., 2020). This is induced by epithelial cell synthetized cytokines, such as interleukin-1 (IL-1), platelet-derived growth factor (PDGF) and transforming growth factor beta (TGF-β), which are able to enter CS through the damaged epithelial basement membrane (Bukowiecki et al., 2017). Mediated by TGF-β and PDGF fibroblast eventually form myofibroblast, exhibiting muscle-specific characteristics, such as contractility and actin-myosin bundles that produce disorganized ECM (Ljubimov & Saghizadeh, 2015; Wilson, 2020; Yam et al., 2020). In normal wound healing the epithelial basement membrane is regenerated after 8–10 days which induces myofibroblast apoptosis as the cytokine concentrations decrease (Wilson, 2020; Yam et al., 2020). Therefore, the corneal transparency is not significantly affected as the myofibroblast have not had time to synthesize enough disorganized ECM (Wilson, 2020).

However, if the normal wound healing process does not occur accordingly persistent corneal epithelial defect follows (Vaidyanathan et al., 2019; Wilson, 2020). The cause is the delayed regeneration of the epithelial basement membrane, which allows the maturation of large number of myofibroblast as the cytokine levels do not decrease (Wilson, 2020). The myofibroblast are able to synthesize large amounts of disorganized ECM, causing CS opacification adversely affecting corneal transparency (Vaidyanathan et al., 2019; Wilson, 2020). In addition, persistent corneal epithelial defect is characterized by epithelial basement membrane thinning as epithelial cells cannot migrate to the injured site (Vaidyanathan et al., 2019). One common cause for persistent corneal epithelial defect is limbal stem cell deficiency (LSCD), due to disease or trauma induced destruction of LESCs niche (Hongisto et al., 2018; Osei-Bempong et al., 2013; Vaidyanathan et al., 2019). Moreover, LSCD is associated with corneal conjunctivalization and opacification, highlighting the importance of LESCs for eyesight (Hongisto et al., 2018; Osei-Bempong et al., 2013; Vaidyanathan et al., 2019).

Damage to the corneal endothelial layer is usually caused by burns or surgeries (Ljubimov & Saghizadeh, 2015). As corneal endothelial cells have limited proliferative capacity, they migrate to the injured site increasing their size in order to close the wound, instead of proliferating (Bukowiecki et al., 2017; Ljubimov & Saghizadeh, 2015). The migration of endothelial cells is stimulated by epithelial cells produced IL-1 (Ljubimov & Saghizadeh, 2015). It has been observed that endothelial cells may undergo endothelial-

mesenchymal transition, acquiring fibroblast-like properties, where they start to proliferate. These cells can deposit fibrous ECM, decreasing corneal transparency and adversely affect endothelial cell or endothelium healing (Bukowiecki et al., 2017; Ljubimov & Saghizadeh, 2015).

2.3.2 Corneal diseases

There are various diseases that affect the cornea, causing corneal blindness by inducing corneal opacification, scaring and vascularization (Tan et al., 2012). It has been estimated that the majority of the corneal blindness cases would be preventable if treated accordingly (Oliva et al., 2012; Whitcher et al., 2001). Next the most common corneal diseases are discussed (Table 1).

Table 1: *Summary of causes, affected corneal layers and treatments for the most common corneal diseases. Peripheral ulcerative keratitis (PUK), Fuchs' endothelial corneal dystrophy (FECD), penetrating keratoplasty (PKP), deep anterior lamellar keratoplasty (DALK), descemet's stripping endothelial keratoplasty (DSEK), Descemet's membrane endothelial keratoplasty (DMEK)*

Disease	Cause	Affected layer	Treatment	Reference
PUK	Bacteria, Viruses, Fungi or Autoimmune diseases	CE and CS	Antimicrobial or immunosuppressive pharmaceuticals and PKP, DALK	Gupta et al., 2021
Trachoma	Chlamydia trachomatis bacterium	CE and CS	Antibiotics or eyelid surgery	Taylor et al., 2014
FECD	Genetic	CS, Endothelium and Descemet's membrane	DSEK/DMEK	Barrientez et al., 2019
Keratoconus	Multifactorial	All layers	PKP, collagen crosslinking	Barrientez et al., 2019

Peripheral ulcerative keratitis (PUK) is a group of diseases that induce epithelial defects and stromal degradation, causing CS thinning, potentially leading to corneal opacity and decreased vision (Gupta et al., 2021). The etiology of PUK is multifactorial and can be caused by autoimmune diseases or bacterial, viral or fungal corneal infections. There are multiple treatments for PUK that have been used such as antimicrobial or immunosuppressive pharmaceuticals. Moreover, corneal surgeries such as full-thickness penetrating keratoplasty (PKP) and deep anterior lamellar keratoplasty (DALK) can be performed to treat PUK (Gupta et al., 2021).

Trachoma is an infectious corneal disease caused by the bacteria chlamydia trachomatis and is the most common reason for corneal blindness (Taylor et al., 2014). It is characterized by inflammation of conjunctiva and if left untreated, it can lead to eyelid scarring and inturning (trichiasis), where the eyelashes touch the cornea. This causes corneal blindness via disruption of Col I organization in CS and thinning of CE. The bacterial infection is treatable with antibiotics and corneal blindness caused by trichiasis can be alleviated by eyelid corrective surgeries (Taylor et al., 2014).

Fuchs' endothelial corneal dystrophy (FECD) is a genetic disease that causes corneal endothelium dysfunction (Barrientez et al., 2019). In FECD the endothelium is not able to regulate the water transport normally, causing corneal swelling. The swelling can lead to corneal opacity by penetrating the stroma. As FECD progresses the endothelium is gradually lost which increases corneal swelling and causes stromal and Descemet's membrane thickening. Initial treatment for FECD includes dehydration of cornea and eye glasses, however with disease progression the severe adverse effects can be treated with Descemet's stripping endothelial keratoplasty (DSEK) and Descemet's membrane endothelial keratoplasty (DMEK) (Barrientez et al., 2019). From the corneal transplantations performed annually 39% are done for patients suffering from FECD (Gain et al., 2016).

The pathophysiology of keratoconus is bulging cornea due to the thinning and decreased structural strength of central or paracentral CS, caused by genetical and environmental factors (Barrientez et al., 2019). Studies have also reported decreased cell density and cell enlargement of basal epithelial cells. Moreover, keratoconus has been associated with breaks in Descemet's membrane, ruptures in Bowman's membrane and increased endothelial cell density. However, the performed studies on keratoconus have yielded contradictory results of the affected layers. To improve patients vision affected by keratoconus collagen crosslinking and penetrating keratoplasty can be performed (Barrientez et al., 2019).

2.3.3 Current treatments

The current gold standard treatment for corneal blindness is corneal transplantation surgery, often referred as keratoplasty (Ahearne et al., 2020; Singh et al., 2019; Wong et al., 2017). PKP is one of the most common keratoplasties, where the whole cornea of the patient is replaced with a donor cornea (Ahearne et al., 2020; Singh et al., 2019; Tan et al., 2012). Other keratoplasty types used are e.g. DALK and DMEK in which only parts of corneal layers are replaced (Ahearne et al., 2020; Singh et al., 2019). The replaced corneal layers in DALK are CE, Bowman's layer and majority of CS (Ahearne et al., 2020; Tan et al., 2012). In DMEK the endothelium and Descemet's membrane are replaced (Ahearne et al., 2020; Barrientez et al., 2019). Keratoplasties have an excellent clinical success rate as the cornea is immune privileged and avascular tissue (Ahearne et al., 2020; Wong et al., 2017). However, the availability of donor corneas is limited, meaning that only 1 in 70 patients can be treated (Gain et al., 2016; Tran et al., 2020). Another challenge related to keratoplasty is the increased risk of graft failure in patients suffering from inflammatory corneal diseases or having a underlying condition such as LSCD and dry eye disease (Holland et al., 2021; Moshirfar et al., 2022; Tan et al., 2012).

To overcome the limitations of keratoplasties, KPros made from transparent synthetic biomaterials have been developed (Ahearne et al., 2020; B. Zhang, Xue, Li, et al., 2019). Widely used KPro is the Boston type I KPro made from poly(methyl methacrylate) (PMMA) front plate and titanium or PMMA backplate (Holland et al., 2021; Moshirfar et al., 2022; Wong et al., 2017). A donor cornea is placed between the two plates and the KPro is implanted to the patients eye (Holland et al., 2021; Moshirfar et al., 2022). Another clinically approved KPro is the modified osteo-odonto-keratoprosthesis (MOOKP) composed from optical cylinder supported by tooth derived alveo-dental lamina and covered with buccal mucosa, a resistant membrane (Holland et al., 2021; Moshirfar et al., 2022). In addition, a modified version of Boston type I KPro has been developed, called Lucia KPro which is more efficient to manufacture (Moshirfar et al., 2022). Although Lucia KPro is commercially available, no clinical trials have been conducted to assess its safety and performance to improve patients eyesight (Moshirfar et al., 2022). While it is possible to restore vision in patients suffering from severe corneal blindness with KPros including LSCD, they are uncomfortable and there is high risk of complications such as calcification and implant extrusion (Holland et al., 2021; Matthyssen et al., 2018; Moshirfar et al., 2022).

As there are major drawbacks in the current treatment methods, more advanced treatment options for corneal blindness are needed (Matthyssen et al., 2018; B. Zhang, Xue,

Li, et al., 2019). An ideal approach would be biomimetic corneal equivalents that can be produced via TE and 3D bioprinting (Gibney et al., 2017; A. Kumar et al., 2021). Cell therapy is another potential treatment option where stem cells are injected into the cornea, where they enhance tissue remodeling and regeneration (A. Kumar et al., 2021). These new treatment strategies are discussed in the following chapters.

2.4 Corneal tissue engineering

TE aims to regenerate or replace damaged tissues with engineered biomimetic tissues (Ovsianikov et al., 2018). As there is shortage of donor corneas and the current KPros are associated with adverse effects, corneal TE has gained interest as a potential solution to this problem (Ahearne et al., 2020; Ghezzi et al., 2015; Matthyssen et al., 2018). In corneal TE the key properties for the used biomaterials are mechanical strength, viscoelasticity and transparency that need to be similar than in the *in vivo* cornea (Ahearne et al., 2020; Matthyssen et al., 2018). In order to perform its intended purpose, the biomaterials need to be biocompatible (Ahearne et al., 2020; Matthyssen et al., 2018). In addition, the biomaterials are desirably biodegradable, thus the corneal cells can replace the biomaterials with cell synthesized ECM as they degrade them (Ahearne et al., 2020; Mahdavi, Abdekhodaie, Mashayekhan, et al., 2020).

There are two main methods in TE, cell-based and scaffold-based methods (Matthyssen et al., 2018; Ovsianikov et al., 2018). In cell-based methods such as sheets and spheroids, the cells are mainly responsible for tissue regeneration (Matthyssen et al., 2018; Ovsianikov et al., 2018). Therefore, this method is suitable for CE and endothelium that are thin cellular layers (Matthyssen et al., 2018). For CS that is much thicker, scaffold-based methods are required. In this method a scaffold with suitable properties is used that mimics the CS microenvironment (Matthyssen et al., 2018). The scaffold must have the mechanical strength to resist forces applied to the cornea such as intraocular pressure and eyelid motion (Ahearne et al., 2020). The scaffold should be porous and designed in a way that it guides cell migration towards the scaffold (Ahearne et al., 2020).

Generally, in corneal TE natural biomaterials are preferred because they are biocompatible and promote cell viability and differentiation as they have excellent cell adhesion properties (Ahearne et al., 2020; Mahdavi, Abdekhodaie, Mashayekhan, et al., 2020). However, natural biomaterials have poor mechanical properties and stability (Mahdavi, Abdekhodaie, Mashayekhan, et al., 2020; Samadian et al., 2020). Synthetic biomaterials on the other hand are tough and durable however they lack cell adhesion sites (Ahearne et al., 2020; Mahdavi, Abdekhodaie, Mashayekhan, et al., 2020). Different surface topological patterns can be applied to synthetic biomaterials which enhance cell viability and

differentiation (Ahearne et al., 2020; Mahdavi, Abdekhodaie, Mashayekhan, et al., 2020). In corneal TE one method to achieve this is with electrospinning that can be used to mimic *in vivo* stromal environment (Mahdavi, Abdekhodaie, Mashayekhan, et al., 2020). Combining natural and synthetic biomaterials is advantageous since a biomaterial incorporating the excellent biological properties and mechanical properties can be created (Mahdavi, Abdekhodaie, Mashayekhan, et al., 2020).

2.4.1 Hydrogels

Hydrogels are widely used in corneal TE, generated from one or more hydrophilic monomers, initiators and crosslinkers (Khosravimelal et al., 2021). Depending on the hydrogel composition the crosslinking can be physical, chemical or enzymatic (Samadian et al., 2020). As hydrogels are highly hydrophilic they have the ability to absorb large amounts of water, leading to hydrogel swelling (Chimene et al., 2020; Khosravimelal et al., 2021; Mahdavi, Abdekhodaie, Mashayekhan, et al., 2020). Hydrogels are versatile and can be fabricated into various structures such as scaffolds, sheets and sponges (Z. Chen et al., 2018). In addition, hydrogels provide a 3D environment for incorporated cells, thus increasing biological accuracy of the structure (Khosravimelal et al., 2021). Furthermore, hydrogels have various advantages such as biocompatibility and ease of modification (Khosravimelal et al., 2021; Mahdavi, Abdekhodaie, Mashayekhan, et al., 2020).

The usual choice of biomaterial in corneal TE are Col I and Col III based hydrogels as cornea mainly consist of collagen (Ahearne et al., 2020; Matthyssen et al., 2018). Collagen hydrogels have excellent biocompatibility and biodegradability, making them relevant for corneal wound healing (Khosravimelal et al., 2021). Various forms of collagen scaffolds have been fabricated such as hydrogels, sponges and films (Ahearne et al., 2020; Matthyssen et al., 2018). The water content of collagen hydrogels is high, which can be decreased by compressing the hydrogel (Ahearne et al., 2020). Although hydrogels made from collagen are able to resemble native corneal structure, the main limitation are its poor mechanical properties (Ahearne et al., 2020). Therefore, chemical or photocrosslinking is needed to improve mechanical properties and stability of the hydrogels (Ahearne et al., 2020; Matthyssen et al., 2018). However, the limitations of these methods are that the chemical crosslinking can be cytotoxic and photocrosslinking decreases cell viability (Ahearne et al., 2020). Collagen based hydrogels have been studied for CS regeneration (Xeroudaki et al., 2020) and to construct 3D corneal equivalents (Hayes et al., 2015). In addition, corneal implants composed of collagen hydrogel and 2-

methacryloyloxyethyl phosphorylcholine (MPC) have been trialed in high-risk patients with promising results in a proof-of-concept study (Buznyk et al., 2015).

Hyaluronic acid (HA) is a polysaccharide, formed of D-gluronic and D-N-acetylglucosamine repeating units and a major constituent of ECM where its function is to hydrate and lubricate tissues (Khosravimelal et al., 2021). Other functions of HA are regulation of cell migration, proliferation and inflammation (Serban & Skardal, 2019). As HA is found in *in vivo* tissues it is highly biocompatible, biodegradable and low-immunogenic (Khosravimelal et al., 2021; Serban & Skardal, 2019). In corneal TE it has been demonstrated that hASC and LESCs seeded dopamine functionalized HA hydrogels are suitable in cell delivery to damaged cornea (Koivusalo et al., 2019). The addition of dopamine improved the hydrogels mechanical properties, reduced swelling and made the hydrogel tissue adhesive (Koivusalo et al., 2019). In addition, HA based hydrogels have been used in CE wound healing (Fernandes-Cunha et al., 2022) and to culture *ex vivo* human corneal epithelial stem cells (hCESCs) in a xeno-free environment (D. Chen et al., 2017).

Gelatin, a natural biomaterial that is derived from collagen hydrolysis, has been used in corneal TE (Ahearne et al., 2020; Khosravimelal et al., 2021). Due to its biocompatibility, low-immunogenicity and biodegradation properties the use of gelatin has been studied for multiple tissues (Khosravimelal et al., 2021; Matthyssen et al., 2018). However, gelatin has poor stability and needs to be crosslinked in order to prevent rapid degradation (Ahearne et al., 2020). It is also possible to modify gelatin with methacrylic anhydride to acquire gelatin methacryloyl (GelMA) (Ahearne et al., 2020; Khosravimelal et al., 2021). GelMA has the advantage that it is photocrosslinkable meaning that cells can be incorporated as the crosslinking process is not cytotoxic (Ahearne et al., 2020). GelMA hydrogels have been studied for CS equivalents in animals with good integration to native tissue and biocompatibility, demonstrating its potential (Kilic Bektas et al., 2019). In addition, gelatin based tissue adhesive hydrogel for corneal regeneration, GelCORE has been developed that is highly transparent and mimics corneal stiffness (Sani et al., 2019). Moreover, recently a bioadhesive glycidyl methacrylate modified gelatin hydrogel, GELGYM suitable for corneal TE including bioprinting with excellent mechanical and biological properties was reported (Sharifi et al., 2021).

2.4.2 Amniotic membrane

Amniotic membrane (AM) is derived from the placenta consisting of three distinct layers, the epithelium, monolayer of cuboidal cells and basement membrane (Jirsova & Jones, 2017). The basement membrane is mostly composed of Col IV and VII. Other structural elements are HA, fibronectin and laminins (Jirsova & Jones, 2017). AM is widely used in

corneal regeneration applications such as burn and persistent corneal epithelial defect treatments (Ahearne et al., 2020; Jirsova & Jones, 2017). The composition of AM supports cellular adhesion and proliferation, making it suitable for wound healing (Jirsova & Jones, 2017). In addition, AM has been implanted to injured corneas and used for LECS culturing (Ahearne et al., 2020; Che et al., 2019). The advantages of AM are its biocompatibility, anti-inflammatory and antimicrobial properties, (Ahearne et al., 2020; Jirsova & Jones, 2017). However, poor availability, batch-to-batch variability and low transparency limits the usefulness of the biomaterial (Ahearne et al., 2020; Che et al., 2019).

AM has been used as a scaffold in simple limbal epithelial transplantation (SLET) in patients suffering from LSCD due to corneal burns (Basu et al., 2016). A CS equivalent constructed with layers of ultrathin AM that was seeded with hCKs has been developed (Che et al., 2019). Analysis of the stromal equivalents revealed ECM produced by hCKs with similar organization as in native CS, associated with increased mechanical strength of the equivalents (Che et al., 2019).

2.4.3 Decellularized cornea

Decellularized tissues have gained interest due to the constantly increasing need for transplantable organs and have been used for various tissues, including cornea (Ahearne et al., 2020; Guruswamy Damodaran & Vermette, 2018). In decellularization cells are removed, leaving the tissues ECM intact that can be used as scaffolds or hydrogels (Ahearne et al., 2020; Guruswamy Damodaran & Vermette, 2018). Thus, with decellularized tissues it is possible to generate biomimetic tissue equivalents as the 3D architecture of the target tissue is preserved (Guruswamy Damodaran & Vermette, 2018). In addition, being highly biocompatible and low-immunogenic, decellularized tissues stimulate cell migration, differentiation and proliferation (Wenhui Zhang et al., 2021). There are various decellularization methods which are physical, chemical and biological methods (Ahearne et al., 2020; Guruswamy Damodaran & Vermette, 2018). Main limitations for different decellularization methods are incomplete removal of DNA and ECM degradation (Ahearne et al., 2020).

Physical methods can be carried out with freeze-thaw cycles, high hydrostatic pressure and supercritical CO_2 (Fernández-Pérez & Ahearne, 2019). Ionic detergents, e.g., sodium deoxycholate, non-ionic detergents, e.g., Triton X-100 and bases, e.g., ammonium hydroxide can be used for chemical methods. In biological methods enzymes such as trypsin and phospholipase A2 are used to remove cells. In addition, DNase nucleases can be used after decellularization in order to fragment any remaining DNA, reducing risk for inflammatory reaction (Fernández-Pérez & Ahearne, 2019). To prepare a hydrogel from

decellularized tissue, pepsin or acetic acid can be used to solubilize the ECM and gelation can be induced by neutralizing the solution and heating it to 37 °C (Ahearne et al., 2020; Wenhui Zhang et al., 2021).

For corneal TE the advantage of decellularized corneas is the possibility to acquire a scaffold that maintains CS ECM organization (Ahearne et al., 2020). This is challenging to mimic with other biomaterials. However, a major disadvantage is the batch-to-batch variability which can change the ECM properties. Majority of studies on decellularized corneas have used porcine corneas. Porcine corneas are a relevant alternative for human corneas as they are anatomically similar. Yet, the limitation for porcine corneas is that they are xenogenic and a robust decellularization protocol is required to minimize rejection risk (Ahearne et al., 2020).

Decellularized porcine corneas have been studied in human clinical trials with promising results (S. Li et al., 2020). CKs migration to the implanted corneas was detected between 3 and 6 months and it was postulated they remodeled the ECM, leading to the observed improvement in transparency (S. Li et al., 2020). In addition, porcine cornea derived hydrogel for CS regeneration has been characterized (Ahearne & Lynch, 2015). Compared to collagen hydrogels the transparency was enhanced, mechanical properties were alike and seeded CS cells had more native CKs gene expression (Ahearne & Lynch, 2015). Recently, the composition, ultrastructure and rheological behavior of porcine cornea derived hydrogel was reported, providing important information for the use of decellularized hydrogels in corneal TE as this kind of extensive characterization has not been done previously (Yazdanpanah et al., 2021).

2.4.4 Scaffold-free approach

Although, scaffold-based approach has favorable properties it contains some limitations (Ovsianikov et al., 2018). Especially cell seeding is difficult as cell densities are inconsistent, and the majority of cells adhere to the scaffold's surface. While hydrogels can be prepared with satisfactory cell densities the stiffness and mechanical properties often hinder cell migration. These disadvantages can be overcome with scaffold-free approach, based on delivering cell sheets, spheroids and suspension to the injured site (Ovsianikov et al., 2018). Cell sheets can be prepared by culturing cells as a monolayer on a coated culture dish and can be collected mechanically or chemically (Ovsianikov et al., 2018; Syed-Picard et al., 2018). Moreover, tissue equivalents can be acquired by stacking cell sheets (Ovsianikov et al., 2018). Cell spheroids can be acquired by culturing cells in suspension or in microfluidic cultures. The advantage of cell spheroids is that they enable extensive cell-cell interactions and mimic the native structure of tissues.

However, the disadvantage of scaffold-free approach are its weak mechanical properties and lack of possibility to incorporate biomolecules (Ovsianikov et al., 2018).

CS regeneration with hCSSC derived hCKs cultured on microgrooved polydimethylsiloxane (PDMS) coated culture dishes has been investigated (Syed-Picard et al., 2018). The cells produced a cell sheet that contained CS specific ECM with similar organization as in native human stroma (Syed-Picard et al., 2018). A proof-of-concept clinical trial has reported the injection of human corneal endothelial cells (hCEnCs) to injured endothelium (Kinoshita et al., 2018). After a five-year follow up period normal corneal thickness was reported in all patients except one, thus hCEnCs injection was safe and effective (Numa et al., 2021). A summary of performed studies in scaffold-free corneal TE is provided in table 2.

Table 2: *Summary of recent research articles on scaffold-free approaches. Peptide amphiphile (PA), embryonic stem cells (ESCs), human corneal epithelial cells (hCEpCs), multilineage-differentiating stress-enduring (Muse) cells.*

Target	Culture substrate	Form	Cell type	Reference
Stroma	PDMS	Sheet	hCSSCs	Syed-Picard et al., 2018
Endothelium	Col I	Suspension	hCEnCs	Kinoshita et al., 2018
Epithelium	AM	Sheet	ESCs	Wei Zhang et al., 2014
Epithelium Stroma	PA	Sheet	hCEpCs, primary hCKs	Gouveia et al., 2017
Endothelium	FNC mix	Suspension	hCEnCs	Xia et al., 2019
Stroma	-	Spheroid	Muse	Guo et al., 2020

2.5 Sources for keratocytes

There are several sources for CKs available, and one major cell source in corneal TE are primary hCKs, isolated from human corneal tissue (Ghezzi et al., 2015). Primary hCKs are suitable for corneal TE applications and have been used to generate CS equivalents with conventional TE (Qi Gao et al., 2021) and with 3D bioprinting (Duarte Campos et al., 2019). However, primary hCKs come with the disadvantage that they are difficult to expand as *in vivo* CKs are inactive and they can acquire fibroblastic properties when cultured (Yusoff et al., 2022). Other relevant cell sources for CKs are stem cells that have

better availability and can be expanded more easily to generate a large number of CKs (A. Kumar et al., 2021; Yam et al., 2020). Next, stem cells as a source for CKs are discussed with the focus on human adipose tissue stem cells (hASCs).

2.5.1 Human stem cells

Stem cells are responsible for tissue formation during development and thereafter for tissue homeostasis (Bacakova et al., 2018; Suman et al., 2019). Stem cells are undifferentiated cells that have two unique properties (Rajabzadeh et al., 2019). They are able to differentiate into various cell types and have self-renewal capacity, thus stem cells can form copies of themselves that are undifferentiated, maintaining their differentiation potential (Bacakova et al., 2018; Rajabzadeh et al., 2019). The differentiation of stem cells can be either symmetric or asymmetric (Kolios & Moodley, 2013). In symmetric differentiation, two differentiated cells and in asymmetric differentiation, one differentiated and one progeny are formed (Kolios & Moodley, 2013). Due to the great differentiation potential stem cells are relevant for TE and regenerative medicine (Bacakova et al., 2018; Rajabzadeh et al., 2019). Adult stem cells are particularly useful for TE applications since almost all tissues contain them (Bacakova et al., 2018; Rajabzadeh et al., 2019). These cells provide a large source of autologous cells as these can be isolated from patients directly (Bacakova et al., 2018; A. Kumar et al., 2021). The use of patients' own cells lowers the risk of inflammation and rejection compared to allogenic cells that are derived from other individuals (Bacakova et al., 2018).

Stem cells are classified according to their differentiation ability termed potency (Bacakova et al., 2018; Suman et al., 2019). Totipotent cells are the most potent stem cells, and they are able to differentiate into any cell type found in the body (Bacakova et al., 2018; Rajabzadeh et al., 2019; Suman et al., 2019). Pluripotent stem cells are capable of differentiating into all cell types of the three embryonic germ layers which are mesoderm, endoderm and ectoderm (Bacakova et al., 2018; Rajabzadeh et al., 2019; Suman et al., 2019). Stem cells residing in adult tissues are either multipotent or unipotent (Suman et al., 2019). Multipotent cells are able to differentiate into the cell types of one germ layer (Suman et al., 2019). Unipotent cells have the lowest potency and can only differentiate into one cell type (Rajabzadeh et al., 2019; Suman et al., 2019).

Other major stem cells used in TE and regenerative medicine are embryonic stem cells (ESCs) (Thomson et al., 1998) and human induced pluripotent stem cells (hiPSCs) (Takahashi et al., 2007). Particularly hiPSCs have gained attention in TE as they can be generated from somatic cells and do not possess similar ethical concerns as ESCs

(Suman et al., 2019). For cornea, hiPSCs derived CKs (Naylor et al., 2016) and LESCs (Hongisto et al., 2018) have been characterized.

2.5.2 Differentiation of hASCs towards keratocytes

hASCs are an excellent autologous cell source of multipotent MSCs that are easily isolated by liposuction (Du et al., 2010; A. Kumar et al., 2019; Lindroos et al., 2009; Lynch & Ahearne, 2017). Isolated hASCs can be identified by the expression of surface markers such as CD29, CD105 and CD90 (Lindroos et al., 2009). Moreover, the cells lack the expression of CD31, CD34 and CD45 marker proteins (Lindroos et al., 2009). Beside, being readily available hASCs possess anti-inflammatory properties, thus reducing inflammation (Du et al., 2010; Lynch & Ahearne, 2017). Therefore, hASCs have been used in clinical trials with promising results as implanted hASCs and decellularized corneal laminas, increased corneal thickness and transparency in keratoconus patients after 1-year (Alió et al., 2019). The same group reported in their 3-year follow-up study that the implantation procedure did not cause any complications and moderately improved patients' eyesight (El Zarif et al., 2021).

The successful differentiation of hASCs towards CKs was reported for the first time in 2010, demonstrating their potential for corneal TE (Du et al., 2010). Since then, several studies have used hASCs as a cell source for CKs (Ahearne et al., 2014; Lynch & Ahearne, 2017; S. Zhang et al., 2013). The differentiation can be induced by culturing hASCs in keratocyte differentiation medium (KDM), containing advanced DMEM, fibroblast growth factor 2 (FGF2) and ascorbic acid-2-phosphate (A2P) (Ahearne et al., 2014; Du et al., 2010). In addition, KDM supplemented with retinoic acid (RA) has been found to enhance hASCs differentiation towards CKs (Lynch & Ahearne, 2017).

Differentiation efficacy towards CKs lineage is verified through expression of CKs specific markers (Du et al., 2010; Lynch & Ahearne, 2017; S. Zhang et al., 2013). Keratan sulfate has been stated to be a robust indication of successful differentiation since its expression is significantly higher in *in vivo* CKs compared to other cell types (Du et al., 2010). Due to the good availability and beneficial properties, hASCs have great potential for corneal TE (A. Kumar et al., 2019; Lynch & Ahearne, 2017). These cells are also suitable for cell therapies as it has been also demonstrated that cryopreservation up to 12 years does not significantly affect viability and differentiation capacity of hASCs (A. Kumar et al., 2019). Therefore, it could be possible to bank hASCs where they are readily available when needed (A. Kumar et al., 2019). In addition, differentiation of hASCs towards neurons (Radhakrishnan et al., 2019), bone cells (Tirkkonen et al., 2013), and cardiomyocytes (Y. S. Choi et al., 2010) have been reported in the literature.

2.6 3D Bioprinting technologies

3D bioprinting is an additive manufacturing technology where cell-laden biomaterial is deposited layer-by-layer, creating a 3D structure (Matai et al., 2020; Vijayavenkataraman et al., 2018). The biomaterials used in 3D bioprinting are called bioinks that are hydrogel-based materials that contain cells and growth factors (Bejoy et al., 2021; Vijayavenkataraman et al., 2018). In bioprinting the bioink is deposited onto a printing platform with high precision with computer-aided design (CAD) that enables the printing of structures with controllable architecture (Vijayavenkataraman et al., 2018). The first step of bioprinting is to generate the CAD file that is a 3D model of the bioprinted structure (Fenton et al., 2020). CAD files can be generated by imaging the desired tissue with computed tomography (CT), magnetic resonance imaging (MRI), X-ray or 3D modeling (Fenton et al., 2020; Vijayavenkataraman et al., 2018). The 3D model is then converted into a STL file that contains information about the shape and geometry of the bioprinted structure and is used in bioprinting (Fenton et al., 2020; Vijayavenkataraman et al., 2018). Then suitable biomaterials and cells are selected to formulate the bioink that is used to bioprint the structure (Bejoy et al., 2021; Fenton et al., 2020). In the executing software of the bioprinter the desired 3D model is selected together with the bioprinting parameters and the bioink is bioprinted into the desired structure (Fenton et al., 2020). Figure 2 depicts the various steps involved in 3D bioprinting. There are various bioprinting technologies available and the most used methods are described next.

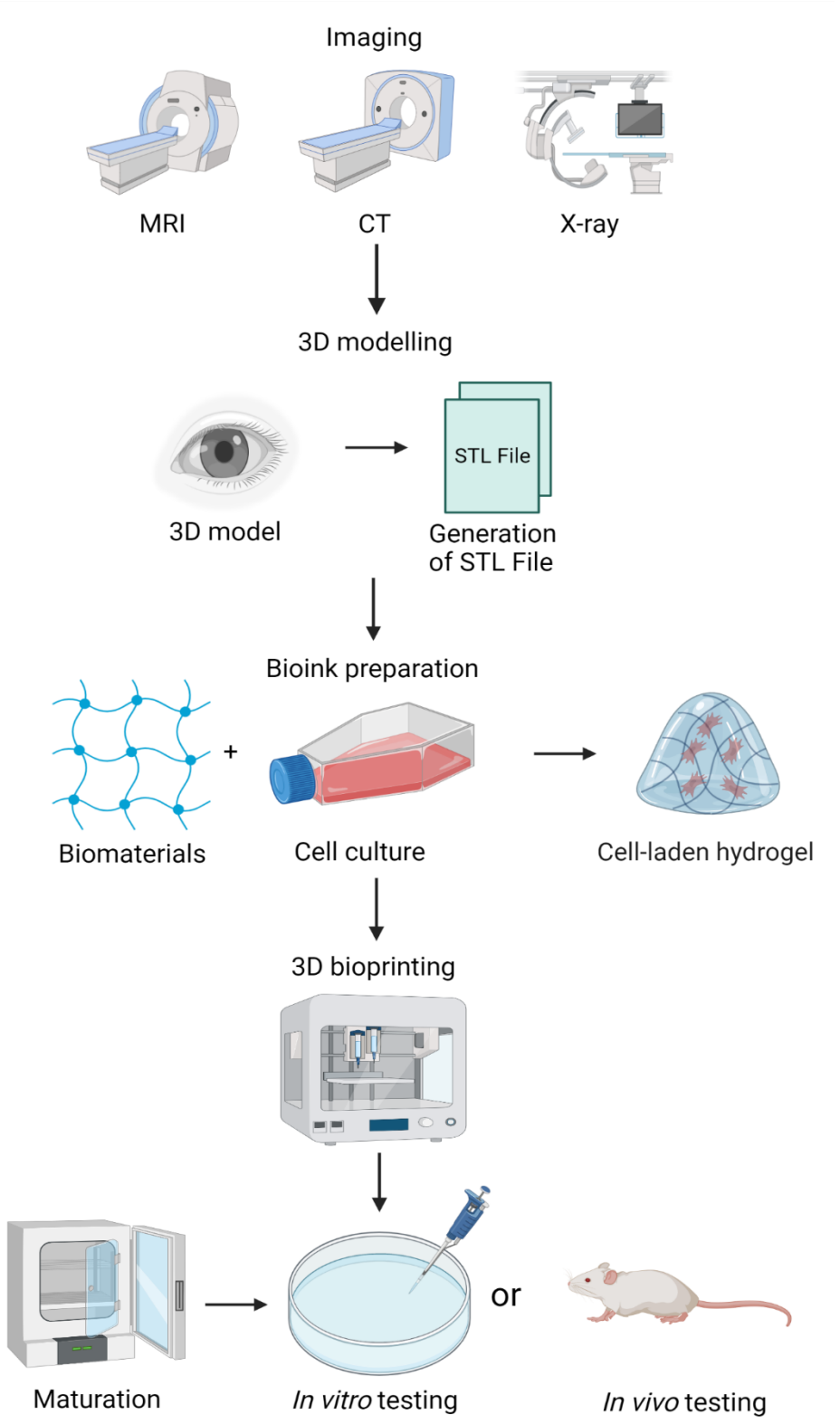

Figure 2: *The initial step in bioprinting is to generate a 3D model of the desired structure by imaging it with e.g., MRI, CT or X-ray. The data is converted into a STL file. Next, the cell-laden bioink is prepared by mixing the desired cell type and biomaterials. After bioprinting the desired 3D structure is maturated by culturing it until the desired biological factors are measured either via in vitro or in vivo testing. Created with BioRender.com. Modified and redrawn from Vijayavenkataraman et al., (2018) and Fenton et al., (2020).*

2.6.1 Extrusion-Based Bioprinting

EBB is a commonly used method to create 2D or 3D structures, because the approach is cost-effective and adjustable (Bejoy et al., 2021; Matai et al., 2020). The principle of EBB is that a continuous filament of bioink is extruded through a nozzle and deposited onto a printing platform (Bejoy et al., 2021; Matai et al., 2020). The extruded filaments are the building blocks of the bioprinted structure and its resolution is determined by the used bioink, printing parameters and nozzle diameter (Schwab et al., 2020; Vijayavenkataraman et al., 2018). Usually, the structures are crosslinked after bioprinting, however with EBB it is possible to use pre-crosslinking, which improves the filament shape retention after deposition (Matai et al., 2020; Schwab et al., 2020).

The filament extrusion can be achieved by pneumatic-, piston- and screw-driven dispensing systems (Figure 3) (Bejoy et al., 2021; Schwab et al., 2020). In pneumatic systems air pressure is used to extrude the filament (Bejoy et al., 2021; Schwab et al., 2020). Piston systems use air pressure or mechanical force to push the piston down (Schwab et al., 2020). These dispensing systems are suitable for bioinks with viscosities lower than 10^7 mPa·s. Rotating screw is used in screw systems to drive the bioink down and through the nozzle (Schwab et al., 2020). The system is more suited for bioinks having a high viscosity up to 10^4 Pa·s (Cui et al., 2020; Schwab et al., 2020).

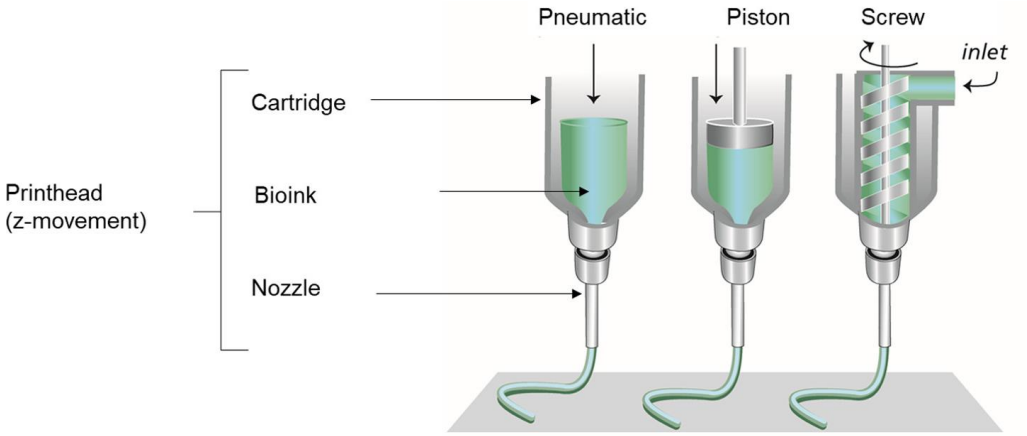

Figure 3: *In EBB the extrusion can be based on pneumatic, piston or screw. These systems use air pressure, mechanical force and screw, respectively to force the bioink through the nozzle, resulting into filament formation. Modified from Schwab et al., (2020). Copyright 2013 John Wiley and Sons.*

The advantage of EEB is its scalability, thus it can be used to create large 3D structures (Schwab et al., 2020; Vijayavenkataraman et al., 2018). Compared to other bioprinting technologies the bioprinting speed is higher and it is possible to bioprint bioinks with high viscosities and cell concentrations (Bejoy et al., 2021; Vijayavenkataraman et al., 2018). High viscosity bioinks improve shape fidelity of printed structures as they retain their

shape more readily (Schwab et al., 2020). In addition, multiple bioinks can be bioprinted simultaneously enabling the creation of structures with different biomaterials and cell types (Bejoy et al., 2021; Schwab et al., 2020). Moreover, various geometries can be achieved and different filaments sizes can be extruded with varying nozzle sizes (Fenton et al., 2020; Schwab et al., 2020).

However, the limitation in EBB is shear stress that cells encounter when going through the nozzle, because it lowers cell viability (Fenton et al., 2020; Schwab et al., 2020). The shear stress increases with high viscosity bioinks, greater pressure and smaller nozzles sizes (Matai et al., 2020; Schwab et al., 2020). Depending on the used bioink characteristics and nozzle size, the post-printing cell viability can vary from 40% to 98% (Bejoy et al., 2021; Vijayavenkataraman et al., 2018). Another problem is nozzle clogging when with high viscosity bioinks and small nozzle sizes which can lead to decreased bioprinting resolution (Fenton et al., 2020; Matai et al., 2020). Therefore, bioinks with shear-thinning properties are preferred in EBB as their viscosity decreases upon pressure reducing nozzle clogging and increasing cell viability (Cui et al., 2020; Schwab et al., 2020). However, this limits the range of usable bioinks with EBB (Vijayavenkataraman et al., 2018),

Despite its drawbacks, EBB is relevant for research and several commercially available bioprinters have been developed such as Bioplotter by EnvisionTEC GmbH, INKREDIBLE by Cellink and Novogen MMX by Organovo (Fenton et al., 2020). Various tissues have been bioprinted with EBB such as bone (Leucht et al., 2020), cardiac (Shin et al., 2021), neural (Salaris et al., 2019) and adipose (Tytgat et al., 2019). In addition, EBB has been used in corneal bioprinting to bioprinting corneal layers and equivalents as discussed later.

2.6.2 Inkjet-Based Bioprinting

Inkjet-based bioprinting is a noncontact bioprinting approach where small bioink droplets (1–100 pL) are layered onto a printing platform to create a 3D structure (Fenton et al., 2020; Matai et al., 2020). The two forms of inkjet bioprinting are continuous inkjet bioprinting (CIJ) and drop-on-demand (DOD) bioprinting (Bejoy et al., 2021; Vijayavenkataraman et al., 2018). In CIJ the bioink flows continuously which causes instability and results in droplet formation (Bejoy et al., 2021; Matai et al., 2020). As the droplets are randomly formed in CIJ, the rate of droplet formation cannot be controlled (Bejoy et al., 2021; Vijayavenkataraman et al., 2018). Therefore, DOD is preferred as it allows control over droplet formation (Bejoy et al., 2021; Vijayavenkataraman et al., 2018). There are three forms of DOD that are thermal, piezoelectric and electrostatic

inkjet bioprinting (Bejoy et al., 2021; Fenton et al., 2020). In thermal bioprinting the printing nozzle is heated, creating air bubbles that eject bioink droplets as they collapse (Bejoy et al., 2021; Fenton et al., 2020). In piezoelectric bioprinting bioink droplets are ejected to the printing platform by a pressure wave that is generated by a piezoelectric actuator (Fenton et al., 2020; Vijayavenkataraman et al., 2018). The droplet formation in electrostatic bioprinting is based on voltage pulses between a pressure plate and electrode (Bejoy et al., 2021). The thermal and piezoelectric inkjet bioprinting approaches are illustrated in figure 4.

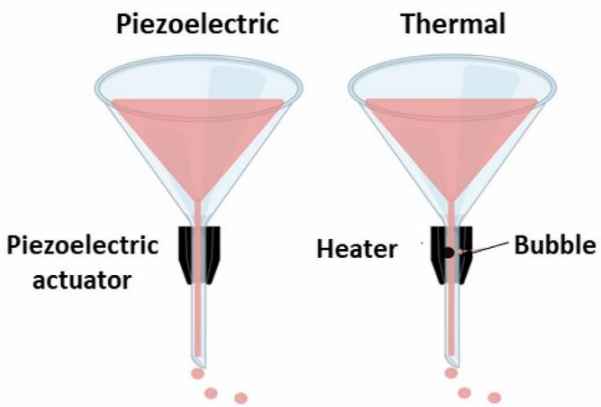

Figure 4: *Piezoelectric and thermal are DOD bioprinting technologies, which use piezoelectric actuator and heater, respectively to generate bioink droplets. Modified from Bejoy et al., (2021).*

The benefit of inkjet bioprinting is its affordability and ease of use compared to other 3D bioprinting technologies (Fenton et al., 2020). In addition, the approach offers fast printing speed, excellent cell viability between 70–90% and printing resolution (50 µm) (Bejoy et al., 2021; Fenton et al., 2020). The disadvantage of inkjet bioprinting is that it can be used for bioinks with low viscosities (1–12 mPa·s) and the control over droplet deposition is limited (Fenton et al., 2020; Vijayavenkataraman et al., 2018). Thermal inkjet is widely used to bioprint cells, however the size of droplets is inconsistent, and the cells are subjected to heat and shear stress, lowering cell viability (Bejoy et al., 2021; Matai et al., 2020). Inkjet bioprinting has been used to bioprint neural (Tse et al., 2016), bone (G. Gao et al., 2015), cartilage (G. Gao et al., 2015) and vascular tissue (Solis et al., 2019). In addition, retina mimicking structures have been created by bioprinting photoreceptor cells (PRs) and retinal pigment epithelium (RPE) (Masaeli et al., 2020).

2.6.3 Laser-Assisted Bioprinting

Laser-assisted bioprinting (LAB) is a noncontact and nozzle free approach that can be classified into laser induced forward transfer (LIFT) and laser guidance direct writing

(LGDW) (Gu et al., 2020). In LIFT, instead of cartridges, the bioink is placed onto an absorptive layer, usually composed of gold or titanium that is attached to a transparent layer of glass or quartz (Gu et al., 2020; Vijayavenkataraman et al., 2018). A laser pulse source is used to focus a laser beam to the absorptive layer through the transparent layer which causes the bioink to evaporate leading to droplet formation (Matai et al., 2020; Vijayavenkataraman et al., 2018). The droplets are ejected to the collector consisting of biomaterials or cell culture medium (Figure 5) (Gu et al., 2020). The working principle of LGDW is to focus a laser to a cell suspension and guide the cells onto a collector (Bejoy et al., 2021; Vijayavenkataraman et al., 2018). As there are only few suitable biomaterials for LGDW and therefore LIFT is the preferred LAB approach (Gu et al., 2020).

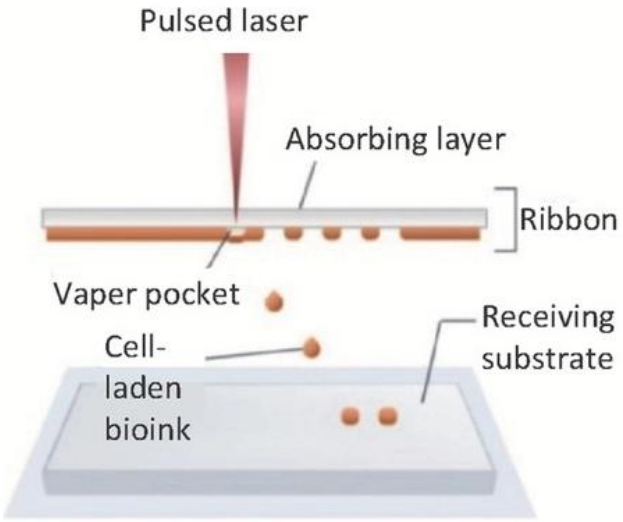

Figure 5: *In LIFT a laser pulse is focused to the absorbing layer, leading to bioink evaporation and droplet formation. The bioink droplets are ejected onto the collector. Modified from Cui et al., (2020).*

In terms of usability LAB is more complicated and expensive to use than extrusion- or inkjet-based bioprinters (Fenton et al., 2020; Vijayavenkataraman et al., 2018). Yet, with LAB it is possible to obtain excellent bioprinting resolution (10–100µm) as it is possible to deposit small bioink droplets (10 pL) (Gruene et al., 2011; Matai et al., 2020). In addition, there is no risk of nozzle clogging thus large variety of different viscosity bioinks can be printed with up to 10^8 cells per milliliter (Fenton et al., 2020; Vijayavenkataraman et al., 2018). As LAB is nozzle free, excellent post-printing cell viabilities up to and over 95% can be achieved (Bejoy et al., 2021; Vijayavenkataraman et al., 2018). However, one disadvantage is that LAB utilizes photocrosslinkable bioinks and the possible cytotoxically effects of the used photoiniators and UV light needs to be assessed for different cell types individually (Fenton et al., 2020). Other limitations include cellular damage due to laser exposure, metallic nanoparticle induced cytotoxicity and poor scalability

(Vijayavenkataraman et al., 2018). LAB has been used to bioprint neural cells (Roversi et al., 2021), skin (Koch et al., 2012) and vascular tissue (Kérourédan et al., 2019).

2.6.4 Lithography-Based Bioprinting

Stereolithography (SLA) and digital light processing (DLP) are lithography-based bioprinting (LBB) approaches in which bioinks are photocrosslinked with laser and light, respectively (Schwab et al., 2020). In both approaches a container with a height controlled platform is filled with the bioink (Gu et al., 2020). SLA utilizes a laser beam that scans each layer initiating gelation and the platform moves upwards after each bioprinted layer (Schwab et al., 2020; Van Hoorick et al., 2019). In DLP the light is patterned to the desired layer shape and focused onto the bioink to crosslink the entire layer simultaneously (Schwab et al., 2020; Van Hoorick et al., 2019). The difference between SLA and DLP is that, in DLP the bottom layer is bioprinted first, thus the platform moves downwards after each layer (Gu et al., 2020).

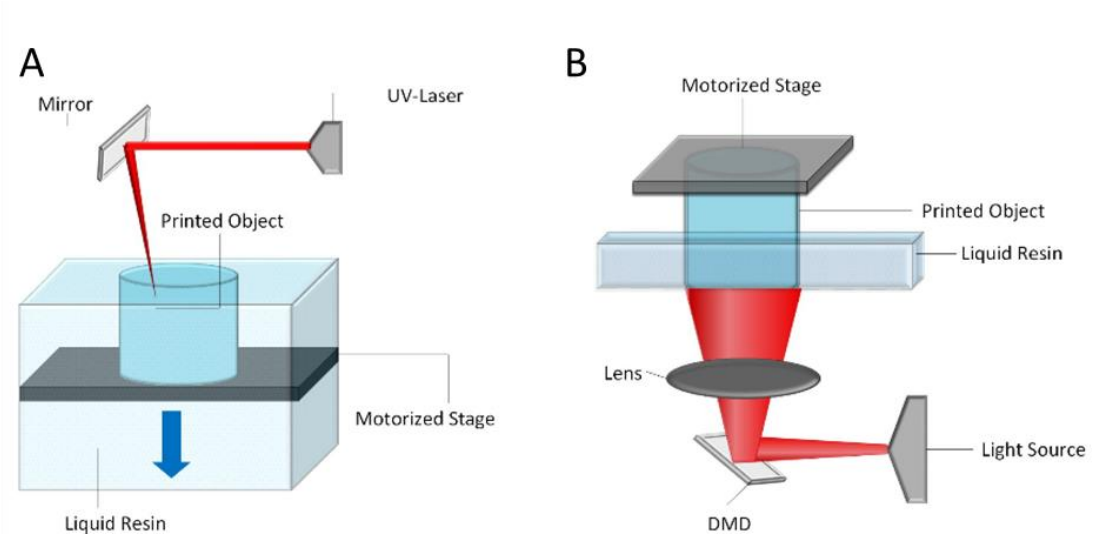

Figure 6: *LBB technologies. A) SLA where a laser is focused onto the printing platform to induce bioink (liquid resin) crosslinking. B) DLP where light is focused onto the printing platform through digital micromirror device (DMD) and lens to induce the bioink crosslinking into the desired layer shape. Modified from Van Hoorick et al., (2019).*

With LBB it is possible to bioprint more complex structures faster with higher resolutions (25–50 µm) compared to EBB (Lim et al., 2020). Since the approach is nozzle-free there are no problems regarding nozzle clogging and shear stress (Gu et al., 2020). In addition, cell viabilities of over 90% can be achieved and high cell concentration bioinks (over 10^6 cells per milliliter) can be used with SLA (Matai et al., 2020; Vijayavenkataraman et al., 2018). In general, a disadvantage for LBB is that only photocrosslinkable bioinks can be

used (Cui et al., 2020). LBB has been used in cardiac (Shenyuan Lee et al., 2021), small intestine (Elomaa et al., 2020) and cartilage (Lam et al., 2019).

2.7 Bioinks

Bioinks are defined as cell-laden biomaterial formulations that can contain bioactive molecules such as growth factors and drug releasing molecules and are printable with 3D bioprinting technologies (Groll et al., 2019; Gungor-Ozkerim et al., 2018; Schwab et al., 2020). Distinct from bioinks are biomaterial inks that can have similar composition however they do not contain cells (Groll et al., 2019; Schwab et al., 2020). Next, the general requirements for bioinks are discussed.

A functional bioink should sustain cell viability by providing an environment for cells with suitable biological, chemical and mechanical properties (Chimene et al., 2020; Gungor-Ozkerim et al., 2018). Majority of the developed bioinks are hydrogel based since hydrogels offer a highly biocompatible and native ECM mimicking environment for cells (Chimene et al., 2020; Gungor-Ozkerim et al., 2018). Bioprinted hydrogel structures are highly porous due to the high water content and permeable for nutrient diffusion, supporting cell migration and proliferation (Chimene et al., 2020; H. Li et al., 2018). In addition, hydrogels are often biodegradable, and cells are able to remodel their environment and deposit their own ECM (Chimene et al., 2020; Gungor-Ozkerim et al., 2018). The hydrogel degradation rate is affected by the bioink formulation and culture conditions and it ideally matches the rate of cellular remodeling (H. Li et al., 2018). Stiffness is one of the important mechanical properties as it influences cell behavior in the bioprinted structure (Chimene et al., 2020; Knowlton et al., 2017). Moreover, external mechanical forces can be applied to hydrogels that cells can sense through a process called mechanotransduction (Chimene et al., 2020). Studies have shown that simulated mechanical forces can improve cell differentiation and alignment, however this is not widely used for bioprinted structures (Chimene et al., 2020).

Bioprinting resolution is dictated by the printability of the bioink, thus it is the central property that needs to be considered during bioink formulation (Cui et al., 2020; Hospodiuk et al., 2017). Main factors influencing printability are the rheological properties such as viscosity, shear stress and yield stress (Chopin-Doroteo et al., 2021; H. Li et al., 2018; Schwab et al., 2020). Viscosity is the fluid's resistance to flow upon encountering stress and a greater viscosity leads to improved shape retention of the bioprinted structure (Chopin-Doroteo et al., 2021; H. Li et al., 2018). The bioink is subjected to shear stress when extruded through the nozzle and is particularly relevant for EBB (Cui et al., 2020; H. Li et al., 2018). Shear stress is defined by printing pressure, nozzle diameter

and bioink viscosity (H. Li et al., 2018; Schwab et al., 2020). High shear stress decreases cell viability, thus the parameters need to be optimized in order to bioprint high resolution structures with adequate cell viability (H. Li et al., 2018). Yield stress is the minimum force required to flow the bioink and is determined by shear stress (Chopin-Doroteo et al., 2021; Cui et al., 2020). Shear-thinning means a decrease in viscosity upon shear stress resulting in improved cell viability, therefore it is a desired bioink property in EBB (H. Li et al., 2018; Schwab et al., 2020). Bioink printability and biocompatibility determine the biofabrication window, meaning the range where both properties are adequate for bioink utilization (Cui et al., 2020; Lim et al., 2020; Schwab et al., 2020). Majority of the current bioinks have a narrow biofabrication window which is a limitation especially for EBB (Cui et al., 2020).

Bioinks can be derived from natural, synthetic or composite hydrogels (Chopin-Doroteo et al., 2021; Gungor-Ozkerim et al., 2018). Generally, natural biomaterials are preferred as they are biocompatible, biodegradable and support cell adhesion compared to synthetic biomaterials (Benwood et al., 2021; Hospodiuk et al., 2017). However, natural biomaterials have poor mechanical properties and therefore bioinks are commonly formulated from various biomaterial types, in order to derive a bioink with the suitable properties (Cui et al., 2020; Hospodiuk et al., 2017). A challenge for hydrogel-based bioinks are their low mechanical properties, limiting the achievable size of the bioprinted structure (Chimene et al., 2020). Therefore, the mechanical properties are enhanced with higher biomaterial concentrations and different crosslinking methods, however these decrease the biocompatibility of the bioink (Chimene et al., 2020; Chopin-Doroteo et al., 2021).

The cell types used in bioinks can be primary cells or stem cells that are differentiated into desired cell type (Matai et al., 2020). Used stem cell types in bioinks include hiPSCs, ESCs and hASCs. Generally, primary cells are useful when bioprinting simple structures and stem cells are suited for more complicated shapes. Stem cells are more susceptible to external forces compared to primary cells and their viability can decrease when printed with EBB. Furthermore, if stem cells are differentiated post-printing, a bioink composition inducing differentiation into the desired cell type must be identified. The suitable cell concentration for bioinks depends on the used bioprinting technology and must account for the cell death occurring during bioprinting so that the bioprinted structure contains enough viable cells. In addition, it is important to note that with increased cell concentrations the bioink viscosity increases, because the space taken by cells (Matai et al., 2020).

There are multiple biomaterials that are studied and used in bioinks. For simplicity in this thesis the focus is on the widely used natural biomaterials in bioinks. Figure 7 illustrates

the general aspects that need to be considered when developing a 3D bioprintable bioink, with a special consideration to EBB.

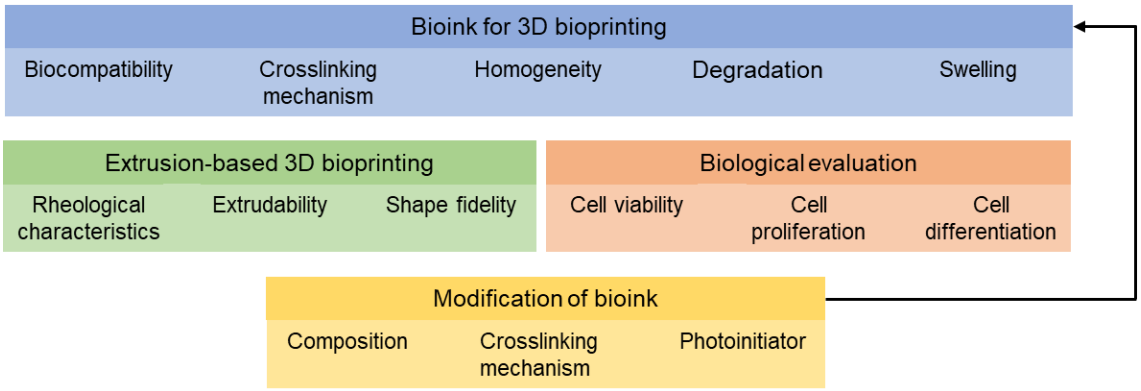

Figure 7: *The aspects that need to be considered when developing bioinks. First, it is important to consider the biocompatibility, crosslinking mechanism, homogeneity, degradation and swelling of the bioink. Second, it is crucial to assess the printability of the bioink. In case of EBB some of the key aspects are rheological characteristics, extrudability and shape fidelity. Third, it is essential to evaluate the biological performance of the bioink which can be done by measuring cell viability, proliferation, and differentiation. Fourth, based on the bioink performance the bioink can be modified by using different composition, crosslinking mechanism and photoinitiator. When the bioink is modified the whole testing process is repeated. Modified and redrawn from Schwab et al., (2020).*

2.7.1 Alginate

Alginate, a polysaccharide derived from algae, resembling GAGs of human ECM, is widely used as it is biocompatible and rapidly crosslinkable (Qiqi Gao et al., 2021; Gungor-Ozkerim et al., 2018; Hospodiuk et al., 2017). It contains carboxylic acid groups (COO^-) and ionic crosslinking can be achieved by calcium chloride ($CaCl_2$) and calcium sulfate ($CaSO_4$) solutions (Qiqi Gao et al., 2021; Hospodiuk et al., 2017). Although alginate is a popular natural biomaterial, it has some limitations such as poor cell adhesion (Gungor-Ozkerim et al., 2018; Hospodiuk et al., 2017). Moreover, it does not support cell proliferation (Benwood et al., 2021). Another disadvantage is that alginate is not biodegradable, and it degrades by dissolving, meaning that the degradation of alginate structures cannot be controlled (Qiqi Gao et al., 2021). Therefore, other biomaterials such as nanocellulose and gelatin have been mixed with alginate to improve its properties (Benwood et al., 2021). In addition, cell-binding arginine-glycine-aspartic acid (RGD) motifs can be added to alginate bioinks to support cell adhesion (Gungor-Ozkerim et al., 2018; Hospodiuk et al., 2017). Examples of tissues that have been bioprinted with alginate-based bioinks are cartilage (Urtaza et al., 2022), neural (Naghieh et al., 2019) and islets of Langerhans (Duin et al., 2019).

2.7.2 Gelatin

As discussed earlier in chapter 2.4.1 gelatin is derived from collagen hydrolysis and has beneficial properties, making it suitable for TE applications. It is commonly used in bioinks as hydrogel formation can be induced at low temperatures (20–30°C) (Benwood et al., 2021; X. Wang et al., 2017). In addition, gelatin is thermosensitive, thus bioink viscosity can be easily controlled by altering the temperature (Benwood et al., 2021; Hospodiuk et al., 2017). However, the stability of gelatin structures is poor due to the thermosensitivity and various approaches have been used to improve the mechanical properties (X. Wang et al., 2017). One method has been to mix gelatin with chemically crosslinkable biomaterials such as alginate and HA (X. Wang et al., 2017). Another approach has been the use of GelMA (Gungor-Ozkerim et al., 2018). GelMA is a popular bioink biomaterial, because it is photocrosslinkable with UV and the degree of crosslinking can be controlled (Benwood et al., 2021; Gungor-Ozkerim et al., 2018). Gelatin-based hydrogels have been used to bioprint aortic valve (Bin Duan et al., 2013), keratinocytes (Piola et al., 2022) and MSCs (Giuseppe et al., 2018). With GelMA on the other hand bone MSCs and human umbilical vein endothelial cells (HUVECs) (Sohyung Lee et al., 2020) have been bioprinted.

2.7.3 Collagen

Collagen based hydrogels are a common biomaterial choice for bioinks as collagen has been used in clinical setting with promising results, thus bioprinted structures with collagen based bioinks have great clinical potential (Hospodiuk et al., 2017; Egor Olegovich Osidak et al., 2020). Collagen hydrogels are mainly formed from Col I which can be crosslinked into a hydrogel at neutral pH and 37 °C (Hospodiuk et al., 2017; Egor Olegovich Osidak et al., 2020). Poor mechanical properties of collagen bioinks are a widely reported limitation in the literature which is related to the low collagen concentrations used in the studied bioinks (Egor Olegovich Osidak et al., 2020). In addition, the gelation is slow, thus the shape fidelity is poor after bioprinting (Benwood et al., 2021; Hospodiuk et al., 2017). Although FRESH can be used to support the structure during printing, it may leave residues to the printed structure which can affect its biocompatibility (Egor Olegovich Osidak et al., 2020). Another approach that has been characterized are high collagen concentrations up to 40 mg/ml which resulted in improved mechanical properties with good cell viability when printed at low temperatures (Egor O. Osidak et al., 2019).

As the majority of pure collagen bioinks have major limitations, collagen is usually supplemented with other biomaterials to improve its strength and printability (Benwood et al., 2021; Egor Olegovich Osidak et al., 2020). Collagen has been supplemented with Pluronic, a synthetic biomaterial synthesized from poly(ethylene glycol) (PEG), which improved printed structure strength due to aligned collagen fibers (Moncal et al., 2019). Moreover, collagen has been combined with decellularized ECM (dECM) and silk-fibroin, resulting in a bioink with excellent biological and mechanical properties suitable for bone regeneration (Hyeongjin Lee et al., 2018). Multiple tissues have been bioprinted with collagen bioinks such as vascular (Muthusamy et al., 2021), cartilage (Yang et al., 2018) and muscle tissue (W. J. Kim et al., 2019).

2.7.4 Decellularized ECM

In vivo, the cells synthesize and secrete different types of proteoglycans and proteins which they organize into ECM, determining the shape and structure of a particular tissue (Kabirian & Mozafari, 2020; B. S. Kim et al., 2020; Wenhui Zhang et al., 2021). Other functions of ECM is to provide adhesion sites for cells, paths for migration and support cell viability (Kabirian & Mozafari, 2020; Wenhui Zhang et al., 2021). As discussed in chapter 2.4.3 dECM can be acquired from the tissue of interest by various decellularization methods that remove cells and leaves the ECM components intact. From the dECM, a tissue-specific bioink can be prepared, containing the native ECM components of the tissue (Nam & Park, 2018; Wenhui Zhang et al., 2021). Thus, structures bioprinted with dECM bioinks provide an environment that mimics the tissues native biochemical composition, inducing tissue-specific cell behavior (B. S. Kim et al., 2020; Nam & Park, 2018; Wenhui Zhang et al., 2021). In addition, cells are able to remodel dECM bioink structures at similar rates as *in vivo* ECM (Kabirian & Mozafari, 2020). The mechanical properties of dECM bioinks are low, which are often enhanced by addition of vitamin B2 or other harder biomaterials (Kabirian & Mozafari, 2020; Nam & Park, 2018). Another challenge is the used decellularization process which may leave residual cells increasing risk on inflammatory response or the removal of some ECM components as discussed previously. In addition, the protein composition of dECM bioinks largely affect the rheological characteristics, thus the same dECM bioink decellularized with different methods can have different rheological properties (Nam & Park, 2018; Pati et al., 2014).

Popular ECM sources used in research are animal and human tissues (Kabirian & Mozafari, 2020; B. S. Kim et al., 2020). Porcine tissues are widely used as they are anatomically and physiologically comparable to human tissues (Kabirian & Mozafari, 2020; B. S. Kim et al., 2020). Lesser used sources are cows, goats and rats (Kabirian &

Mozafari, 2020). However, animal tissues are xenogeneic and there is the risk of rejection and transmission of zoonosis if implanted to humans (Kabirian & Mozafari, 2020; Wenhui Zhang et al., 2021). Therefore, human tissues derived from cadavers or donors are superior due to the lower risk of eliciting immune reaction although their availability is limited (Kabirian & Mozafari, 2020; Wenhui Zhang et al., 2021).

Bioinks derived from dECM have been characterized for various tissues and table 3 summarizes the recent performed studies in the field. Pati et al. performed the first study in which tissue-specific dECM bioink from cardiac, adipose and cartilage tissue was bioprinted with hASCs or human turbinate-tissue derived mesenchymal stromal cells (hTMSCs) (Pati et al., 2014). It was observed that the bioinks induced stem cells to differentiate into tissue-specific lineages and supported the maintenance of mature cell phenotype. Moreover, the bioinks showed shear-thinning behavior, which was linked to the observed high post-printing cell viability (Pati et al., 2014). More recently, skin constructs were bioprinted with skin derived dECM bioink which incorporated primary human skin fibroblasts (PHSFs) (Jorgensen et al., 2020). The bioink was supplemented with fibrinogen, which improved printability together with enhanced cell viability. Furthermore, the bioink exhibited shear-thinning behavior and the microstructure of the constructs mimicked native skin structure (Jorgensen et al., 2020). In addition, a cornea-specific dECM bioink with excellent transparency and shear-thinning behavior has been characterized (H. Kim et al., 2019). The bioink was bioprinted with hTMSCs, demonstrating excellent biocompatibility *in vitro* and *in vivo* rabbit model (H. Kim et al., 2019).

Table 3: *Summary of relevant recent research articles on decellularized bioinks. Neonatal rat cardiomyocytes (NRCM), human bone marrow-derived mesenchymal stem cells (BMMSCs), human hepatocellular carcinoma (HepG2), human skeletal muscle cells (hSKMs).*

Tissue	Origin	Decellularization method	Cell type	Reference
Skin	Human	Enzymatic Chemical	PHSFs	Jorgensen et al., 2020
Cardiac	Porcine	Chemical	NRCM	Das et al., 2019
Liver	Porcine	Chemical	BMMSCs HepG2	Hyungseok Lee et al., 2017
Skeletal muscle	Porcine	Chemical	hSKMs	Y. J. Choi et al., 2019
Vascular				
Cartilage	Porcine	Physical Chemical	Chondrocyte	Visscher et al., 2021
Cornea	Bovine	Chemical	hTMSCs	H. Kim et al., 2019
Small intestine submucosa	Porcine	Chemical	hASCs	Rueda-Gensini et al., 2021
Adipose	Porcine	Chemical	hASCs	Pati et al., 2014

Recently, an alternative option for tissues has gained attention, called cell-derived matrix (CDM), where primary cells or stem cells are cultured *in vitro* in 2D, 3D or aggregates to acquire ECMf (Chan et al., 2021; Fitzpatrick & McDevitt, 2014; Wenhui Zhang et al., 2021). After culture the cells are removed with similar methods than ECM and the CDM is collected from the culture system (Chan et al., 2021). The biochemical composition of CDM is alike to *in vivo* ECM, however the structural organization differs significantly (Chan et al., 2021; Fitzpatrick & McDevitt, 2014). Fortunately, this is not required for bioinks since the ECM organization is disrupted during the preparation process (Chan et al., 2021). In addition, the stem cells can be genetically modified or different cell culture conditions can be used to produce different compositions of CDM for a large variety of applications (Chan et al., 2021; Fitzpatrick & McDevitt, 2014). The amount of deposited CDM by cells can be increased with macromolecule crowding (MMC), where inert macromolecules of natural or synthetic origin are added to the culture medium (C. Chen et al., 2011; P. Kumar et al., 2015). The polysaccharide carrageenan is one MMC agent, which has been used effectively for human corneal fibroblasts (hCFs) (Gürdal et al., 2020; P. Kumar et al., 2015). While CDM can be used to acquire ECM with homogenous quality, the scaling up of the technique is challenging due to lack of suitable technologies (Chan et al., 2021).

2.7.5 Hyaluronic acid

Similarly to traditional TE, the excellent properties of HA has made it a common biomaterial choice for bioinks (Hospodiuk et al., 2017; Matai et al., 2020). In order to make HA suitable for bioink preparation chemical modification of its functional groups is required to improve the rheological properties (Hospodiuk et al., 2017; Nam & Park, 2018; Serban & Skardal, 2019). The chemical functionalization can be achieved by various methods such as with thiol, amine, methacrylic anhydride, and hydrazine sulfate group mediated chemical reactions (Serban & Skardal, 2019). HA bioinks have to be mixed with other biomaterials to improve the crosslinking speed, mechanical properties and stability (Benwood et al., 2021; Hospodiuk et al., 2017; Nam & Park, 2018). Moreover, the cell adhesion properties are inadequate and cell adhesion promoting factors like ECM components must be added (Benwood et al., 2021).

Although HA is found in almost all tissues, it is the major ECM component in cartilage tissue, thus it has been used extensively to print cartilaginous tissue (Antich et al., 2020; Hauptstein et al., 2020). In addition, HA modified with methacrylate has been used for cartilage 3D bioprinting (Lam et al., 2019). Other bioprinted tissues with HA containing bioinks have been neural tissue (Liu et al., 2021), heart tissue (B. Duan et al., 2014) and liver tissue (Mazzocchi et al., 2019)

2.8 Crosslinking methods

Structures bioprinted with hydrogel-based bioinks need to be crosslinked in order to maintain the shape fidelity and improve the mechanical stability of the structure post-printing (Chimene et al., 2020; Cui et al., 2020; Hospodiuk et al., 2017). The crosslinking methods for bioinks are either classified as chemical or physical (Figure 8) (Cui et al., 2020; GhavamiNejad et al., 2020). In chemical crosslinking bioink gelation is achieved by covalent bond formation and the different chemical methods that have been used are radical polymerization, thiol-ene chemistry, Schiff's base and click chemistry. Physical crosslinking methods are based on weak bond formation within the bioink and the methods that can be used include ionic and electrostatic interactions (Cui et al., 2020; GhavamiNejad et al., 2020). Additional methods that can be employed, which are not discussed here, are enzymatic reactions and stereo-complexation for chemical and physical crosslinking, respectively (Cui et al., 2020). Structures bioprinted with chemically crosslinkable bioinks have in general, greater mechanical properties as the process is nonreversible unlike physical crosslinking (Chimene et al., 2020; GhavamiNejad et al., 2020).

A functional bioink has excellent printability and provides a biomimetic environment, supporting cellular functions such as proliferation and migration (Chimene et al., 2020; H. Li et al., 2018). The challenge with current crosslinking methods is that a relatively high bioink crosslinking degree is required in order to bioprint larger structures (Chimene et al., 2020). This leads to a decrease in bioink permeability and porosity, negatively affecting cell behavior. Therefore, new methods such as biomaterial functionalization and nanocomposite-based bioinks are researched to improve the mechanical properties without compromising cell viability (Chimene et al., 2020).

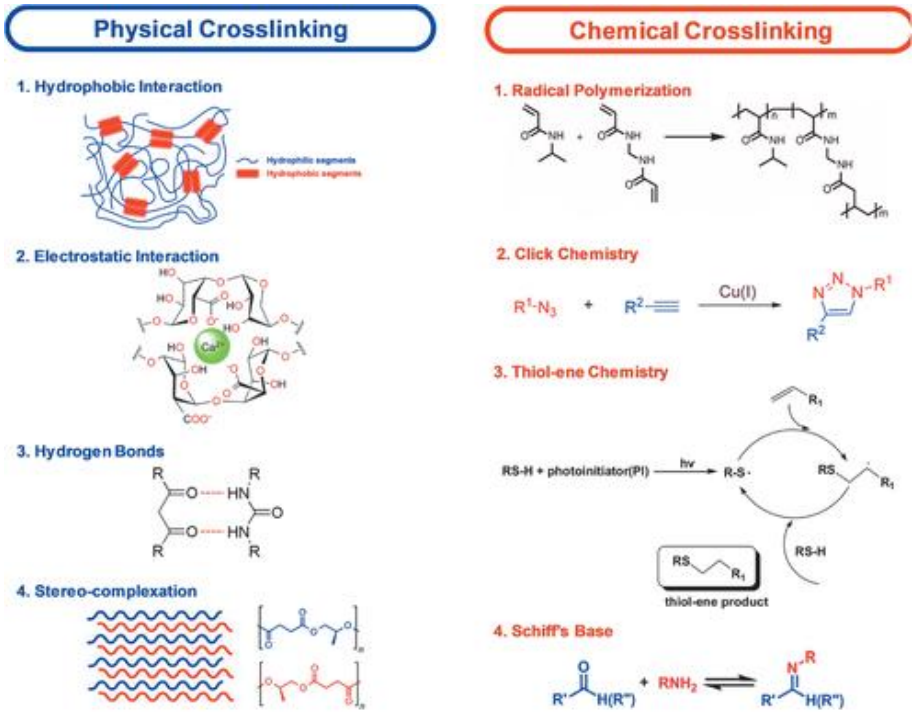

Figure 8: *Schematic of physical and chemical crosslinking approaches that are used in bioinks. Modified from. Cui et al., (2020).*

2.8.1 Chemical crosslinking

In chemical crosslinking crosslinkers are used to create covalent bonds between hydrogels polymer chains, leading to hydrogel gelation (Cui et al., 2020; Hospodiuk et al., 2017). Compared to physical crosslinking, chemical crosslinking offers improved mechanical properties and stability, however crosslinkers may cause unexpected reactions in the hydrogel, lowering biocompatibility (Hospodiuk et al., 2017). There are various methods to achieve chemical crosslinking in bioinks and next Schiff's-based reactions and click chemistry are discussed.

Schiff's-based reactions occur between aldehyde and amine or alcohol group containing polymers at physiological conditions where the reaction of these groups leads to formation of covalent bond (Cui et al., 2020; GhavamiNejad et al., 2020; Hospodiuk et al., 2017). Bioinks that are crosslinked with this method contain biomaterials with amine groups that are mixed with aldehyde containing crosslinkers like glutaraldehyde (GhavamiNejad et al., 2020; Hospodiuk et al., 2017). The degree of crosslinking can be controlled with varying crosslinker concentrations and a higher concentration generates hydrogels with greater mechanical properties and stability (Hospodiuk et al., 2017). In addition, higher reaction pH can be used to achieve a higher crosslinking degree (GhavamiNejad et al., 2020). The benefit of Schiff's-based reactions is that the generated bioinks have shear-thinning properties, however the aldehyde groups may react with amine group containing biological molecules (Cui et al., 2020). Although glutaraldehyde is widely used in crosslinking, it is cytotoxic and more cell friendly crosslinkers such as genipin have been identified (Hospodiuk et al., 2017). The by-product of Schiff-based reactions is water, thus it is a condensation reaction and the formation of water can degrade bioinks via hydrolysis (GhavamiNejad et al., 2020). Figure 9 illustrates the Schiff-based reaction between gelatin and oxidized dextran.

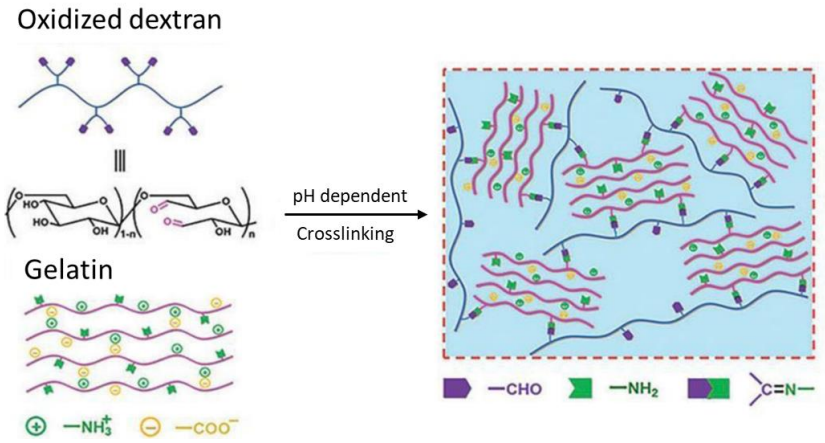

Figure 9: *Schiff-based reaction between oxidized dextran and gelatin, which leads to a pH dependent bioink crosslinking. Modified from GhavamiNejad et al., (2020).*

A bioink crosslinkable by click chemistry can be formed by mixing at least two reactive precursors (Gopinathan & Noh, 2018; Mueller et al., 2022). This induces a fast spontaneous gelation without the need for additional crosslinkers or energy (Gopinathan & Noh, 2018; Mueller et al., 2022). The benefit of click chemistry is that the bioink gelation speed and degradation can be adjusted by using different precursors (Mueller et al., 2022). In addition, this crosslinking method does not generate toxic by-products as it is usually water or nothing (Gopinathan & Noh, 2018; Mueller et al., 2022). Furthermore, click chemistry is often bio-orthogonal, thus there are minimal undesired side reactions with

cells or ECM (Cui et al., 2020; Mueller et al., 2022). Click chemistry can be achieved with various ways and a popular method is to mix alkyne and azide functional groups containing precursors (Cui et al., 2020). However, in this approach copper is commonly used as a catalyzer, which can be cytotoxic (Cui et al., 2020; Gopinathan & Noh, 2018; Mueller et al., 2022). Although cyclooctyne can be used instead of copper, the gelation is slower which can decrease cell viability as cells are subjected to nonphysiological conditions for a longer time (Gopinathan & Noh, 2018; Mueller et al., 2022).

Another click chemistry is hydrazone crosslinking, a reaction between aldehyde and hydrazide groups (GhavamiNejad et al., 2020; Koivusalo et al., 2018; Mueller et al., 2022). This approach has been used for a HA based hydrogel in which HA was functionalized with aldehyde and hydrazide (Koivusalo et al., 2018). The HA based hydrogel was supplemented with Col I, inducing elongated hASCs morphology and proliferation (Koivusalo et al., 2018). Later the hydrogel was modified with dopamine, making the hydrogel tissue adhesive as discussed in chapter 2.4.1. Another study has reported a bioink with aldehyde and 1-Ethyl-3-(3-dimethylaminopropyl)carbodiimide (EDC) functionalized HA (L. L. Wang et al., 2018). In addition, a gelatin based bioink composed of hydrazide functionalized gelatin and aldehyde functionalized carboxymethylcellulose (CMC) with potential for vascular bioprinting has been reported (Kageyama et al., 2016). Moreover, hydrazone crosslinking has been used in alginate and gellan gum based hydrogels (Karvinen et al., 2019).

2.8.2 Photocrosslinking

Photocrosslinking is a widely used form of chemical crosslinking and it is based on light intensity and exposure duration that induce bioink gelation (Cui et al., 2020; Samadian et al., 2020). The advantage of photocrosslinking is that it enables the spatiotemporal control of crosslinking reactions (Knowlton et al., 2017; Lim et al., 2020; Samadian et al., 2020). In addition, photocrosslinking can be performed for the whole structure after printing, for individual layers, continuously throughout printing or before printing (Knowlton et al., 2017; Lim et al., 2020). However, to induce bioink gelation the photoinitiators are excited by exposure to UV light, inducing cellular DNA damage and reducing cell viability (GhavamiNejad et al., 2020; Knowlton et al., 2017). Thus, the lowest possible light intensity should be used (Lim et al., 2020). The three forms of photocrosslinking that are used in bioprinting and discussed here are free-radical polymerization, thiol-ene and photomediated redox photocrosslinking (Figure 10).

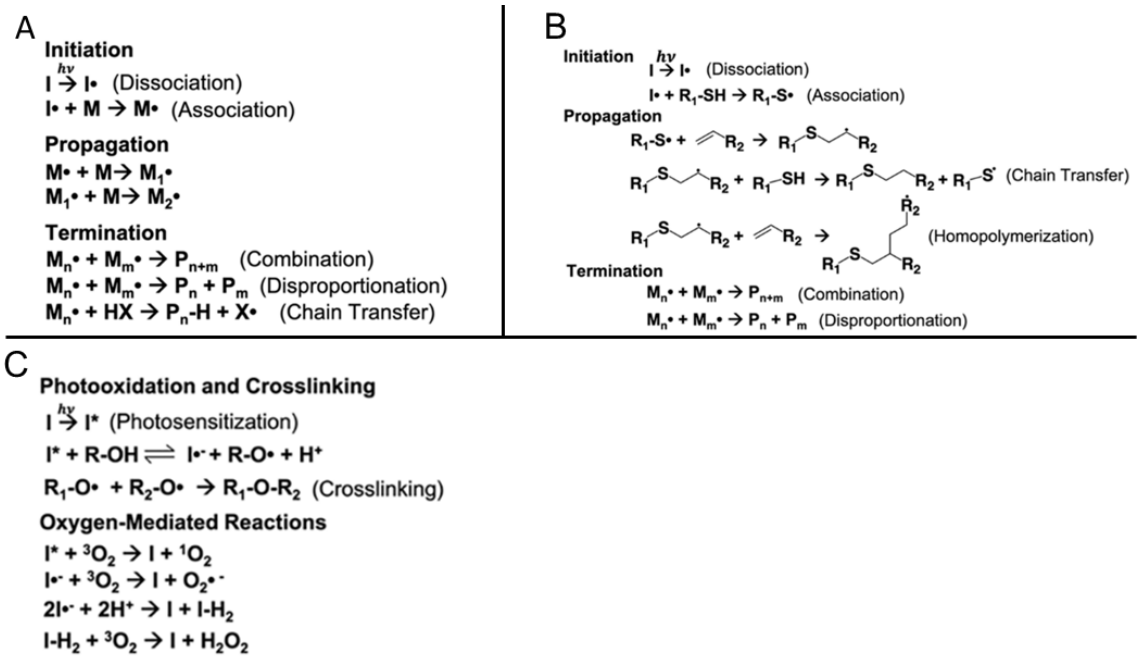

Figure 10: *The chemical mechanism of (A) free-radical polymerization, (B) thiol-ene and (C) photo-mediated redox photocrosslinking. Free-radical polymerization and thiol-ene photocrosslinking have three distinct phases that are initiation, propagation and termination. In photo-mediated redox a photoinitiator is excited with light, inducing the chemical reaction. Moreover, oxygen-mediated side reactions can occur which generate singlet oxygen species, superoxides and hydrogen peroxide. Modified from Lim et al., (2020).*

In initiation reactive radicals are generated from photoinitiators with light, that react with the functional groups of polymers such as methacrylate and acrylate, resulting in formation of covalent bonds (Lim et al., 2020). This forms a radical intermediate that reacts during propagation with functional groups of other polymers, leading to polymer chain growth. Propagation can be terminated in several ways which are combination, disproportionation and chain transfer (Lim et al., 2020).

The rate of radical formation, determining the speed and degree of free radical polymerization, depends on the used light intensity, photoinitiator efficiency and concentration (Lim et al., 2020). In addition, the reactivity of functional groups can be increased by adding groups that attract electrons (Lim et al., 2020). A challenge in free radical polymerization is oxygen inhibition that can occur in chain transfer due to the formation of peroxyl radicals (Lim et al., 2020; Van Hoorick et al., 2019). This can decrease bioink crosslinking degree, lowering bioprinted structure shape fidelity and mechanical properties (Knowlton et al., 2017; Lim et al., 2020). Another disadvantage is that the formed radicals are cytotoxic, decreasing cell viability (Lim et al., 2020; Samadian et al., 2020).

The principle of thiol-ene crosslinking is similar to free radical polymerization and it is based on reactive thiyl radical intermediates, produced when sulfide groups of thiol-containing molecules react with reactive radicals (Lim et al., 2020). The thiyl intermediates

react with carbon double bonds (‘ene’), forming thioether bonds (Lim et al., 2020; Van Hoorick et al., 2019). Growth of the polymer chain occurs via a combination of polymers or macromers, named step growth mechanism (Lim et al., 2020). The reaction is terminated either by combination or disproportionation, like in free radical polymerization (Lim et al., 2020; Van Hoorick et al., 2019). A thiol-ene crosslinkable bioink can be formulated by incorporating ‘ene’ containing groups such as norbornene or vinyl esters to a biomaterial and inducing crosslinking with a thiolated crosslinkers (e.g dithioretinol (DTT)) (Van Hoorick et al., 2019). Another way is to functionalize the biomaterial with thiols and performing crosslinking with a ‘ene’ crosslinker (e.g. poly(ethylene glycol)-diacrylate (PEGDA) (Van Hoorick et al., 2019).

Compared to free radical polymerization, the polymers crosslinking degree and mechanical properties can be modified more precisely with thiol-ene reactions (Lim et al., 2020). Furthermore, the required radical concentrations for crosslinking to occur are lower as thiol-ene reactions are not inhibited by oxygen (Lim et al., 2020; Van Hoorick et al., 2019). Another advantage is the possibility to control the unreacted ‘ene’ and thiol amounts after crosslinking which allows the incorporation of signaling ligands via post crosslinking, increasing the biological activity of the hydrogel (Lim et al., 2020; Van Hoorick et al., 2019). However, a limitation of thiol-ene photocrosslinking is the chance of disulfide formation during crosslinking, decreasing hydrogel stability (Van Hoorick et al., 2019).

Photomediated redox is the third option that has been used to photocrosslink polymers containing phenol groups (Lim et al., 2020). It relies on photosensitizers such as eosin-Y and flavin that are light absorbing dyes or additives which are excited upon light exposure. These oxidize the reactive groups of polymers that react with each other, leading to crosslink formation. The reaction is terminated when all reactive groups are depleted or when the photosensitizers return to their ground state. In addition, the products formed during the oxygen-mediated side reactions regenerate ground state photoinitiators, increasing the rate of crosslinking (Lim et al., 2020).

Widely used photoinitiators in bioinks are 2-hydroxy-l-[4-(hydroxyethoxy)phenyl]-2-methyl-1-propanone (Irgacure 2959) and lithium phenyl-2,4,6-trimethylbenzoylphosphinate (LAP). (Samadian et al., 2020; Van Hoorick et al., 2019). Irgacure 2959 absorbs light between 200–370 nm UV-range and usually a wavelength of 365 nm is used as lower light wavelength induces DNA mutations (Lim et al., 2020; Van Hoorick et al., 2019). Advantages of Irgacure 2959 are its water solubility and biocompatibility at low concentrations. However, a limitation of Irgacure 2959 is the poor light absorption at 365 nm, thus long exposure time and light intensity are required to induce bioink crosslinking (Lim

et al., 2020; Van Hoorick et al., 2019). Alternatively, LAP can be used that is more hydrophilic and has greater light absorption at 365 nm, superior biocompatibility (Samadian et al., 2020; Van Hoorick et al., 2019).

2.8.3 Physical crosslinking

In physical crosslinking methods bioink gelation occurs due to weak bond formation and compared to chemical crosslinking methods the bioinks are more biocompatible (GhavamiNejad et al., 2020). In addition the crosslinking process is reversible and can be controlled with varying pH and temperature (Cui et al., 2020; GhavamiNejad et al., 2020). However, the mechanical strength of physically crosslinked bioinks is low, which can be compensated by incorporation of nanofillers or chemical functionalities that enhance the stability of bioprinted structures (GhavamiNejad et al., 2020). Multiple physical crosslinking methods have been used in bioprinting and next ionic and electrostatic interactions are discussed.

The crosslinking of bioinks via ionic interactions can be achieved when biomaterials and multivalent metal ions with opposite charges are combined (GhavamiNejad et al., 2020; Hospodiuk et al., 2017). The opposite charges attract each other, leading to rapid bioink gelation at mild and physiological conditions (GhavamiNejad et al., 2020; Hospodiuk et al., 2017). The limitations of this method include low mechanical properties and potential release of the metal ions from the printed structure (GhavamiNejad et al., 2020). $CaCl_2$ is the most popular ionic crosslinker, since it is easily dissolved and allows rapid crosslinking (GhavamiNejad et al., 2020; Mueller et al., 2022). However, this may lead to poor structure stability as the crosslinking occurs faster on the surface than inside of the structure, therefore addition of $CaCl_2$ should be controlled (GhavamiNejad et al., 2020; Mueller et al., 2022). Moreover, studies have indicated that high concentrations of Ca^{2+} damages cells (GhavamiNejad et al., 2020). Alginate is a common choice of biomaterials crosslinked with $CaCl_2$ as it contains carboxylic groups that react with Ca^{2+} ions (Figure 11) (Cui et al., 2020; Qiqi Gao et al., 2021).

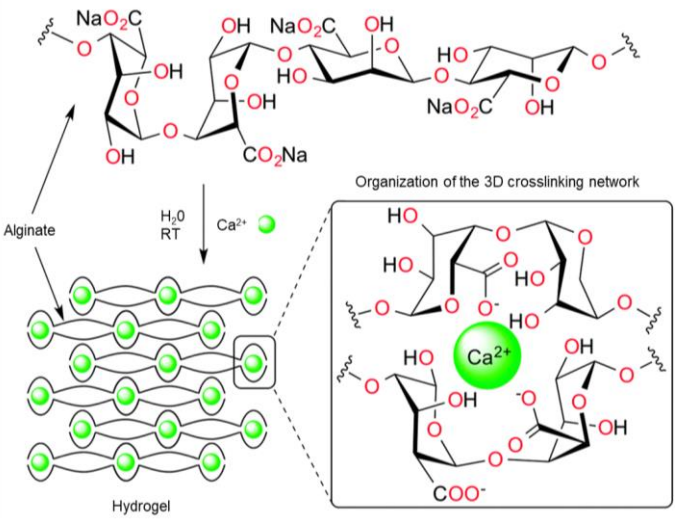

Figure 11: *Chemical structure of alginate and illustration of its ionic crosslinking by solution containing Ca^{2+} ions at RT. Modified from Kühbek et al., (2015).*

Electrostatic interactions have a similar principle to ionic interactions, but the weak bonds form between ionic groups of the polymers without the need for metal ions (GhavamiNejad et al., 2020). Biomaterials can be classified based on their charges, negatively charged (e.g. alginate), positively charged (e.g. gelatin) and neutral (e.g. dextran). When biomaterials from different categories are combined, the bioink gelation is induced by electrostatic interactions. Majority of electrostatically crosslinkable bioinks have shear-thinning property, resulting in excellent cell viability post-printing. However, the internal crosslinking can be low, because the electrostatic interactions are stronger at the interface of oppositely charged biomaterials (GhavamiNejad et al., 2020).

2.9 State of the art 3D bioprinting of cornea

The shortage of donor corneas limits the number of corneal transplantation surgeries that can be performed and the alternative solution, KPros possess risk of complications (Gain et al., 2016; Holland et al., 2021; Matthyssen et al., 2018; B. Zhang, Xue, Li, et al., 2019). Conventional TE has been used to create biosynthetic corneas, however formation of layered structures is time consuming and control over structural architecture is limited with these methods (Ruiz-alonso et al., 2021; B. Zhang, Xue, Li, et al., 2019). With 3D bioprinting it is possible to precisely control printed structure architecture, thus structural elements of cornea such as shape, thickness, curvature and mechanical properties can be mimicked in the corneal equivalents (Ruiz-alonso et al., 2021; B. Zhang, Xue, Li, et al., 2019). In addition, 3D bioprinting offers excellent repeatability and different biomaterial and cell types can be incorporated into the printed structures, increasing the resemblance to native tissues (Ruiz-alonso et al., 2021; Vijayavenkataraman et al., 2018;

B. Zhang, Xue, Li, et al., 2019). Due to the shortage of donor corneas, there is a need for corneal equivalents that could answer the unmet clinical need (Ruiz-alonso et al., 2021; Sommer & Blumenthal, 2019).

In the field of ophthalmology 3D bioprinting has gained interest as the eye is easily accessible, immunologically privileged and avascular, which makes the implementation of the technology easier compared to other tissues (Ruiz-alonso et al., 2021; Sommer & Blumenthal, 2019). The performed studies on corneal 3D bioprinting to date are presented in table 4. Furthermore, 3D bioprinting has been studied for retina and conjunctiva, but these studies are not discussed (Ruiz-alonso et al., 2021).

Table 4: *Summary of research articles on 3D bioprinting of cornea. Cornea-derived extracellular matrix (Co-dECM), human corneal epithelial cells (HCECs), human corneal stromal cells (hCSCs).*

Printed tissue	3D bioprinting method	Bioink biomaterials	Cell type	Cell density (cell/ml)	Reference
Stroma	EBB	Alginate with methacrylated Col I	hCKS	2×10^6	Isaacson et al., 2018
Stroma	LIFT	Human Col I with plasma and thrombin	hASCs	30×10^6	Sorkio et al., 2018
Epithelium		Laminin-521 with HA	hESC-LESCs		
Cornea	EBB	Co-dECM	hTMSCs	1×10^6	H. Kim et al., 2019
Stroma	DOD	Bovine Col I with agarose	hCKs	1×10^6	Duarte Campos et al., 2019
Cornea	Extrusion-DLP	Alginate with GelMA	HCECs	2×10^6	B. Zhang, Xue, Hu, et al., 2019
Stroma	EBB	GelMA	hCKs	1×10^6	Kilic Bektas & Hasirci, 2020
Stroma	EBB	Alginate with gelatin and bovine Col I	hCKs	3×10^6	Kutlehria et al., 2020
Stroma	SLA	GelMA	hCSCs	8×10^6	Mahdavi, Abdekhodaie, Kumar, et al., 2020
Epithelium	EBB	Alginate with gelatin and rat Col I	hCEpCs	1×10^6	Wu et al., 2016

The most used 3D bioprinting technology for the bioprinted corneal structures is extrusion, which has been reported for stroma (Isaacson et al., 2018; Kilic Bektas & Hasirci, 2020; Kutlehria et al., 2020), epithelium (Wu et al., 2016) and cornea equivalent (H. Kim et al., 2019). LIFT has been used for stroma and epithelium (Sorkio et al., 2018). Other technologies that have been used for stroma are DOD (Duarte Campos et al., 2019) and SLA (Mahdavi, Abdekhodaie, Kumar, et al., 2020). In addition, a corneal equivalent has been printed with an integrated Extrusion-DLP 3D bioprinter (B. Zhang, Xue, Hu, et al., 2019).

The biomaterial components of the used bioinks have been sodium alginate (Isaacson et al., 2018; Wu et al., 2016; B. Zhang, Xue, Hu, et al., 2019), Col I (Duarte Campos et al., 2019; Isaacson et al., 2018; Kutlehria et al., 2020; Sorkio et al., 2018; Wu et al., 2016), gelatin (Kutlehria et al., 2020; Wu et al., 2016; B. Zhang, Xue, Hu, et al., 2019), agarose (Duarte Campos et al., 2019), GelMA (Kilic Bektas & Hasirci, 2020; Mahdavi, Abdekhodaie, Kumar, et al., 2020; B. Zhang, Xue, Hu, et al., 2019), Laminin 521 (Sorkio et al., 2018) and ECM of cornea (H. Kim et al., 2019). In these bioinks, the most used cell type has been hCKs (Duarte Campos et al., 2019; Isaacson et al., 2018; Kilic Bektas & Hasirci, 2020; Kutlehria et al., 2020). Other cell types that have been used are hASCs (Sorkio et al., 2018), hESC-LESCs (Sorkio et al., 2018), hTMSCs (H. Kim et al., 2019), HCECs (B. Zhang, Xue, Hu, et al., 2019), hCSCs (Mahdavi, Abdekhodaie, Kumar, et al., 2020) and hCEpCs (Wu et al., 2016). As seen in table 4, the cell densities used have been between 1–8 million per ml, except in the study performed by Sorkio et al., (2018) where a cell density of 30 million per ml was used as LIFT can be used with very high cell densities (Vijayavenkataraman et al., 2018).

To the best of my knowledge, the study performed by Kim et al. is the only one that has incorporated cornea ECM into a bioink. The developed cornea-derived extracellular matrix (Co-dECM) bioink showed similar transparency and biochemical composition to native cornea (H. Kim et al., 2019). In addition, excellent biocompatibility and improved maintenance of CKs phenotype were observed when Co-dECM bioink was injected into mice and rabbits. The study demonstrated that addition of cornea ECM results into a bioink with cornea-specific properties that is suitable for corneal 3D bioprinting (H. Kim et al., 2019). The curvature of cornea is difficult to replicate and maintain, thus some studies have used a support structure to improve the curvature of the bioprinted structures (Isaacson et al., 2018; Kutlehria et al., 2020; B. Zhang, Xue, Hu, et al., 2019). While all studies listed in table 4 have reported excellent cell viability post-printing, another challenge has been the rounded morphology of cells in the bioprinted corneal structures, which may decrease cellular interactions and migration (Duarte Campos et al., 2019;

Isaacson et al., 2018; Kilic Bektas & Hasirci, 2020; Kutlehria et al., 2020; Sorkio et al., 2018). However, some studies have reported retention of cell morphology during the culture of bioprinted structures (Duarte Campos et al., 2019; Mahdavi, Abdekhodaie, Kumar, et al., 2020; Sorkio et al., 2018). Although promising results have been obtained from the performed studies, most of them have focused only on a single corneal layer with a single cell type and currently there is only one study that has combined multiple corneal layers and cell types (Sorkio et al., 2018).

3. AIM OF THE STUDY

The aim of this study was to develop and characterize a cornea-specific bioink by hASC-CKs differentiation, which were used to produce Co-CDM. The Co-CDM was processed and decellularized before incorporation into the bioink. Majority of current treatments for damaged corneas depend on donor corneas that are scarce, meaning that not all patients can be treated. Although a bioink derived from decellularized human corneas have been characterized, it is not ideal as it requires donor corneas. Therefore, the cornea-specific component of the bioink was chosen to be hASC-CKs produced Co-CDM. The first objective of this study was to determine suitable bioink formulations and optimal printing parameters. This was followed by characterization of bioink, bioprinted structures and hASCs bioprinted with Co-dCDM. The properties of Co-dCDM bioink were compared against the properties of Col I bioink. The characterized Co-dCDM bioink in this study provides an alternative approach to cornea-specific bioinks that is suitable for corneal 3D bioprinting. The hypothesis for the study is that incorporation of Co-dCDM enhances bioink printability, shape fidelity and biocompatibility.

4. MATERIALS AND METHODS

This chapter describes the used materials and methods in the thesis experimental part. Figure 13 illustrates the workflow of the conducted study. The thesis began by hASC-CKs differentiation in order to produce the Co-CDM, which was incorporated into the Co-dCDM bioink. Before incorporation the Co-CDM was decellularized, freeze-dried and solubilized. Then the bioink composition and printing parameters were optimized for satisfactory printability. After discovering the suitable bioink compositions and printing parameters, the bioink was characterized. The final step in this thesis was to print Co-dCDM bioink with hASCs in order to study bioink biocompatibility by assessing cell viability and proliferation.

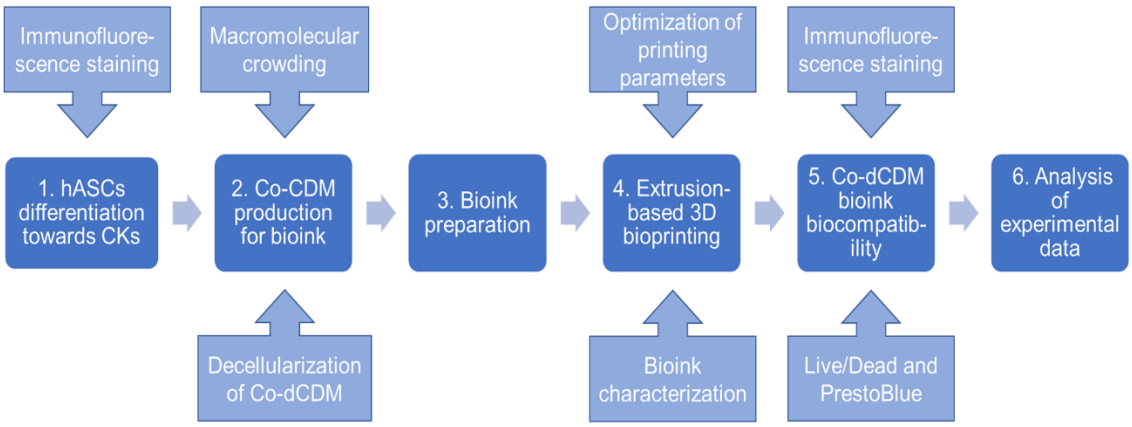

Figure 13: *The workflow of the thesis experimental part. 1: hASCs were differentiated towards CKs and immunofluorescence staining was performed to study differentiation. 2: Co-CDM for the bioink was produced. 3: The bioinks were prepared for extrusion-based 3D bioprinting. 4: For bioprinting the printing parameters were optimized and bioink characterization was performed. 5: Biocompatibility of Co-dCDM was studied by immunofluorescence staining, Live/Dead and PrestoBlue. 6: Finally, the experimental data was statistically analyzed.*

4.1 hASC ethical statement

The hASCs 4/18 were used in accordance with the Tampere University Hospital Ethics Committee, Tampere, Finland (R15161). The hASCs were isolated from an adipose tissue sample obtained from surgical procedure conducted in the Department of Plastic Surgery, Tampere University Hospital. The donor gave a written informed consent for the utilization of the adipose tissue sample in research settings.

4.1.1 hASCs differentiation towards keratocytes for Co-CDM

A frozen-stock of hASCs were thawed and the cell suspension was mixed with 2 ml of prewarmed hASC medium containing DMEM/F-12 (Gibco, USA), 5% Human Serum (Human Serum AB male Hiv tested, Biowest, France), 1% Glutamax (Gibco, USA) and 1% Penicillin-Streptomycin (Gibco, USA). The cells were centrifuged at 1200 rpm for 5 minutes and the supernatant was removed. Next, the cells were mixed with 3 ml of hASC medium. Then the cells were plated to T75 culture flasks (Nunc EasYFlask Cell Culture Flask, Thermo Fisher, USA) with 9 ml of hASC medium and stored in an incubator at 37 °C 5% CO_2. The cells were cultured for 7 days to expand the cell amount. The cell culture medium was changed three times per week.

After 7 days of expansion the hASCs were briefly washed with PBS (Phosphate-buffered saline, Lonza, Switzerland) and detached with 3 ml of TrypLE Select (Gibco, USA). After 8 minutes of incubation 5 ml of prewarmed hASC medium was added to the flasks. The cell suspension was thoroughly mixed to ensure maximum cell detachment and the suspension was collected. The cells were centrifuged as described above and resuspended in hASC medium. Next, the cells were counted with Bürker chamber, and the volume of needed cell suspension was calculated.

Next, the hASCs were plated in order to begin Co-CDM production. To induce hASCs differentiation towards hASC-CKs, the cells were cultured in KDM. The production of Co-CDM and the detailed composition of the KDM is described in the confidential supplement 2

4.1.2 Co-CDM Decellularization

After two weeks of cell culture of hASC-CKs in KDM the Co-CDM was collected and decellularized. The cells were briefly washed with PBS. Then 2.5 ml of TrypLE was added and the culture dishes were incubated for 8 minutes. Thereafter, 3 ml of KDM was added to stop the effects of TrypLE. The culture dishes were carefully rinsed with the cell suspension to detach the remaining cells. Next, the cell suspension was removed with care in order to avoid the removal of ECM. Then 4 ml of PBS was added, and the Co-CDM was detached with a cell scraper and collected.

The collected Co-CDM was decellularized to get rid of any residual DNA, because that is known to decrease the ECM's biocompatibility. In all steps the centrifuging was done at 3000 rpm for 5 minutes. The samples were washed twice with PBS and centrifuged. After, the washes 4 ml of sodium deoxycholate (SD) (Sigma, USA), dissolved in Milli-Q water at a concentration of 10 mg/ml, was added. The samples were incubated at RT for

10 minutes, after which they were centrifuged. Then, the ECM samples were washed three times with PBS with 5 minutes incubation and centrifuged. Next, DNase 1 was added in Milli-Q water at a concentration of 400 U/µl for 30 minutes in RT to fragment residual DNA. Two DNase 1 reagents were used in this thesis that were DNase 1 (RNase-free, 1 U/µL, Thermo Fisher, USA) and DNase 1 (Roche, Switzerland). To remove the DNase 1 the samples were washed with PBS and centrifuged. Lastly, the samples were washed with PBS with 15 minutes incubation and centrifuged. This was repeated four times after which the decellularized Co-CDM was resuspended to 1 ml of PBS and transferred to pre-weighted tubes. The decellularized Co-CDM is referred to as cornea-specific decellularized cell-derived matrix (Co-dCDM) throughout the thesis when discussing the bioink containing Co-CDM. Co-CDM is used when discussing the production, characterization and decellularization.

In addition, the efficacy of the used decellularization protocol was examined by performing DNA extraction with QIAamp DNA Mini Kit (Qiagen, Germany) for the collected Co-CDM. To determine if the decellularization protocol decreases DNA concentrations, the collected Co-CDM was handled with three different methods. In the first method, the Co-CDM was collected after cells were dissociated and in the second method, the Co-CDM was decellularized without addition of DNase 1. In the third method, the Co-CDM was decellularized as described previously. For all individual handling methods, there were three biological replicates. The DNA extraction for Co-dCDM was performed according to the manufacturer's instructions. To summarize, PBS was removed and Buffer ATL was added. Then, proteinase K was added, and the samples were incubated at 56 °C until the samples were completely solubilized. Next, Buffer AL was added, and the samples were incubated at 70 °C for 10 minutes. Subsequently, 100% ethanol was added to the samples. Then, the samples were moved to QIAamp Mini spin columns and centrifuged at 8000 rpm for 1 minute. After this, Buffer AW1 was added, followed by centrifuging as previously. This was followed by Buffer AW2 addition and centrifuging at 14 000 rpm for 3 minutes. Next, Buffer AE was added, and the samples were incubated at RT for 1 minute. Finally, the DNA was collected by centrifuging the samples at 8000 rpm for 1 minute and the DNA concentrations were measured immediately with Nanodrop (NanoDrop 2000 Spectrophotometer, Thermo Fisher, USA).

4.1.3 Co-dCDM freeze-drying and dissolving

To incorporate the Co-dCDM into the bioink it was freeze-dried and dissolved. The samples were immersed into liquid nitrogen for 2 minutes after decellularization. Then the

samples were freeze-dried for 24 hours in a freeze dryer (ScanVac MaxiVac with 4L CoolSafe -110 °C condenser, LaboGene, Denmark). Thereafter, the samples were weighed to determine the Co-dCDM yield. The Co-dCDM was dissolved in 0.1 M HCl into the desired concentration. In addition, sterile-filtered pepsin (Roche, Switzerland) 10 mg/ml stock-solution was prepared into 0.01 M HCl and added so that the pepsin concentration in the samples was 0.5 mg/ml. The Co-dCDM was incubated at RT on a shaker for 48 hours, after which the Co-dCDM was aliquoted and ready to be used in bioink preparation.

4.2 Characterization of Co-CDM

hASCs used for immunofluorescence stainings were dissociated similarly as stated above and plated at a density of 7000 cells/cm^2 to 24-well plate (CellBind 24-well Clear Multiple Well Plates, Corning, USA). The medium used was KDM as the immunofluorescence was used to study the differentiation protocols efficacy and the presence of cornea-specific ECM proteins. The hASCs were cultured for 14 days, after which the immunofluorescence stainings were performed as described in chapter 4.7.3.

4.3 Macromolecular crowding

In addition, hASC-CKs were differentiated under MMC conditions to determine if MMC increases ECM protein deposition as reported for human corneal fibroblasts (hCF) in the literature by Gürdal et al. The hASCs were dissociated as previously and plated similarly as in chapter 4.2. The experimental set-up for MMC was to use three modified KDM mediums, one without growth factor 4 and one supplemented with growth factor 4. The third medium contained carrageenan (Sigma, USA) with growth factor 4, because Gürdal et al. reported increased ECM deposition with the addition of carrageenan. The well plates were fixed on days 14 and 21. The same protocol for the fixing and staining was used to study the hASC-CKs differentiation and effects of MMC. The protocol is described in chapter 4.7.3.

4.4 Bioink preparation

The studied bioinks in this thesis were Col I and Co-dCDM bioinks. Used bioink components and the exact compositions of the studied bioinks in this thesis are confidential, thus they are discussed in the confidential supplement 1. For this reason, only a general protocol for bioink preparation is described here. The detailed component preparations and their specific volumes and dissolutions can be found in the supplement 1.

All bioink preparation steps were performed under the laminar hood without lights due to the light sensitivity of some bioink components. First, two 2.5 ml syringes with a luer lock tip were equipped with a needle. Then the bioink components were carefully pulled into the syringes. Next the syringes were connected with a female-female luer lock connector and the components were thoroughly mixed by pushing the pistons multiple times. After bioink mixing, the bioink was transferred into a printing barrel with a tip cap to prevent bioink outflow. Also, a piston was inserted in the middle of the barrel. Finally, the tip cap was changed into a printing needle and an air lock adapter was attached to the barrel. The barrel containing the bioink was placed to the low-temperature tool head of the printer to start the bioprinting process. All materials used to prepare and print the bioink are listed in table 5.

Table 5: *Summary of materials used in bioink preparation and 3D bioprinting*

Bioink preparation and 3D bioprinting materials	**Manufacturer**
2.5 ml syringe with Luer Lock Tip	Terumo, Japan
20G, 1 ½, KD-FINE	KD Medical GmbH Hospital Products, Germany
Female-Female Luer Lock Connector	Health Care Logistics, USA
Optimum Syringe Barrel, clear, 30cc	Nordson, USA
Optimum Tip Cap, blue	Nordson, USA
Optimum Piston, white	Nordson, USA
Standard Blunt Needle 32 G	CELLINK, Sweden
Optimum Adapter	Nordson, USA

4.5 3D Bioprinting

In the following chapters the 3D bioprinting workflow of this thesis is described. First, the used 3D bioprinter and the printed structures are described. In addition, the set-up of the printer is discussed. Second, the printing process itself is described, which printing parameters were used and how the printed structures were handled post-printing.

4.5.1 3D Extrusion-based Bioprinter

In this study all printing steps were performed with the extrusion-based 3D-Bioplotter Manufacturer Series (EnvisionTEC GmbH, Germany) (Figure 14). The bioprinter was

equipped with a temperature controllable printing platform, built-in camera and a dispensing head, with temperature range from 0 – 70°C. In addition, the system had a UV Curing head, but this was not used during printing. The 3D structures used in printing were designed as a STL file with the Perfactory RP software. Subsequently the desired dimensions were set to the structure and the model was sliced into a layer thickness that was 80% from the used needle size. Next, the STL file was converted and saved as a Borland Package Library (BPL) file. The BPL file was opened in Visual Machines, which is the software used to control the bioprinter. The desired 3D structure was selected in the project editor tab, the corresponding bioink was selected in the material editor tab and the printing parameters were set in the programming tab of the software. The used bioink was also assigned to the dispensing head in the project editor tab and the head temperature was set to 20°C.

After the printing process was set up with the software, the printing platform was cleaned with 70% ethanol. Finally, the needle was calibrated with the Visual Machine's calibrate command. The calibration was done according to the manufacturer's instructions.

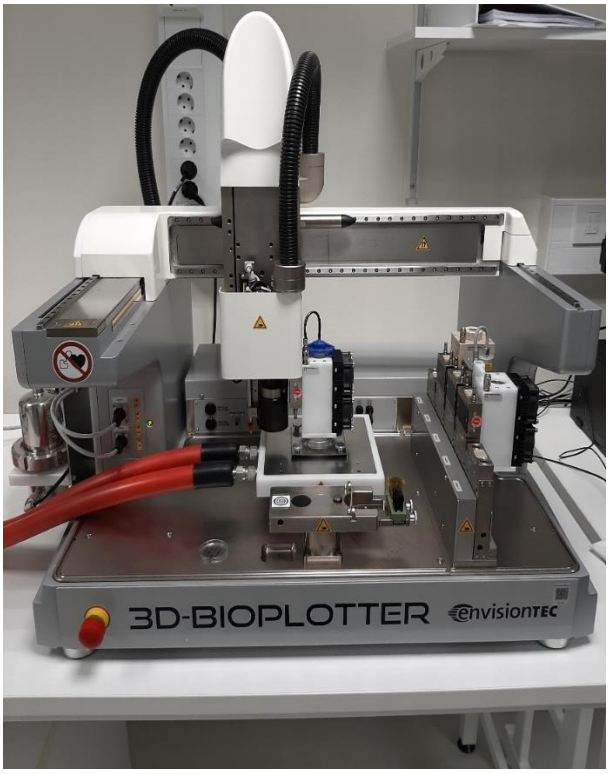

Figure 14: *3D-Bioplotter Manufacturer Series (EnvisionTEC GmbH, Germany) 3D bioprinter used in this study.*

4.5.2 Bioink printing

All samples were printed onto 35 mm dishes (Falcon TC-treated Easy Grip Style Cell Culture Dish, Corning, USA) which were placed onto the printing platform. The printing started by selecting the desired printing project as previously described. The printed structures in this work to study the bioink printability were 6-layered lattices and 8-layered 3D cylinder models. The distance between adjacent filaments was set to 0.25 in printing. Also, various other shapes were printed with Co-dCDM bioink to demonstrate its versatility. The printing parameters for lattices were 1.3 bar pressure and 6 mm/s speed and for 3D cylinder models 1.4 bar and 6 mm/s. Both studied bioinks were printed with the same parameters to improve the comparability of results. Additionally, the optimal parameters for improved printability of Co-dCDM bioink were determined.

Col I and Co-dCDM bioinks were printed without cells to compare differences in printability, shape fidelity and stability, as described later in chapter 4.6. After sample printing, they were allowed to stabilize at 37 °C 5% CO_2 by pipetting PBS or hASC medium to the dish edges for preventing the samples from drying. Lattices were stabilized for 30 minutes and 3D cylinder models for 1 hour, after which the structures were immersed in 1-2 ml of PBS or hASC medium. The samples were stored at 37 °C 5% CO_2.

For the Co-dCDM bioink biocompatibility assessment, the bioink was printed with hASC to determine cell viability and proliferation in the printed structures as described in chapter 4.7. The structures for the cellular printing were the lattices and 3D cylinder models. Printing parameters were 1.0–1.1 bar pressure and 7-6 mm/s speed for lattices and 1.2 bar and 5 mm/s for 3D models. After printing the samples were handled similarly as samples without cells. All samples were stored in hASC medium at 37 °C 5% CO_2.

4.6 Bioink characterization

The Col I and Co-dCDM bioinks were characterized by printing them with the same parameters and measuring their shape fidelity and swelling behavior. In addition, the transparency was analyzed by measuring the bioink transmittance. Finally, shear-thinning properties of the bioinks were investigated by rheometer.

4.6.1 Shape Fidelity

Shape fidelity of the bioinks containing Col I and Co-dCDM was studied to determine if the biomaterials shape fidelity characteristics are affected by the addition of Co-dCDM. For each timepoint and condition three biological replicate lattice structures were printed.

The samples were imaged immediately after printing and at 7- and 14-days post-printing with the build-in camera. The liquid was carefully removed before imaging at later timepoints. The images were analyzed with ImageJ Fiji (2.0.0-rc-69/1.52n; Java 1.8.0_172 [64 bit]) to measure the filament width and the distance between adjacent filaments. For each sample the filament width and distance between filaments was calculated from nine places as shown in figure 15. In addition, as illustrated in the figure 15, the pore factor (Pr) was calculated for the samples at day 0 from three places according to the equation 1:

$$\mathrm{Pr} = \frac{(pore\ perimeter)^2}{16\ x\ (pore\ area)} \quad (1)$$

The Pr value provides information about how well the pores in the printed structures match the designed square pores. Perfectly square pores are indicated by a Pr value of 1, whereas Pr < 1 and Pr > 1, indicate under- and overgelled pores, respectively (Soltan et al., 2019).

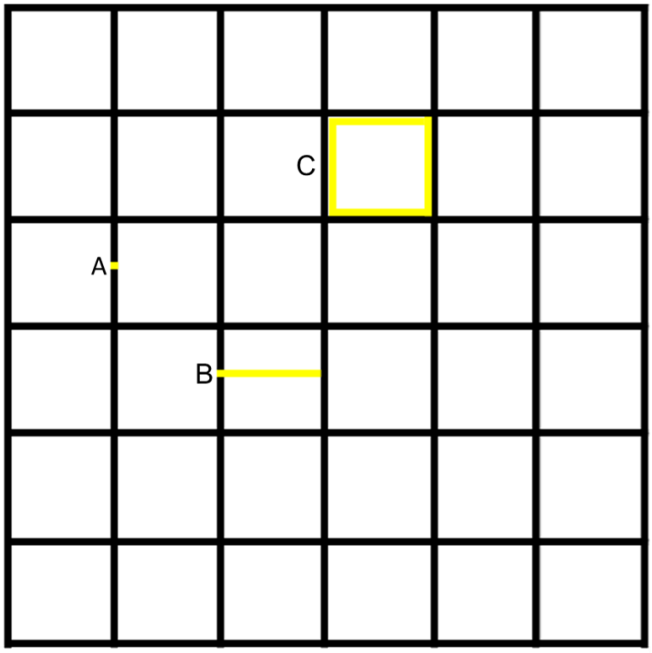

Figure 15: *Illustration how the (A) filament width, (B) distance between adjacent filaments and (C) pore factor (Pr) was calculated from the printed lattice structures.*

4.6.2 Swelling behavior

The swelling characteristics of the two bioinks was measured by weighing printed cylinderic structures at specific timepoints to investigate how different bioink composition affects bioink swelling and stability. Two biological replicate structures of both bioinks were prepared. The samples were printed onto pre-weighted culture dishes and the dishes

were weighed immediately after printing to determine the initial weight of the printed 3D structures. The samples were weighted at 30 minutes, 6 hours, 24 hours and 7 days post-printing. Before weighting the hASC medium was carefully removed and after weighting the samples were immersed to hASC medium and put back to the incubator at 37 °C 5% CO_2. To determine the swelling behavior of the bioinks in various the swelling ratio (SR) was calculated according to the equation 2:

$$SR = \frac{W_{swollen} - W_{initial}}{W_{initial}} * 100\% \quad (2)$$

In the equation $W_{initial}$ is the weight of the structures right after printing and $W_{swollen}$ is the weight of the structures after incubation in hASC medium.

4.6.3 Transparency

The transparency of Col I and Co-dCDM bioinks were determined to assess if the addition of Co-dCDM affects the biomaterials transparency. The transparency of the bioinks were determined by measuring transmittance of the bioinks with Lamda 35 UV/VIS spectrophotometer (PelkinElmer, USA). For the measurement 2 ml of the two bioinks were prepared into semi-micro cuvettes (polystyrene semi-micro cuvette, Sarstedt, Germany). After bioink preparation the cuvettes were placed into a 50 ml falcon tube and centrifuged at 1000 rpm for 1 minute to remove air bubbles. The cuvettes were stored under a wet tissue before measurements to prevent the bioinks from drying. Transmittance was measured 1 and 2 hours after bioink preparation. The wavelengths used ranged from 300 to 900 nm and as a blank an empty cuvette was used.

4.6.4 Viscosity

Discovery HR-2 hybrid rheometer (TA Instruments, USA) was used to determine the shear-thinning properties by measuring viscosities of Col I and Co-dCDM bioinks. The geometry used for the measurements was a 20 mm parallel plate with a gap of 1 mm which was manually set for every sample to prevent over- and underfill. In the TRIOS software from the calibrate tab the inertia, friction and rotational mapping were calibrated. The measurement temperature was set to 20 °C. The bioinks were prepared as previously described and from each bioink three 350 µl technical replicates were pipetted onto a 20 mm x 20 mm cover glass. The samples were let to crosslink for 30 minutes before starting the viscosity measurements.

The measurements were performed with continuous flow sweep for all samples. The shear rate range for flow sweep measurements was from 0.01 1/s to 100 1/s to determine

the bioink viscosity under different shear rates. From the acquired viscosity data, the average and standard deviation for the parallel replicates was calculated. The average values for bioink viscosity were plotted.

4.7 Bioink biocompatibility assessment

The biocompatibility of Co-dCDM was studied by printing the bioink with hASCs. The undifferentiated hASCs were cultured similarly as described in chapter 4.1.1. For the Co-dCDM bioink containing hASCs, the needed cell suspension was centrifuged and resuspended in a specific volume of culture medium so that the cell concentration in the bioink was 1.1 million/ml. Live/Dead and PrestoBlue assays were used to determine cell viability and proliferation, respectively. In addition, immunofluorescence staining was performed to visualize cell proliferation. These analyses were done at 1-, 4- and 7-days post-printing.

4.7.1 Live/Dead

The viability of hASCs in the printed structures was determined by Live/Dead Viability/Cytotoxicity Kit (Invitrogen, USA). The samples were briefly washed with PBS before adding 1ml of the reagent solution containing 1.25 µl Calcein-AM (stains live cells green) and 1.25 µl ethidium homodimer-1 (stains dead cells red) diluted in 10 ml of PBS. The samples were incubated for 30 minutes at 37 °C 5% CO_2. Next, the samples were imaged with IX51 fluorescence microscope (Olympus Corporation, Japan). The images were analyzed with Corel Photo-Paint 2021 software (23.1.0.389).

4.7.2 PrestoBlue

Cell proliferation was measured by PrestoBlue Cell Viability Reagent (Invitrogen, USA). At day 1 and 4 timepoints, two biological replicates were used, whereas three biological replicates were used at day 7 timepoint. From all biological replicates, including blank, four technical replicates were prepared. A reagent solution was prepared by mixing 1 ml of PrestoBlue stock reagent with 9 ml of prewarmed hASC medium. Then 1 ml of the reagent solution was added to the samples, and they were incubated for 30 minutes at 37 °C 5% CO_2. An empty 35 mm culture dish with 1ml reagent solution was used as a blank to calculate the background of the PrestoBlue reagent. After incubation, 100 µl of the solution was pipetted from the samples to a 96-well plate (Nunc MicroWell 96-Well, Nunclon Delta-Treated, Flat-Bottom Microplate, Thermo Fisher, USA). The well plate was covered with aluminum foil to protect the samples from light. Fluorescence was

measured with Wallac 1420 VICTOR2 Multilabel Counter (PelkinElmer, USA). The average fluorescence from the four technical replicates was calculated and the average blank fluorescence was subtracted from the sample values to acquire the fluorescence without the background.

4.7.3 Immunofluorescence staining

Before immunofluorescence staining, the cells were imaged with phase contrast microscope (ZEISS, Axio Vert.A1, Germany). Differentiation of hASC-CKs used in Co-CDM production and MMC culture conditions was studied by staining the cells on a well plate with cornea-specific protein markers. After two weeks of culture in KDM the cells were washed twice with PBS and fixed with 4% paraformaldehyde (PFA, Sigma) for 12 minutes. Then the cells were washed three times with PBS before adding 0.1% Triton X-100 in PBS for 15 minutes. Next, the cells were blocked for 1 hour with 3% bovine serum albumin (BSA, Sigma) in PBS to avoid unspecific binding of the antibodies. This was followed with addition of primary antibodies in 0.5% BSA in PBS and with overnight incubation at +4 °C on a shaker. The following day the cells were washed three times with PBS with 5 minutes incubations. Then, the secondary antibodies in 0.5% BSA in PBS were added onto the cells and incubated for 1 hour after which the cells were washed with PBS as previously. The final step was mounting with Prolong Gold (Thermo Fisher, USA) and careful insertion of coverslip onto the samples. The lattices which were printed with hASCs were stained according to the same protocol, however the used markers were proliferation markers and mounting was done with Vectashield Antifade Mounting Medium (Vector Laboratories, USA). The used primary and secondary antibodies are listed in table 6 and 7, respectively. The stained cellular and lattice samples were stored at +4 °C before imaging with IX51 fluorescence microscope. The images were analyzed with Corel Photo-Paint 2021 software.

The 3D cylinder structures were stained with the same protocol with slight modifications. Fixing was done with 4% PFA for 1 hour. Next, the samples were washed with PBS as previously and then the samples were stored overnight at +4°C. Permeabilization and blocking were performed with 5% BSA in PBS with 0.1% Triton X-100 overnight at room temperature. Then, the 3D structure was cut in half and the primary antibody in 5% BSA in PBS was added and incubated for 3 days. This was followed with PBS washes for 2 days and the PBS was changed three times. Secondary antibody was added in 5% BSA in PBS and the samples were incubated at room temperature overnight. The antibodies used to stain the 3D structures are given in table 6 and 7. Thereafter, the samples were washed with PBS overnight at room temperature and the solution was changed three

times. Before mounting the samples were transferred to MatTEK 35mm glass bottom dishes (MatTEK corporation, USA). Mounting was done by adding 150 µl of Vectashield Antifade Mounting Medium and storing the samples overnight at +4°C. Thereafter, excess mounting medium was removed, and a 13 mm cover slip was placed onto the samples. The 3D cylinder structures were imaged with ZEISS LSM 800 confocal microscope (ZEISS, Germany) and the images were analyzed with ImageJ.

Table 6: *Summary of the primary antibodies used in immunofluorescence stainings of well plates and printed structures.*

Antibody	**Dilution**	**Manufacturer**	**Use**
Rabbit anti-Collagen V	1:100	Sigma	Visualization collagen V
Goat anti-Lumican	1:100	R&D systems	Visualization of lumican
Mouse anti-Collagen I	1:100	Abcam	Visualization of collagen I
Rabbit anti-ALDH3A1	1:200	Abcam	Visualization of ALDH34 I
Rabbit anti-Keratocan	1:50	Bioss	Visualization of keratocan
Mouse anti-Keratan Sulfate	1:50	Santa Cruz Biotechnology	Visualization of keratan sulfate
Rabbit anti-Ki-67	1:400	Sigma	Proliferation marker
Rabbit anti-Connexin 43	1:100	Abcam	Visualization of gap junctions

Table 7: *Summary of secondary antibodies, other stainings and mounting mediums used in immunofluorescence stainings of well plates and printed structures.*

Type		Dilution	Manufacturer	Use
Secondary antibodies	Donkey anti-Rabbit lgG, Alexa Fluor 568	1:400	Invitrogen	Binds to primary antibodies from rabbit
	Donkey anti-Goat lgG, Alexa Fluor 488	1:400	Invitrogen	Binds to primary antibodies from goat
	Donkey anti-Mouse lgG, Alexa Fluor 488	1:400	Invitrogen	Binds to primary antibodies from mouse
Other	Hoechst 33342	1:1000	Invitrogen	Nuclei stain
	Phalloidin	1:150	Sigma	Cellular actin cyto-skeleton stain
	ProLong Gold Anti-fade Mountant		Invitrogen	Mounting medium
	Vectashield Antifade Mounting Medium		Vector Laboratories	Mounting medium

4.8 Statistical analyses

The statistical significance for decellularization, printability and PrestoBlue was determined with Mann Whitney U test. For statistical significance the p-value < 0.05 was chosen. All analyses were performed with IBM SPSS Statistics 27.0 software.

5. RESULTS

The first step in this study was to study the presence of specific corneal markers in the produced Co-CDM, followed by its decellularization and solubilization. In addition, the effects of MMC on the deposition of ECM proteins in the Co-CDM was assessed. The solubilized Co-dCDM was incorporated into a bioink and its printability and desired bioink characteristics, such as shape fidelity, swelling behavior, transparency and viscosity, were compared against those of Col I bioink. After these analyses the final step in this study was to investigate biocompatibility Co-dCDM by printing it with hASCs and analyze cell viability, proliferation and maturation in the printed structures. The bioink composition used in this study is presented in classified supplement 1 and the different structures printed with Co-dCDM bioink demonstrating its versatility are presented in appendix 1.

5.1 Characterization of produced Co-CDM

The hASC-CKs cultured on well plate in KDM were stained at day 14 with specific corneal markers to study differentiation towards CKs lineage. In addition, the presence of cornea-specific ECM proteins in the produced Co-CDM was studied (Figure 16). The CKs specific markers Lumican (Figure 16 A) and ALDH3A1 (Figure 16 B) and Keratocan (Figure 16 C) were expressed in the samples. Lumican and ALDH3A1 can be seen outside the cells with a fibrous appearance. Keratocan is expressed inside the cells and is seen more as a dot like shape. In addition, native cornea ECM proteins Col I (Figure 16 A) and Col V (Figure 16 B) were expressed and can be seen outside the cells with fibrous appearance. Keratan sulfate, a glycosaminoglycan in the *in vivo* cornea, was not expressed (Figure 16 C). Negative image for primary antibodies derived from mouse and rabbit (Figure 16 D) demonstrated absence of unspecific binding of secondary antibodies, although cells were present in the sample as seen with nuclein stain DAPI (Figure 16 E).

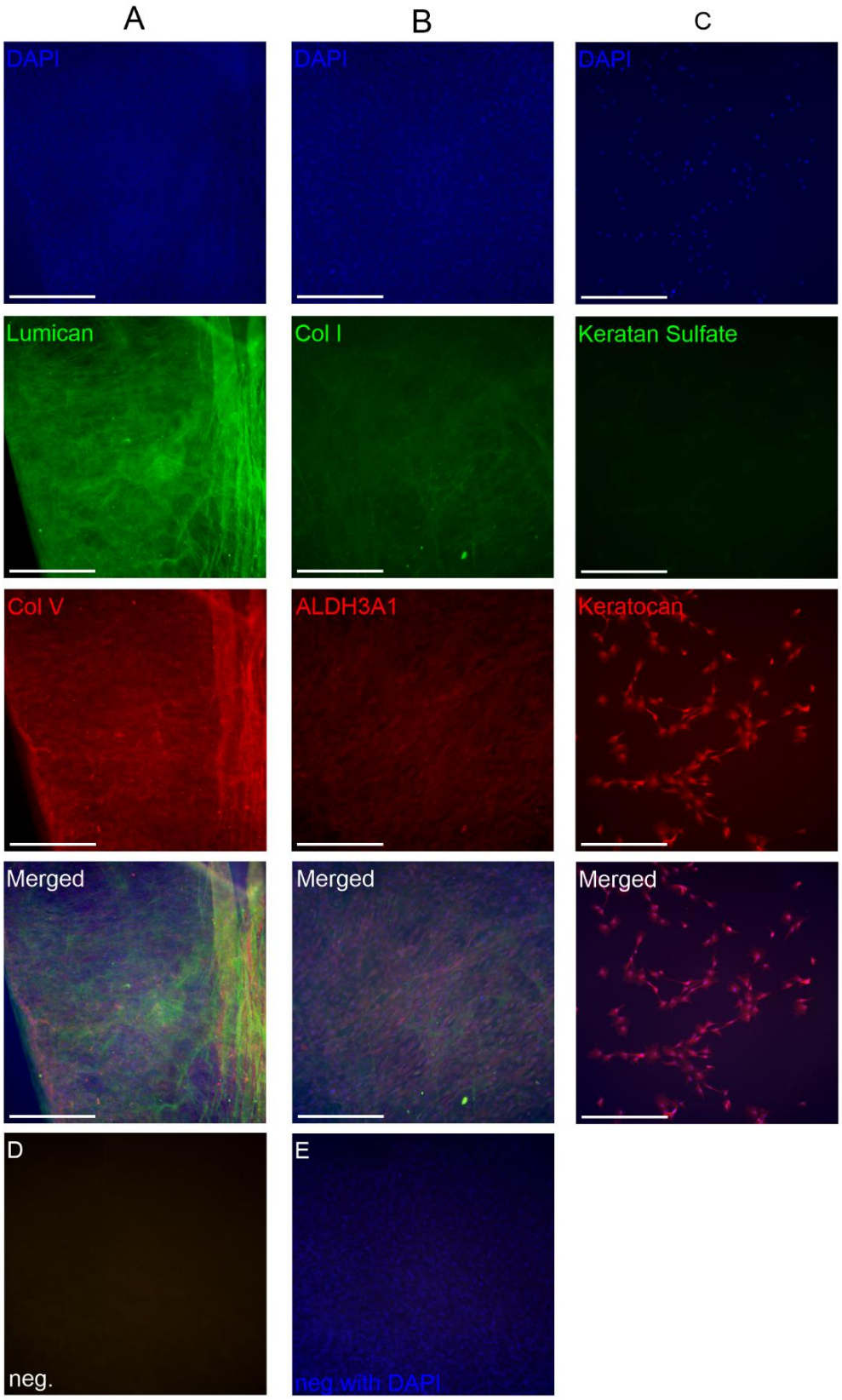

Figure 16: *Immunofluorescence staining of Co-CDM deposited by hASC-CKs at day 14. Nuclei stain DAPI (blue) (A, B and C). Shown in green Lumican (A), Col I (B) and Keratan sulfate (C). Shown in red Col V (A), ALDH3A1 (B) and Keratocan (C). Negative for primary antibodies derived from mouse and rabbit (D). Negative for primary antibodies derived from mouse and rabbit with nuclei stain DAPI (E). Scale bar 400 µm.*

5.2 Co-CDM decellularization

The efficacy of the decellularization protocol used for the Co-CDM that was incorporated into the Co-dCDM bioink was assessed by performing DNA extraction for Co-CDM treated in three different methods (Figure 17). In the non-decellularized samples the DNA amount was highest and was 337 ng/µL. The residual DNA amount in the samples decellularized without DNase 1 and with DNase 1 were 54 ng/µL and 76 ng/µL, respectively. Although there was a decrease in the amount of DNA compared to the non-decellularized samples, the difference observed between the treatments was not statistically significant.

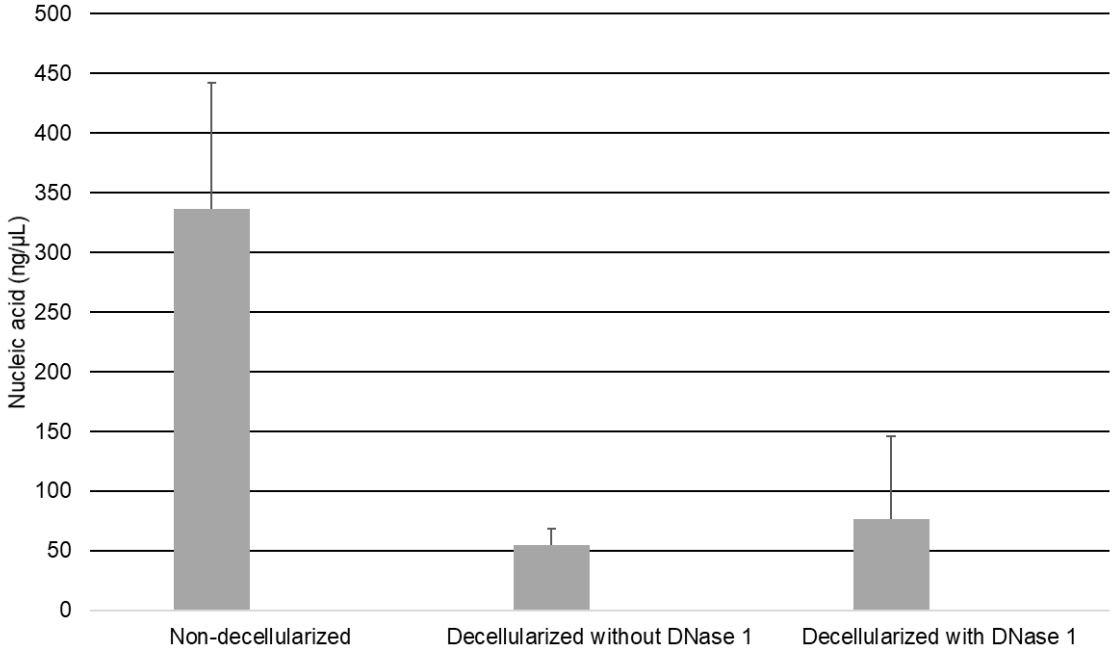

Figure 17: *Amount of remaining DNA in the Co-CDM after three different treatments: non-decellularized (n = 3), decellularized without DNase 1 (n = 2) and decellularized with DNase 1 (n = 3).*

5.3 Macromolecular crowding

The effects of MMC on cornea-specific ECM protein production were determined by cultured hASC-CKs in three different mediums, which were stained for immunofluorescence at days 14 and 21 (Figure 18). Phase contrast image shows spreading of hASC-CKs with elongated morphology in KDM medium at day 14. Similar morphology can be observed for cells cultured in KDM supplemented with growth factor 4, although cell detachment has occurred as rounded hASC-CKs can be seen. Clear detachment of cells with rounded morphology in KDM medium supplemented with growth factor 4 and carrageenan is evident. The respective, immunofluorescence images show weak or non-

existent expression of lumican. Collagen V and DAPI are weakly expressed in KDM and KDM supplemented with growth factor 4.

Phase contrast images at day 21 show significant detachment of hASC-CKs in all mediums, except KDM used as a control in this experiment (Figure 18). The morphology of hASC-CKs in KDM medium is similar to day 14. In addition, clear proliferation has occurred, since cells growing on top of each other can be recognized. In immunofluorescence staining the expression of lumican, collagen and DAPI are either weak or nonexistent with all conditions due to the detachment of hASC-CKs. Although hASC-CKs had proliferated in KDM medium at day 14 and 21, the weak expression of the used antibodies indicates detachment of cells during stainings in both time points.

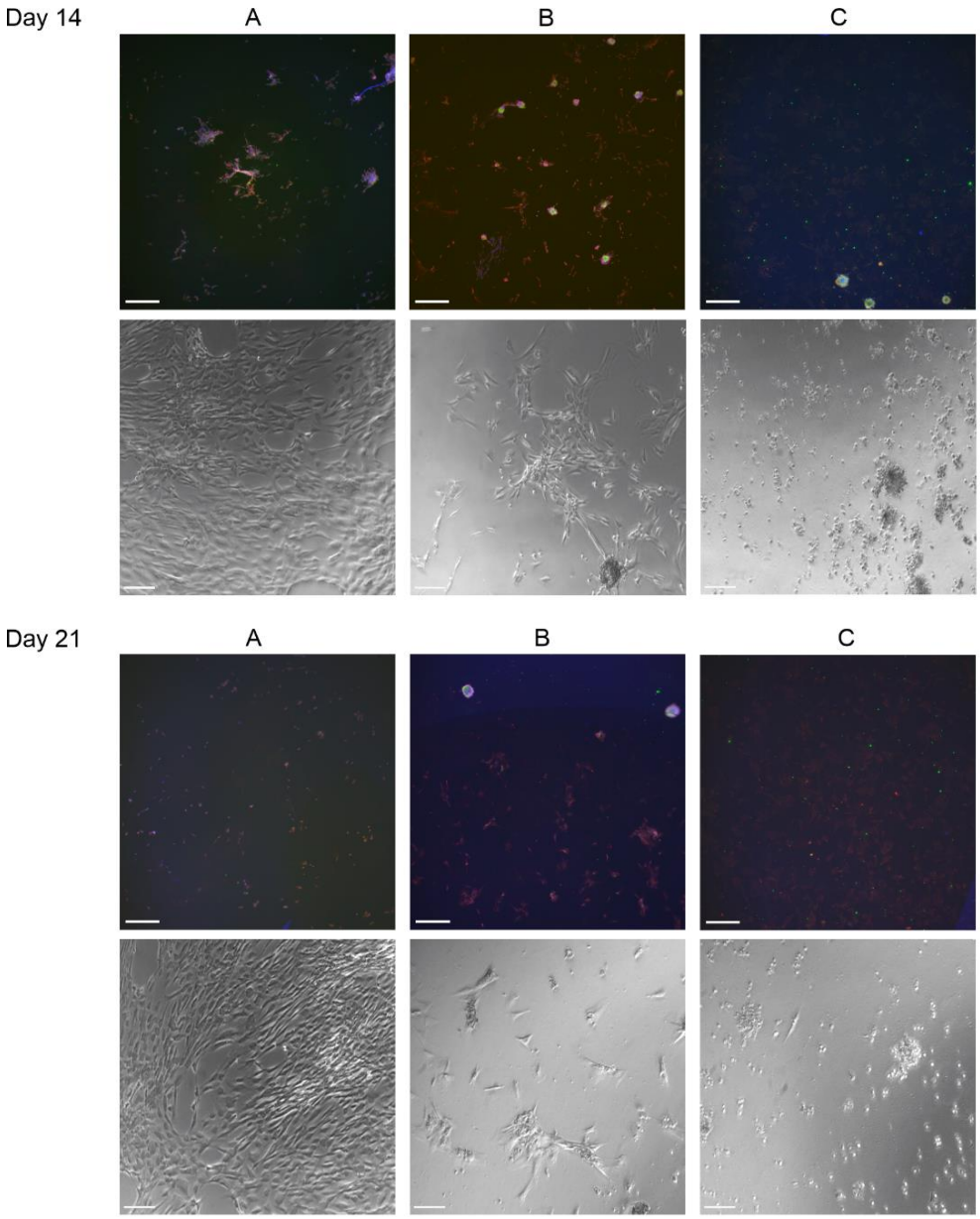

Figure 18: *hASC-CKs cultured in three different conditions (A = KDM, B = KDM with growth factor 4, C = KDM with growth factor 4 and carrageenan) and their respective phase contrast images at day 14 and day 21. Immunofluorescence stainings with nuclei stain DAPI (blue), anti-lumican (green) and anti-collagen V (red). Scale bars 200 µm for immunofluorescence and phase contrast images.*

5.4 Bioink printability

The printability of the studied bioinks was assessed without cells by printing lattice structures with printing parameters of 1.3 bar pressure and 7 mm/s speed, that delivered overall good printing resolution for both bioinks. Both bioinks were printable for approximately 1 hour and towards the end nozzle clogging occurred more frequently. The used printing parameters were not optimal for Co-dCDM bioink, which were used as it was

desirable to print the studied bioinks with the same parameters. Therefore, optimal printing parameters for improved printability of Co-dCDM bioink were determined separately.

The printability assessment for Col I and Co-dCDM bioinks is presented in figure 19. For Col I bioink the printed filaments are uniform and minor filament merging is observable at the crossroads (Figure 19 A). Filaments with more evident filament merging at the crossroads can be seen in lattice printed with Co-dCDM bioink (Figure 19 B). With appropriate printing parameters for Co-dCDM bioink the printed structures showed fine and uniform filaments with minor filament merging (Figure 19 C).

For both bioinks the width and distance between adjacent filaments was measured, to assess the differences in printability. The lattice structures used in analysis were printed with the same parameters to increase the comparability of the results. Average filament thickness was greater for structures printed with Col I bioink (0.38 mm) compared to Co-dCDM printed structures (0.31 mm) and was statistically significant ($p < 0.05$). The distance between adjacent filaments was similar for both bioinks (2.53 mm) and was close to the distance set in the 3D model (2.5 mm). Moreover, the pore factor (Pr) was calculated and was larger for Col I bioink (0.93) compared to Co-dCDM (0.90) and was statistically significant ($p < 0.05$).

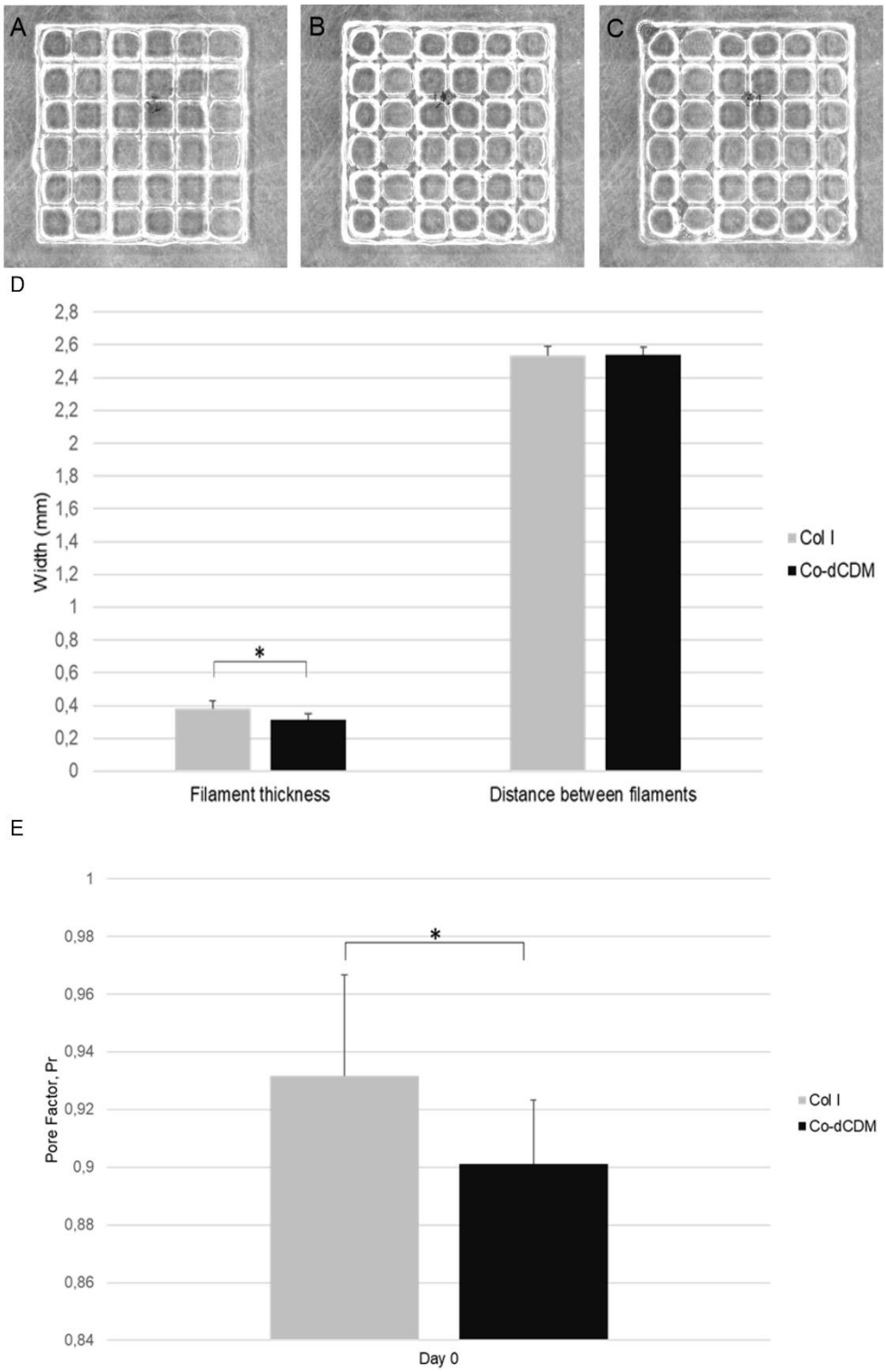

Figure 19: *Printability of Col I (A) and Co-dCDM (B) bioink at 1.3 bar pressure and 7 mm/s speed. Improved Co-dCDM printability at printing parameters 1.1 bar pressure and 6 mm/s speed (C). Average filament thickness ($p^{*} < 0.05$) and distance between filaments for Col I (n = 12) and Co-dCDM (n = 11) bioinks (D). Pore factor (Pr) ($p^{*} < 0.05$) after printing for Col I (n = 12) and Co-dCDM bioinks (n = 11) (E).*

5.5 Bioink characterization

In addition to printability, shape fidelity, swelling behavior and transmittance of the bioinks were characterized. Viscosity was also measured to determine bioink shear-thinning property. The measured properties were compared against each other to investigate if Co-dCDM bioink characteristics differ from Col I bioink.

5.5.1 Shape fidelity

Printed structures were incubated in PBS or hASC medium and the filament thickness was measured on day 7 and 14, to assess how different bioink composition and incubation conditions affect structure shape fidelity (Figure 20). On day 7, the average filament thickness of Col I structures was 1.2 and 1.5 times larger compared to the normalized initial filament thickness right after printing (Day 0) in PBS and hASC medium, respectively. Filament thickness of the Co-dCDM structures on day 7 increased 1.7 and 2.3 times in PBS and hASC medium, respectively. For both bioinks the difference of average filament thickness between the two conditions was statistically significant ($p < 0.05$). On day 14 there was a slight increase in filament thickness compared to day 7, except for Co-dCDM structures incubated in hASC medium. Filament thickness was 1.3 and 1.5 times greater in structures printed with Col I compared to initial filament thickness in PBS and hASC medium, respectively. Co-dCDM structures had 1.7- and 2.6-times larger filament thickness in PBS and hASC medium, respectively. The difference observed in average filament thickness was statistically significant between the two conditions for both bioinks ($p < 0.05$). Moreover, the differences in average filament thickness between Col I and Co-dCDM bioink incubated in the same conditions was statistically significant in both timepoints ($p < 0.05$).

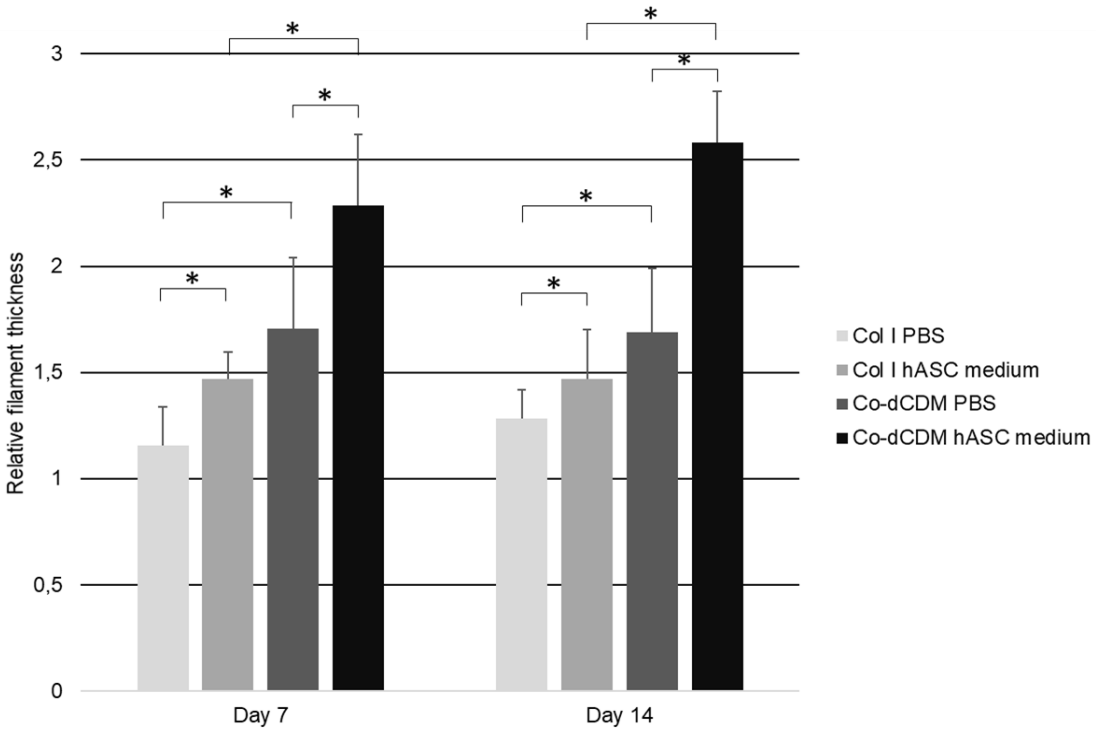

***Figure 20**: Relative filament thickness compared to day 0 of Col I (n = 12) and Co-dCDM (n = 11) bioink in two different conditions at day 7 and 14 ($p^{*} < 0.05$).*

5.5.2 Swelling behavior

The SR was determined by printing 3D cylinder structures with both bioinks and incubating them in hASC medium for 7 days (Figure 21). After 30 minutes of post-printing and incubation, SR was observed to be 20% for Col I and 32% for Co-dCDM. For both bioinks, the SR increased and reached a maximum value of 50% and 51% at 6h for Col I and Co-dCDM, respectively. Thereafter, at 24h SR decreased for both bioinks and was 35% for Col I and 41% for Co-dCDM. At day 7 SR had again increased and was 41% and 44% for Col I and Co-dCDM, respectively.

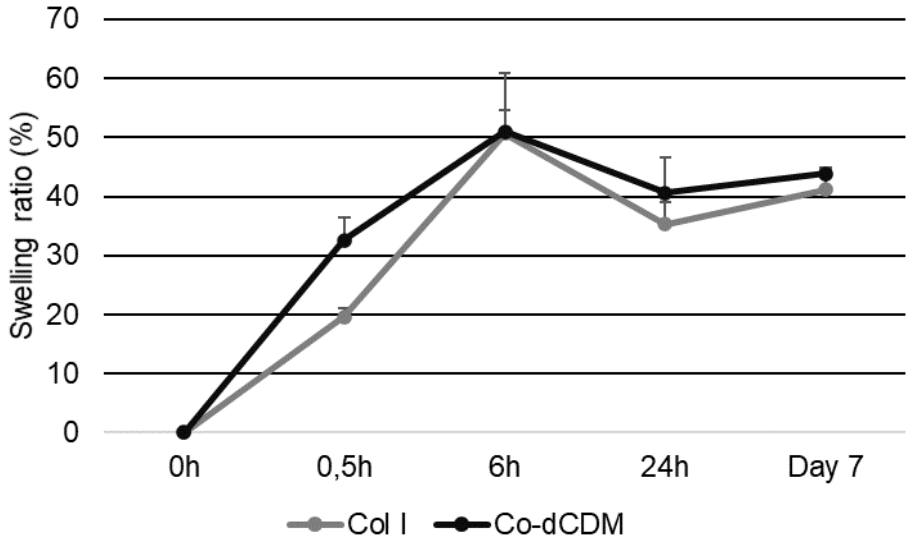

Figure 21: *Swelling ratio for 3D structures printed with Col I (n = 3) and Co-dCDM (n = 2) bioinks at different timepoints of incubation in hASC medium.*

5.5.3 Transmittance

Transparency was determined by measuring their transmittance between wavelengths 300 nm to 900 nm after 1 h and 2 h of bioink preparation (Figure 22). In the range of visible light (400–750 nm), the transmittance values of the Col I bioink ranged from 83% to 97% after 1 h. The transmittance values of the Co-dCDM bioink were between 76% to 93% within the same wavelength range and thus were lower compared to Col I. After 2 h of bioink preparation transmittance values were slightly lower compared to the measurements after 1 h. Generally, both bioinks had excellent transmittance values between visible light wavelengths.

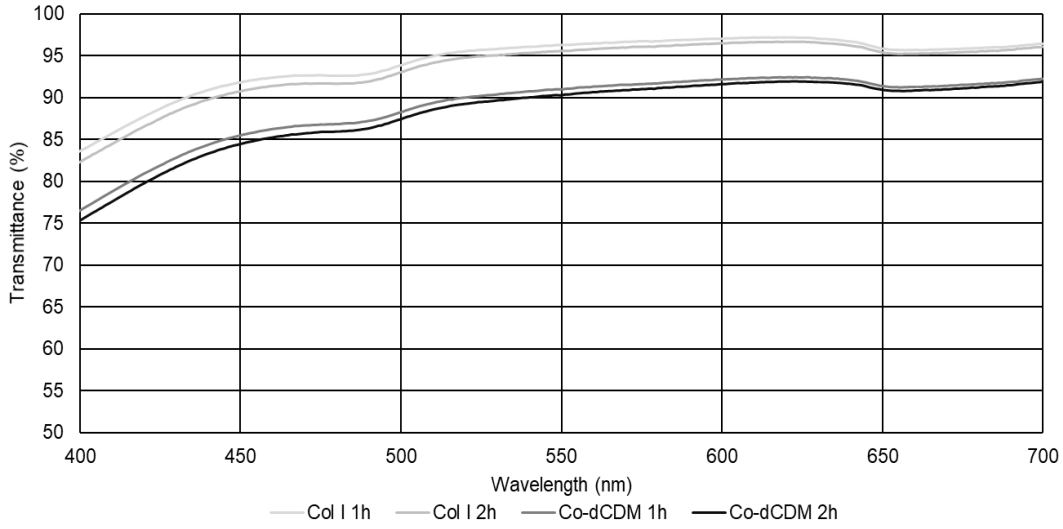

Figure 22: *Transmittance values for Col I and Co-dCDM after 1h and 2h of bioink preparation (n = 1).*

5.5.4 Viscosity

Viscosity at different shear rates was measured by a rheometer at 20 °C to investigate the shear-thinning properties of the bioinks (Figure 23). The observed initial viscosity value for Col I was 65 Pa·s and with increasing shear rates viscosity quickly reached its highest value of 104 Pa·s. Thereafter, the viscosity of Col I decreased steadily with greater shear rates. The viscosity for Co-dCDM was clearly greater. The initial viscosity was 296 Pa·s which increased to a maximum value of 635 Pa·s which was followed by sudden drop in viscosity with greater shear rates. After the shear rate of 0.15 1/s the sudden decrease in viscosity stopped and the viscosity began to decrease steadily, similarly to Col I bioink. Although, the initial and peak viscosity values differ clearly for Co-dCDM and Col I bioink, with greater shear rates their viscosities approach each other.

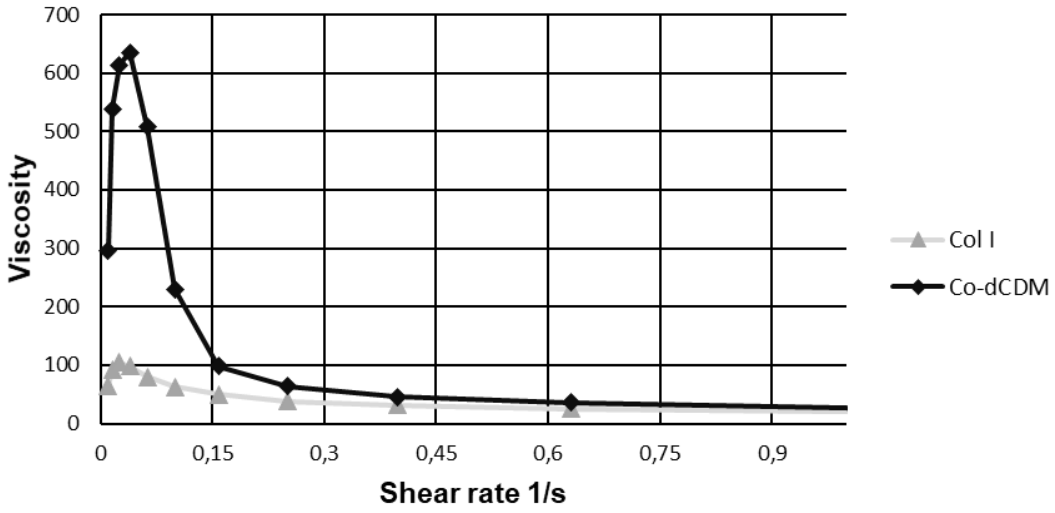

Figure 23: *Measured viscosity values for Col I and Co-dCDM at 20 °C with increasing shear rates (n = 3).*

5.6 Bioink biocompatibility

In this thesis biocompatibility assessment was only performed for structures printed with Co-dCDM bioink. The structures were incubated in hASC medium after printing and cultured until further analysis. The assays performed were Live/Dead, PrestoBlue, and immunofluorescence staining and the selected timepoints were days 1, 4 and 7.

5.6.1 Live/Dead

The viability of printed hASCs in Co-dCDM bioink was investigated by performing Live/Dead assay (Figure 24). The number of live hASCs in printed lattices were excessively higher to the number of dead cells in all time points (Figure 24 A). The total number

of hASCs on day 1 was lower and cell migration had not yet occurred as cell morphology was rounded. On day 4, cells have migrated from the filament to the lattice pores. On day 7 the number of hASCs had increased and the viability is very high (approximately 99%) as only one dead cell can be seen. In addition, the intersection of two filaments can be seen, and hASCs have migrated to the pores of the filament intersections. The morphology and increased number of hASCs is shown in phase contrast images taken from the respective samples in the right column.

Moreover, hASCs were printed within 3D cylinder structures to study tissue formation and if any change in cell viability occurs (Figure 24 B). Similarly, to the lattice structures the cell viability is high in the 3D structures and dead cells are not apparent. In the phase contrast images it is clear that hASCs number increased from day 1 to 7. It is worth mentioning that the printed 3D structures were not ideal as only 5 to 6 layers were managed to be printed. This was due to nozzle clogging during printing. However, both structures printed with Co-dCDM showed excellent cell viability of hASCs.

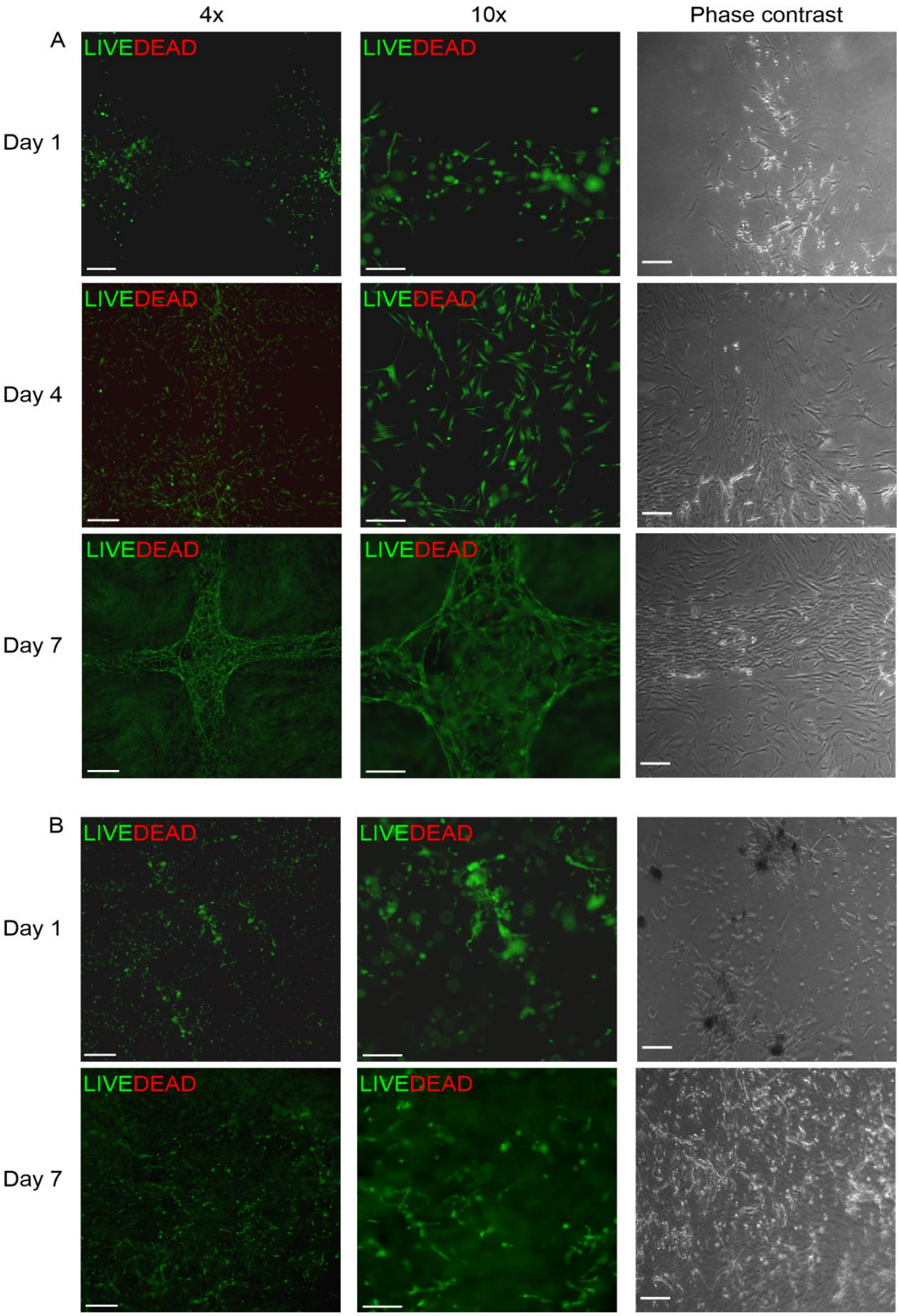

Figure 24: *Viability of hASCs (1.1*10^6 cells/ml) in Co-dCDM printed lattices (n = 1) and phase contrast image from the respective sample to demonstrate increased number of cells (A). Cell viability of hASCs (1.1*10^6 cells/ml) printed with 3D structures (n = 1) and phase contrast image from the respective sample (B). Scale bars 200µm (left column), 400µm (middle and right column).*

5.6.2 PrestoBlue

In order to assess hASCs proliferation in the printed structures PrestoBlue assay was performed (Figure 25). The fluorescence values at day 4 and 7 were higher compared to day 1, and the difference was statistically significant ($p < 0.05$). On day 7 the fluorescence was clearly higher compared to day 1 and 4. The difference in fluorescence values between day 4 and 7 was statistically significant ($p < 0.05$). Thus, hASCs proliferation increased in Co-dCDM printed structures during the culture period and the fluorescence value was approximately four times greater at day 7 compared to day 1.

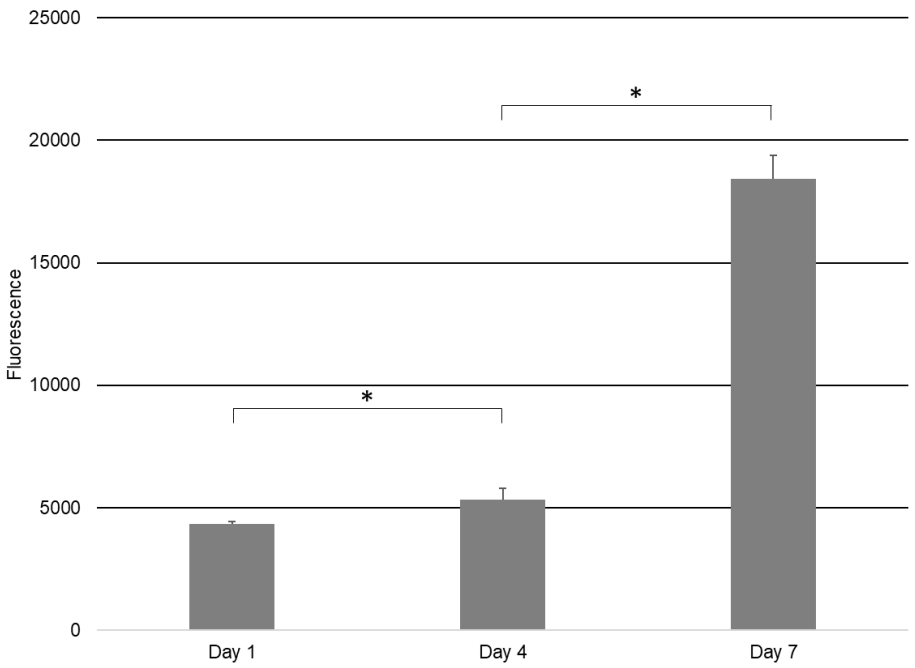

Figure 25: *PrestoBlue data for hASCs ($1.1*10^6$ cells/ml) proliferation in Co-dCDM printed structures cultured in hASC medium ($n = 1$, $p^* < 0.05$).*

5.6.3 Immunofluorescence

The cell proliferation and maturation efficacy were studied by immunofluorescence staining Co-dCDM printed lattice and 3D cylinder structures containing hASCs. The results of immunostaining are given below in their own figures. Results for immunofluorescence of lattice structures are shown in figure 26. On day 1 there was expression of nuclei stain DAPI and proliferation marker Ki-67. In addition, the hASCs morphology can be recognised by the phalloidin stained actin cytoskeleton. Expression of these stains is increased on day 4 which is expected as cell number has increased through proliferation. In addition, on day 4 there are cells neighbouring the filament that is in the center of the image. This verifies the presence of migrating cells in the lattice pores that were observed in Live/Dead assay. Although the expression of DAPI and phalloidin was evident on day 7,

the expression of Ki-67 is lower compared to day 4. This suggests that cell proliferation has decreased presumably via contact inhibition as cell density increases.

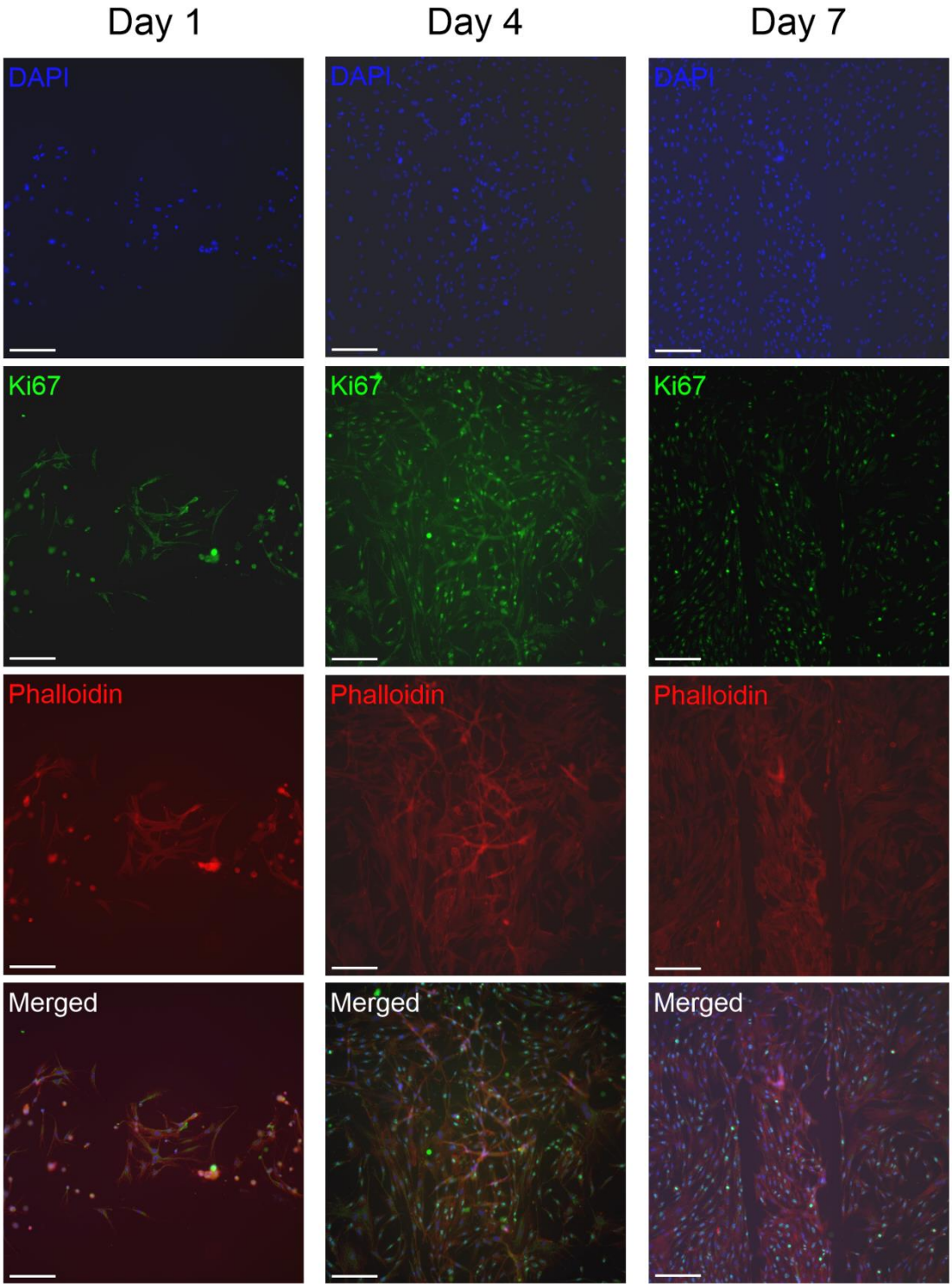

Figure 26: *hASCs (1.1*10^6 cells/ml) printed with Co-dCDM lattice structures. Immuno-fluorescence staining with nuclei stain DAPI (blue), proliferation marker Ki-67 (green) and Phalloidin (red). Scale bars 400 µm.*

In figure 27, the confocal image of immunofluorescence staining for hASCs containing 3D cylinder structures on day 7 is presented, stained with DAPI, connexin 43 and phalloidin. The elongated morphology from hASCs can be clearly seen by phalloidin stained actin filaments, suggesting that hASCs are proliferating and migrating in the Co-dCDM bioink structure. This is further supported by the observation that cells seen to be close to each other as multiple adjacent cell nuclei can be identified. In addition, connexin 43, a gap junction protein, is expressed as bright dots, which could suggest that hASCs have formed gap junctions with each other. These observations indicate that hASCs are viable and proliferative, indicating that the cells are able to form tissue in the 3D Co-dCDM structure.

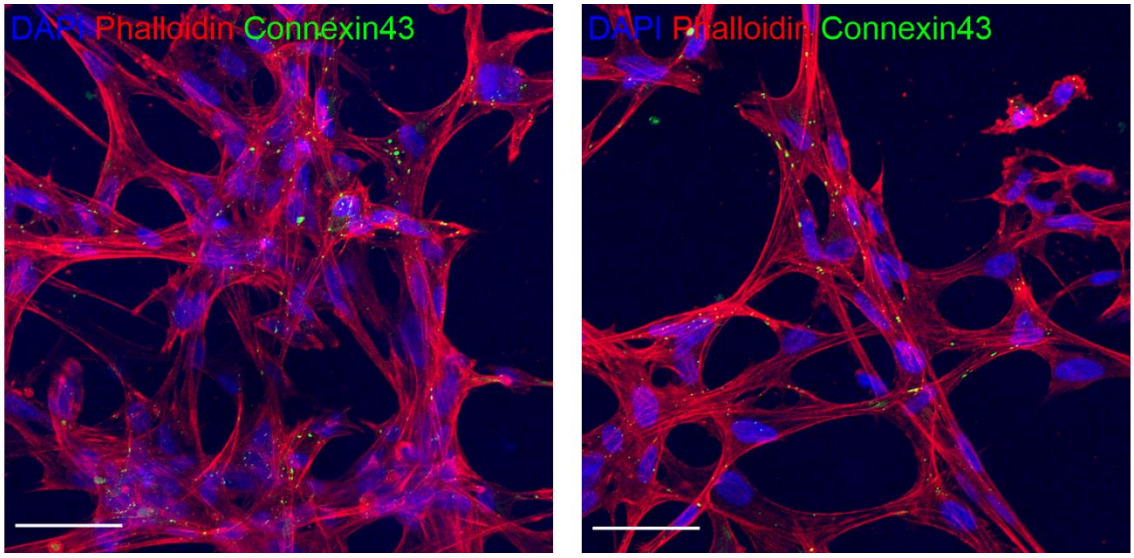

Figure 27: *hASCs (1.1*10^6 cells/ml) printed into Co-dCDM 3D structures. Immunofluorescence staining with nuclei stain DAPI (blue), gap junction protein Connexin 43 (green) and Phalloidin (red). Scale bars 50 µm.*

6. DISCUSSION

Injuries and diseases induce corneal damage, adversely affecting vision as they reduce corneal transparency (Yam et al., 2020). While corneal transplantation can be performed to improve vision, the availability of donor corneas is poor, meaning that only a small portion of patients suffering from corneal blindness can be treated (Gain et al., 2016; Singh et al., 2019). Although KPros can be used instead of donor corneas, they come with high complications risk, limiting their use (Holland et al., 2021; Matthyssen et al., 2018). Therefore, there is a huge need for corneal equivalents which could be transplanted similarly as donor corneas (B. Zhang, Xue, Li, et al., 2019). 3D bioprinting enables the generation of 3D structures with precision and controllable architecture, thus this technology has the potential to produce corneal equivalents for corneal blindness patients (Ruiz-alonso et al., 2021; B. Zhang, Xue, Li, et al., 2019). Recently, dECM bioinks have gained interest as these bioinks provide a similar microenvironment than in *in vivo* tissues, promoting tissue specific cell behavior (B. S. Kim et al., 2020; Nam & Park, 2018). Previously, a dECM bioink has been explored for cornea (H. Kim et al., 2019). However, as the bioink is derived from scarce donor corneas, it has limited potential. The aim of this thesis was to characterize a cornea-specific bioink for EBB without the need for donor corneas.

6.1 Characterization of Co-CDM

To study successful differentiation of hASC-CKs, the previously reported specific markers used have been lumican, ALDH3A1 and keratocan (Du et al., 2010; Lynch & Ahearne, 2017). In this study, the expression of these specific CKs markers was studied with immunofluorescence staining. In addition, expression of Col I and Col V was studied, because they are major constituents of native corneal ECM produced by CKs (Espana & Birk, 2020; Yam et al., 2020). However, keratan sulfate, which has been stated to be a reliable marker of successful differentiation of hASC-CKs (Du et al., 2010), was not expressed. Previous studies have successfully shown differentiation of hASC-CKs with KDM (Ahearne et al., 2014; Du et al., 2010; Lynch & Ahearne, 2017; S. Zhang et al., 2013). It is worth mentioning that the hASC-CKs differentiated in this study were immature compared to *in vivo* CKs as they were only differentiated for 2 weeks. This is supported by the non-existent keratan sulfate expression. Therefore, it could be beneficial to compare primary CKs and hASC-CKs gene expression to study the efficacy of the differentiation protocol. However, the reason for non-existent keratan sulfate could be

due to the used primary antibody, thus another primary antibody could be used in the immunofluorescence staining for keratan sulfate.

6.2 Decellularization and solubilization of Co-CDM

Although CDM are derived from cultured cells and not native tissues, they can be processed and decellularized similarly as native ECM (Chan et al., 2021). The objective in decellularization is to remove the cells from the ECM, in this case CDM, which improves its biocompatibility, lowering the risk of inflammatory response (Fernández-Pérez & Ahearne, 2019; H. Kim et al., 2019; Hyungseok Lee et al., 2017). Additionally, after decellularization DNase 1 can be used to fragment residual DNA (Fernández-Pérez & Ahearne, 2019). For ECM derived from native tissues, decellularization is successful when the DNA content is less than 3% compared to the non-decellularized tissue or the amount of DNA is less than 50 ng/mg after decellularization (H. Kim et al., 2019). Subsequently, the decellularized ECM is frozen in -80 °C or with liquid nitrogen and freeze-dried and turned into a powder by grinding or milling machine before digestion with pepsin in HCl or acetic acid (Ahearne & Lynch, 2015; Fernández-Pérez & Ahearne, 2019; H. Kim et al., 2019; Hyungseok Lee et al., 2017). In order to prepare a bioink from the solubilized ECM, it is subsequently neutralized with NaOH to induce hydrogel formation (Ahearne et al., 2020; Ahearne & Lynch, 2015; H. Kim et al., 2019). The Co-dCDM was decellularized and turned into a hydrogel similarly as described in the literature. However, Co-dCDM was not turned into a powder as the literature has only described protocols for tissues ECM that are mechanically much tougher than CDM. Therefore, powdering of Co-dCDM was not required for solubilization.

In this study, the efficacy of the used decellularization protocol was analyzed by performing DNA extraction for Co-CDM collected in three different methods. The Co-CDM samples decellularized without DNase 1 and with DNase 1 contained less DNA than the non-decellularized samples. Interestingly, the samples decellularized with DNase 1 contained more DNA than the group decellularized without DNase 1. Thus, the decellularization protocol decreased the DNA content of the Co-CDM and addition of DNase 1 did not enhance the decellularization outcome. The DNA contents compared to non-decellularized Co-CDM (100%) were 16% and 22.5% for decellularized without and with DNase 1, respectively. Therefore, the decellularization was not successful as discussed previously. A possible cause for this result may be the fact that according to the manufacturer's instructions DNase 1 requires Mg^{2+} to fragment DNA effectively, which was not done in this experiment. DNase 1 prepared in $MgCl_2$ solution has been used with excellent results (Ahearne & Lynch, 2015; Fernández-Pérez & Ahearne, 2019), which suggest

that similar approach could have improved decellularization results in this experiment. Furthermore, the sample size in decellularization was small and differed between groups, thus reliability of statistical analysis is probably questionable.

6.3 Macromolecular crowding

In MMC *in vivo* environment is mimicked by addition of inert macromolecules to the culture medium, which exclude volume and increase the density of culture conditions (C. Chen et al., 2011; Gürdal et al., 2020; P. Kumar et al., 2015). This has been associated with increased ECM protein deposition by cells as MMC increases the rate of procollagen conversion to collagen (C. Chen et al., 2011; Gürdal et al., 2020; P. Kumar et al., 2015). From the various macromolecules that have been used, the highest increase in ECM protein deposition has been achieved with carrageenan (Gürdal et al., 2020). In corneal applications carrageenan has been used effectively for hCF to form stromal-like assemblies (Gürdal et al., 2020; P. Kumar et al., 2015).

The effects of MMC on Co-CDM deposition was investigated by culturing keratocytes in three different conditions. Phase contrast images showed excellent proliferation of keratocytes in KDM at day 14 and 21 compared to the other formulations. On day 14 there was some cell detachment evident in KDM supplemented with growth factor 4. Detachment had increased on day 21. In KDM supplemented with growth factor 4 and carrageenan, the cell morphology was mostly round with significant detachment in both time points. A reason for the detachment of hASC-CKs and their rounded morphology could be the increased deposition of ECM proteins caused by the culture mediums. Presumably, the increase in ECM protein deposition initially led to Co-CDM detachment, which then caused the cells to detach as they are adhered to the Co-CDM. Surprisingly, the expression of used antibodies was poor for all culture conditions including KDM, which indicate cell detachment during immunofluorescence staining. This is supported by the relatively low number of DAPI stained cell nuclei in the immunofluorescence images. Based on these results, MMC could be experimented with KDM supplemented with carrageenan in the future.

6.4 Bioink printability

The printability of a bioink is a major characteristic that is influenced by the bioink composition (Cui et al., 2020; Matai et al., 2020; Ruiz-alonso et al., 2021). Printability in EBB is analysed by filament formation, shape fidelity and bioink extrudability (Schwab et al., 2020). In this study, the printability was assessed by printing both bioinks without cells.

The previously optimized parameters for Col I bioink were used when printing both bioinks. Col I and Co-dCDM bioinks extruded well with the used printing parameters and showed overall good filament formation. The filament thickness was smaller for Co-dCDM, which could be explained by the bioink accumulation to the lattice crossroads. This can be seen as filament merging at the crossroads from the images of lattice printed with Co-dCDM bioink. No clear filament spreading was observed for Col I bioink, thus it is unlikely that the difference between filament thickness would be caused by larger spreading of Col I bioink post-printing. However, the distance between filaments was almost identical for both bioinks and close to the designed value, which is desired in bioprinting. Interestingly, the Pr was larger for Col I, which suggests better shape fidelity around the pores compared to Co-dCDM. The obtained result could indicate that Co-dCDM bioink filament merging was larger, leading to a smaller Pr value, although the overall filament thickness was smaller. From the images of printed structures, it can be observed that filament merging at the crossroads is more pronounced in the Co-dCDM structure, supporting the acquired lower Pr value.

Greater printing pressure and smaller needle size increase shear stress encountered by cells during printing, lowering cell viability (Matai et al., 2020; Soltan et al., 2019; Vijayavenkataraman et al., 2018). Thus, the optimized parameters for printing Co-dCDM with hASC were determined. Moreover, the structures printed with the lower pressure and speed looked visually more uniform with less filament merging at the crossroads. This is supported by the literature as pressure and speed are key determinants for printing resolution (Matai et al., 2020; Van Hoorick et al., 2019).

It is challenging to achieve adequate printability and biocompatibility for single biomaterial bioink which cause a narrow biofabrication window (Chimene et al., 2020; Cui et al., 2020; Schwab et al., 2020). A way to improve the biofabrication window is using multi biomaterial bioinks which also retain the desired bioink characteristics (Chimene et al., 2020; Cui et al., 2020). Wide range of multi biomaterial bioinks have been characterized such as Col I and HA containing bioink and dECM with vitamin B2 (Cui et al., 2020). In this study the biofabrication window after the required crosslinking time was similar for both bioinks. It could be interesting to print both bioinks with varying component concentrations to assess if a longer biofabrication window is achieved, while maintaining printability and the bioink characteristics discussed next.

6.5 Bioink characterization

The bioink used in 3D bioprinting should possess adequate mechanical strength in order to support and maintain the shape of the printed structure (Benwood et al., 2021;

Hospodiuk et al., 2017; H. Li et al., 2018). To maintain cell viability the bioink should allow diffusion of oxygen and nutrients (Chimene et al., 2020; Chopin-Doroteo et al., 2021). In addition, the bioink ideally mimics the *in vivo* environment of the target tissue, thus supporting native cell behavior (Chimene et al., 2020; Montero et al., 2019).

A common method to assess bioink shape fidelity is to print lattice structures and measure the filament width (Gillispie et al., 2020; Schwab et al., 2020). In this study shape fidelity of the studied bioinks was investigated by incubating printed lattice structures in two different conditions. In both timepoints and conditions, structures printed with Co-dCDM bioink had larger relative filament thickness than Col I bioink structures. In addition, the observed differences in the timepoints between bioink groups and conditions were statistically significant. Hydrogels have the ability to absorb large amounts of water, leading to their swelling (Chimene et al., 2020; Wenhui Zhang et al., 2021), which explains the larger filament width after incubation. Interestingly, the relative filament thickness was clearly larger for structures incubated in hASC medium. Previously, different swelling behavior has been reported for hydrogel structures incubated in PBS and hASC medium (Koivusalo et al., 2019), which can be due to the inflow of various nutrients found in the culture medium. This finding could explain the greater relative filament thickness observed for the lattice structures in hASC medium.

Due to the swelling ability of hydrogels in aqueous environment, the swelling characteristics of both bioinks was analyzed by printing 3D cylinder structures without cells, which were weighted after 0.5, 6, 24 hours and 7 days of incubation in hASC medium. There was a clear increase in the weight of the printed samples after 0.5 hours and the weight peaked at 6 hours for both bioinks. Thereafter, the weight slightly decreased at 24 hours and was again increased when weighing at day 7. Although both bioinks behaved similarly the weight of Co-dCDM structures was greater, except for the peak value, which was almost identical compared to Col I bioink. A possible cause for the peak value at 6 hours, could be that the structures had absorbed almost the maximum amount of medium at that point. However, an equilibrium had not been reached, which could explain the drop in weight at 24 hours. The increase in weight at day 7 could imply that an equilibrium could have been reached. Therefore, the structures could have been incubated for a longer time period to study if this was the case. The observed increase weight of the structures as well the increase in filament width discussed earlier, was expected due to the previously mentioned hydrogel ability to absorb water. Similar method to assess bioink water content as used in this study has been reported for corneal 3D bioprinting (Kilic Bektas & Hasirci, 2020; Mahdavi, Abdekhodaie, Kumar, et al., 2020; B. Zhang, Xue, Hu, et al., 2019). A reason for the larger swelling of Co-dCDM bioink, could be the

presence of proteoglycans such as lumican and keratocan, ECM proteins produced by keratocytes *in vivo,* which bind water (Espana & Birk, 2020; Yam et al., 2020). In addition, native ECM contains HA, which is important for tissue hydration (B. S. Kim et al., 2020). The composition of the produced Co-CDM could be characterized, in order to assess if the amount of these factors in the bioink significantly affect swelling characteristics. However, it should be mentioned that higher crosslinking, degree decreases bioink swelling (Koivusalo et al., 2018). Consequently, it is possible that the crosslinking degree was lower for Co-dCDM, leading to greater swelling.

The transparency of cornea is crucial for eyesight as its purpose is to refract and transmit light (Meek & Knupp, 2015; Yam et al., 2020). Therefore, the transparency of the used bioinks is important when bioprinting corneal structures, which is often characterized for bioinks used in corneal 3D bioprinting by measuring their transmittance. Previous studies have reported bioink transmittance values of 75–90% (Kutlehria et al., 2020), 78–95% (Mahdavi, Abdekhodaie, Kumar, et al., 2020), over 75% (Kilic Bektas & Hasirci, 2020; H. Kim et al., 2019) and 85–94% (B. Zhang, Xue, Hu, et al., 2019). Similar method was used in this study to measure Col I and Co-dCDM bioink transparency 1 and 2 hours after preparation. In the range of visible light, the transmittance ranged from 83% to 97% and 76% to 92% for Col I and Co-dCDM bioink, respectively. After 2 hours of preparation the transmittance values are slightly lower for both bioinks. The transmittance acquired in this study is similar as reported in relevant research articles and the transmittance of Co-dCDM is alike to the transmittance reported for Co-dECM bioink by Kim et al. (2019). In addition, the transmittance values of the studies bioinks is close to the transmittance of native cornea, which has been measured to be 86–94% between 450–600 nm and over 95% in the range of 600–1000 nm (Beems & Van Best, 1990). Hence, Co-dCDM bioink is suitable for corneal 3D bioprinting in terms of transparency.

Viscosity is an important factor in shape retention as structures printed with high viscosity bioink, have improved shape fidelity after printing, before crosslinking has stabilized the structure (Benwood et al., 2021; Cui et al., 2020). Therefore, in EBB shear thinning is a desired bioink property, as the decrease in viscosity during extrusion, reduces shear stress experienced by cells, increasing their viability post-printing (Benwood et al., 2021; Cui et al., 2020; Schwab et al., 2020). Some studies have reported viscosity for bioink used in corneal 3D bioprinting (Duarte Campos et al., 2019; H. Kim et al., 2019; Kutlehria et al., 2020). In this study bioink viscosity was measure with a rheometer and the initial viscosities were 65 Pa·s and 296 Pa·s for Col I and Co-dCDM bioink, respectively. With increasing shear rates both bioinks behaved similarly as their viscosity increased until shear rate of 0.15 1/s reaching a peak value of 296 Pa·s and 635 Pa·s, respectively.

When exceeding this shear rate, a drop in the viscosity of both bioinks was observed, thus Col I and Co-dCDM had shear-thinning property.

Shear thinning property has been reported for Col I (Duarte Campos et al., 2019) and Co-dECM (H. Kim et al., 2019) bioink. For 0.3% Col I bioink the viscosity values were below 0.1 mPa·s and viscosity decreased only slightly with higher shear rates (Duarte Campos et al., 2019). When the Col I bioink was supplemented with agarose the initial viscosity was 10 mPa·s and decreased clearly with higher shear rates (Duarte Campos et al., 2019). The observed low viscosity for pure Col I bioink supports the notion made in the literature that pure Col I bioinks have poor properties for bioprinting and need to be supplemented with other biomaterials (Benwood et al., 2021). Overall, the viscosities for both bioinks were quite low, which is likely due to the low Col I concentration in the bioinks. For Co-dECM the reported viscosity values varied between 65–2.4 Pa·s at shear rate of 1 s^{-1} and higher Co-dECM concentration was associated with higher viscosity values (H. Kim et al., 2019). As the shear rate increased the viscosity decreased, thus the Co-dECM bioink showed shear-thinning property (H. Kim et al., 2019). The larger viscosity measured for Co-dCDM was interesting as generally, dECM bioinks are less viscous due to the loss of ECM proteins during decellularization, which also decreases their printability (B. S. Kim et al., 2020). Yet, it is possible that the presence of proteoglycans in Co-dCDM lead to greater viscosity as discussed previously for swelling behavior. It is worth mentioning that in the rheological measurement the gap for the geometry was manually adjusted and the amount of bioink was estimated from the syringe scale. These aspects are prone to errors, thus these would need to be optimized.

6.6 Co-dCDM biocompatibility

Besides being printable and support printing of 3D structures, a functional bioink should be highly biocompatible, enabling native cellular functions such as proliferation, migration and differentiation (Gungor-Ozkerim et al., 2018; Matai et al., 2020; Montero et al., 2019). In addition, the bioink should ideally accurately mimic the *in vivo* environment of the target tissue (Bejoy et al., 2021; Gungor-Ozkerim et al., 2018; Montero et al., 2019). There are various aspects that can be analyzed to determine bioink biocompatibility such as cell viability, proliferation and maturation, which are discussed next.

Previously in corneal 3D bioprinting, cell viability has been shown to be over 80% (Mahdavi, Abdekhodaie, Kumar, et al., 2020; B. Zhang, Xue, Hu, et al., 2019) and over 90% (Duarte Campos et al., 2019; Kilic Bektas & Hasirci, 2020; Kutlehria et al., 2020). In this study, the viability of hASCs printed with Co-dCDM were approximately 99.9% in

all timepoints as there were virtually no dead cells apparent, thus the finding is in accordance with the previously reported values. In fact, the cell viability reported in this study is clearly higher than in the literature, which would suggest that Co-dCDM bioink has superior biocompatibility in terms of cell viability. Moreover, Live/Dead images showed cell proliferation and change from rounded cell morphology into elongated, over time. Previous studies have made similar observations in the change of cell morphology with increased incubation time (Duarte Campos et al., 2019; Mahdavi, Abdekhodaie, Kumar, et al., 2020; Sorkio et al., 2018). It is worth mentioning that although Kim et al. (2019) reported excellent cell viability in Co-dECM bioink, the analysis was only done at day 1, thus they are not comparable with Co-dCDM bioink. In addition, the study performed by Kim et al. (2019) did not present results on retention of cell morphology over time as seen in this study. PrestoBlue has been used to measure the cell proliferation in the printed structures (Sorkio et al., 2018). In this experiment the assay verified cell proliferation, since the values increased over time and were almost four times greater at day 7 compared to the value at day 1.

Immunofluorescence staining has been used to analyzed cell maturation in the bioink previously (Duarte Campos et al., 2019; Kilic Bektas & Hasirci, 2020; H. Kim et al., 2019; Kutlehria et al., 2020; Sorkio et al., 2018). In this study proliferation and growth of hASCs in Co-dCDM was analyzed by staining the structures with proliferation marker Ki-67 and phalloidin, respectively. Ki-67 was expressed in all timepoints, indicating proliferation of cells. This was associated with increased phalloidin expression from day 1 to 7, thus demonstrating growth of hASCs. In addition, the phalloidin stained cytoskeleton showed the elongated morphology of cells. Moreover, at day 7 cellular migration was observed from the lattice filaments. For hASCs this has been previously reported that were printed in Col I based bioink, where elongated cell morphology was observed after printing (Sorkio et al., 2018). Moreover, cells in these structures showed increased proliferation and migration post-printing (Sorkio et al., 2018). Another study reported initial rounded morphology for printed cells (Duarte Campos et al., 2019), which was interestingly not seen in this study. The observations from immunofluorescence images are further supported by the confocal image of the 3D Co-dCDM structure, that clearly shows elongated cell morphology. Also, connexin 43 is expressed, pointing to possible formation of gap junctions between cells. The immunofluorescence stainings suggest that Co-dCDM bioink supports normal cellular functions, which is highly desirable for bioinks.

6.7 Future directions

In this study a cornea-specific bioink was developed and characterized. The Co-dCDM bioink demonstrated favorable properties, thus it has potential in corneal 3D bioprinting. However, in the future the bioink should be analyzed in depth in order to evaluate its strength and possible areas of improvement. It is important to understand that the hASC-CKs differentiated in this study were not mature CKs. It is highly likely that this negatively affects the cornea-specify of the produced Co-CDM. Therefore, the composition of the produced Co-CDM should be analyzed. In addition, it should be studied if the decellularization protocol causes removal of corneal ECM proteins. The differentiation protocol efficacy should also be studied by comparing hASC-CKs and *in vivo* CKs gene expression. Moreover, after improving the Co-dCDM bioink, it could be evaluated against a dECM bioink derived from bovine or donor cornea.

Lastly, in the field of corneal 3D bioprinting majority of the studies have focused only on one or two corneal layers. As the cornea consists of multiple layers and cell types, these should ideally be incorporated into a single printed structure, in order to generate more accurate corneal equivalent (B. Zhang, Xue, Li, et al., 2019). This is challenging as the composition of the corneal layers is different, thus these should be studied thoroughly, which is time consuming. The Co-dCDM bioink reported in this study could preferably be used to print the CS layer. The reason is that the incorporated Co-CDM is produced by hASC-CKs and ideally contains the major ECM proteins found in native CS. As the CS is the largest layer of cornea (Yam et al., 2020), achieving a highly biomimetic CS layer, would significantly contribute toward bioprinting a full-thickness corneal equivalent.

7. CONCLUSION

In this thesis a novel cornea-specific bioink with optimized composition for EBB that avoids the need for donor corneas was characterized. To produce the Co-CDM hASCs were differentiated towards CKs, and the ECM secreted by the cells was collected. Before incorporation to the bioink, the Co-CDM was decellularized and solubilized after freeze-drying. Moreover, the efficacy of decellularization was studied by performing DNA extraction for the decellularized Co-CDM. MMC was used to determine if the amount of the produced Co-CDM can be increased. To achieve adequate bioink printability, the printing parameters were optimized. Thereafter, the bioink was characterized by analyzing its shear-thinning properties, transparency, shape fidelity and swelling behavior. In addition, biocompatibility was studied by analyzing the hASCs viability and proliferation from cell-laden bioprinted structures.

Analysis of the Co-CDM revealed presence of cornea-specific ECM proteins, thus hASCs were differentiated towards CKs. Thus, the incorporation of Co-CDM into the bioink made it cornea-specific to some degree. In addition, decellularization decreased the amount of DNA in the Co-CDM, although the decrease could have been greater. While literature has reported increased deposition of ECM proteins with MMC, this was not achieved in this study. Overall, Co-dCDM bioink demonstrated adequate printability and the structures were stable in different incubation conditions. In addition, the bioink demonstrated shear-thinning behavior, a desired property in EBB. Moreover, the transparency of Co-dCDM bioink was found to be excellent due to transmittance over 75%. Finally, the biocompatibility of Co-dCDM bioink was excellent as virtually no dead cells were present and hASCs were able to proliferate in the bioprinted structures. Thus, Co-dCDM bioink characterized in this thesis demonstrated suitable properties for corneal 3D bioprinting.

Although the results reported here are promising, further research is needed to better understand the properties of Co-dCDM bioink. In this study only hASCs were printed with CO-dCDM bioink and cultured for a relatively short period. Therefore, structures should be printed with hASC-CKs laden Co-dCDM bioink and cultured as long as cells remain viable. With this approach cell organization, maturation and tissue formation could be studied. This novel cornea-specific bioink holds great potential for corneal 3D bioprinting and provides an attractive alternative approach to produce tissue-specific bioinks.

REFERENCES

Ahearne, M., Fernández-Pérez, J., Masterton, S., Madden, P. W., & Bhattacharjee, P. (2020). Designing Scaffolds for Corneal Regeneration. *Advanced Functional Materials*, *30*(44). https://doi.org/10.1002/adfm.201908996

Ahearne, M., & Lynch, A. P. (2015). Early Observation of Extracellular Matrix-Derived Hydrogels for Corneal Stroma Regeneration. *Tissue Engineering - Part C: Methods*, *21*(10), 1059–1069. https://doi.org/10.1089/ten.tec.2015.0008

Ahearne, M., Lysaght, J., & Lynch, A. P. (2014). Combined influence of basal media and fibroblast growth factor on the expansion and differentiation capabilities of adipose-derived stem cells. *Cell Regeneration*, *3*(1), 3:13. https://doi.org/10.1186/2045-9769-3-13

Alió, J. L., Alió Del Barrio, J. L., El Zarif, M., Azaar, A., Makdissy, N., Khalil, C., Harb, W., El Achkar, I., Jawad, Z. A., & De Miguel, M. P. (2019). Regenerative Surgery of the Corneal Stroma for Advanced Keratoconus: 1-Year Outcomes. *American Journal of Ophthalmology*, *203*, 53–68. https://doi.org/10.1016/j.ajo.2019.02.009

Antich, C., de Vicente, J., Jiménez, G., Chocarro, C., Carrillo, E., Montañez, E., Gálvez-Martín, P., & Marchal, J. A. (2020). Bio-inspired hydrogel composed of hyaluronic acid and alginate as a potential bioink for 3D bioprinting of articular cartilage engineering constructs. *Acta Biomaterialia*, *106*, 114–123. https://doi.org/10.1016/j.actbio.2020.01.046

Bacakova, L., Zarubova, J., Travnickova, M., Musilkova, J., Pajorova, J., Slepicka, P., Kasalkova, N. S., Svorcik, V., Kolska, Z., Motarjemi, H., & Molitor, M. (2018). Stem cells: their source, potency and use in regenerative therapies with focus on adipose-derived stem cells – a review. *Biotechnology Advances*, *36*(4), 1111–1126. https://doi.org/10.1016/j.biotechadv.2018.03.011

Barrientez, B., Nicholas, S. E., Whelchel, A., Sharif, R., Hjortdal, J., & Karamichos, D. (2019). Corneal injury: Clinical and molecular aspects. *Experimental Eye Research*, *186*, 1–35. https://doi.org/10.1016/j.exer.2019.107709

Basu, S., Sureka, S. P., Shanbhag, S. S., Kethiri, A. R., Singh, V., & Sangwan, V. S. (2016). Simple Limbal Epithelial Transplantation: Long-Term Clinical Outcomes in 125 Cases of Unilateral Chronic Ocular Surface Burns. *Ophthalmology*, *123*(5), 1000–1010. https://doi.org/10.1016/J.OPHTHA.2015.12.042

Beems, E. M., & Van Best, J. A. (1990). Light transmission of the cornea in whole human eyes. *Experimental Eye Research*, *50*(4), 393–395. https://doi.org/10.1016/0014-4835(90)90140-P

Bejoy, A. M., Makkithaya, K. N., Hunakunti, B. B., Hegde, A., Krishnamurthy, K., Sarkar, A., Lobo, C. F., Keshav, D. V. S., G, D., S, D. D., Mascarenhas, S., Chakrabarti, S., Kalepu, S. R. R. D., Paul, B., & Mazumder, N. (2021). An insight on advances and applications of 3d bioprinting: A review. *Bioprinting*, *24*(June), e00176. https://doi.org/10.1016/j.bprint.2021.e00176

Benwood, C., Chrenek, J., Kirsch, R. L., Masri, N. Z., Richards, H., Teetzen, K., & Willerth, S. M. (2021). Natural biomaterials and their use as bioinks for printing tissues. *Bioengineering*, *8*(2), 1–19. https://doi.org/10.3390/bioengineering8020027

Bukowiecki, A., Hos, D., Cursiefen, C., & Eming, S. A. (2017). Wound-healing studies in cornea and skin: Parallels, differences and opportunities. *International Journal of Molecular Sciences*, *18*(6), 1–24. https://doi.org/10.3390/ijms18061257

Buznyk, O., Pasyechnikova, N., Islam, M. M., Iakymenko, S., Fagerholm, P., & Griffith, M. (2015). Bioengineered Corneas Grafted as Alternatives to Human Donor Corneas in Three High-Risk Patients. *Clinical and Translational Science*, *8*(5), 558–562. https://doi.org/10.1111/cts.12293

Chan, W. W., Yu, F., Le, Q. B., Chen, S., Yee, M., & Choudhury, D. (2021). Towards

biomanufacturing of cell-derived matrices. In *International Journal of Molecular Sciences* (Vol. 22, Issue 21, pp. 1–13). https://doi.org/10.3390/ijms222111929

Che, X., Wu, H., Jia, C., Sun, H., Ou, S., Wang, J., Jeyalatha, M. V., He, X., Yu, J., Zuo, C., Liu, Z., & Li, W. (2019). A novel tissue-engineered corneal stromal equivalent based on amniotic membrane and keratocytes. *Investigative Ophthalmology and Visual Science*, *60*(2), 517–527. https://doi.org/10.1167/iovs.18-24869

Chen, C., Loe, F., Blocki, A., Peng, Y., & Raghunath, M. (2011). Applying macromolecular crowding to enhance extracellular matrix deposition and its remodeling in vitro for tissue engineering and cell-based therapies. *Advanced Drug Delivery Reviews*, *63*(4), 277–290. https://doi.org/10.1016/j.addr.2011.03.003

Chen, D., Qu, Y., Hua, X., Zhang, L., Liu, Z., Pflugfelder, S. C., & Li, D. Q. (2017). A hyaluronan hydrogel scaffold-based xeno-free culture system for ex vivo expansion of human corneal epithelial stem cells. *Eye*, *31*(6), 962. https://doi.org/10.1038/EYE.2017.8

Chen, Z., You, J., Liu, X., Cooper, S., Hodge, C., Sutton, G., Crook, J. M., & Wallace, G. G. (2018). Biomaterials for corneal bioengineering. *Biomedical Materials (Bristol)*, *13*(3). https://doi.org/10.1088/1748-605X/aa92d2

Chimene, D., Kaunas, R., & Gaharwar, A. K. (2020). Hydrogel Bioink Reinforcement for Additive Manufacturing: A Focused Review of Emerging Strategies. *Advanced Materials*, *32*(1). https://doi.org/10.1002/adma.201902026

Choi, Y. J., Jun, Y. J., Kim, D. Y., Yi, H. G., Chae, S. H., Kang, J., Lee, J., Gao, G., Kong, J. S., Jang, J., Chung, W. K., Rhie, J. W., & Cho, D. W. (2019). A 3D cell printed muscle construct with tissue-derived bioink for the treatment of volumetric muscle loss. *Biomaterials*, *206*, 160–169. https://doi.org/10.1016/J.BIOMATERIALS.2019.03.036

Choi, Y. S., Dusting, G. J., Stubbs, S., Arunothayaraj, S., Han, X. L., Collas, P., Morrison, W. A., & Dilley, R. J. (2010). Differentiation of human adipose-derived stem cells into beating cardiomyocytes. *Journal of Cellular and Molecular Medicine*, *14*(4), 878. https://doi.org/10.1111/J.1582-4934.2010.01009.X

Chopin-Doroteo, M., Mandujano-Tinoco, E. A., & Krötzsch, E. (2021). Tailoring of the rheological properties of bioinks to improve bioprinting and bioassembly for tissue replacement. *Biochimica et Biophysica Acta - General Subjects*, *1865*(2). https://doi.org/10.1016/j.bbagen.2020.129782

Cui, X., Li, J., Hartanto, Y., Durham, M., Tang, J., Zhang, H., Hooper, G., Lim, K., & Woodfield, T. (2020). Advances in Extrusion 3D Bioprinting: A Focus on Multicomponent Hydrogel-Based Bioinks. *Advanced Healthcare Materials*, *9*(15). https://doi.org/10.1002/adhm.201901648

Das, S., Kim, S. W., Choi, Y. J., Lee, S., Lee, S. H., Kong, J. S., Park, H. J., Cho, D. W., & Jang, J. (2019). Decellularized extracellular matrix bioinks and the external stimuli to enhance cardiac tissue development in vitro. *Acta Biomaterialia*, *95*, 188–200. https://doi.org/10.1016/j.actbio.2019.04.026

DelMonte, D. W., & Kim, T. (2011). Anatomy and physiology of the cornea. *Journal of Cataract and Refractive Surgery*, *37*(3), 588–598. https://doi.org/10.1016/j.jcrs.2010.12.037

Du, Y., Roh, D. S., Funderburgh, M. L., Mann, M. M., Marra, K. G., Peter Rubin, J., Li, X., & Funderburgh, J. L. (2010). Adipose-derived stem cells differentiate to keratocytes in vitro. *Molecular Vision*, *16*(December), 2680–2689.

Duan, B., Kapetanovic, E., Hockaday, L. A., & Butcher, J. T. (2014). Three-dimensional printed trileaflet valve conduits using biological hydrogels and human valve interstitial cells. *Acta Biomaterialia*, *10*(5), 1836–1846. https://doi.org/10.1016/j.actbio.2013.12.005

Duan, Bin, Hockaday, L. A., Kang, K. H., & Butcher, J. T. (2013). 3D Bioprinting of heterogeneous aortic valve conduits with alginate/gelatin hydrogels. *Journal of Biomedical Materials Research - Part A*, *101 A*(5), 1255–1264. https://doi.org/10.1002/jbm.a.34420

Duarte Campos, D. F., Rohde, M., Ross, M., Anvari, P., Blaeser, A., Vogt, M., Panfil, C., Yam, G. H. F., Mehta, J. S., Fischer, H., Walter, P., & Fuest, M. (2019). Corneal bioprinting utilizing collagen-based bioinks and primary human keratocytes. *Journal of Biomedical Materials Research - Part A*, *107*(9), 1945–1953. https://doi.org/10.1002/jbm.a.36702

Duin, S., Schütz, K., Ahlfeld, T., Lehmann, S., Lode, A., Ludwig, B., & Gelinsky, M. (2019). 3D Bioprinting of Functional Islets of Langerhans in an Alginate/Methylcellulose Hydrogel Blend. *Advanced Healthcare Materials*, *8*(7), 1801631. https://doi.org/10.1002/ADHM.201801631

El Zarif, M., Alió, J. L., Alió Del Barrio, J. L., Abdul Jawad, K., Palazón-Bru, A., Abdul Jawad, Z., De Miguel, M. P., & Makdissy, N. (2021). Corneal Stromal Regeneration Therapy for Advanced Keratoconus: Long-term Outcomes at 3 Years. *Cornea*, *40*(6), 741–754. https://doi.org/10.1097/ICO.0000000000002646

Elomaa, L., Keshi, E., Sauer, I. M., & Weinhart, M. (2020). Development of GelMA/PCL and dECM/PCL resins for 3D printing of acellular in vitro tissue scaffolds by stereolithography. *Materials Science and Engineering: C*, *112*, 110958. https://doi.org/10.1016/J.MSEC.2020.110958

Espana, E. M., & Birk, D. E. (2020). Composition, structure and function of the corneal stroma. *Experimental Eye Research*, *198*(June), 108137. https://doi.org/10.1016/j.exer.2020.108137

Fenton, O. S., Paolini, M., Andresen, J. L., Müller, F. J., & Langer, R. (2020). Outlooks on Three-Dimensional Printing for Ocular Biomaterials Research. *Journal of Ocular Pharmacology and Therapeutics*, *36*(1), 7–17. https://doi.org/10.1089/jop.2018.0142

Fernandes-Cunha, G. M., Jeong, S. H., Logan, C. M., Le, P., Mundy, D., Chen, F., Chen, K. M., Kim, M., Lee, G. H., Na, K. S., Hahn, S. K., & Myung, D. (2022). Supramolecular host-guest hyaluronic acid hydrogels enhance corneal wound healing through dynamic spatiotemporal effects. *The Ocular Surface*, *23*, 148–161. https://doi.org/10.1016/J.JTOS.2021.09.002

Fernández-Pérez, J., & Ahearne, M. (2019). The impact of decellularization methods on extracellular matrix derived hydrogels. *Scientific Reports*, *9*(1), 1–12. https://doi.org/10.1038/s41598-019-49575-2

Fitzpatrick, L. E., & McDevitt, T. C. (2014). Cell-derived matrices for tissue engineering and regenerative medicine applications. *Biomaterials Science*, *3*(1), 12–24. https://doi.org/10.1039/C4BM00246F

Funderburgh, J. L., Funderburgh, M. L., & Du, Y. (2016). Stem Cells in the Limbal Stroma. *Ocular Surface*, *14*(2), 113–120. https://doi.org/10.1016/j.jtos.2015.12.006

Gain, P., Jullienne, R., He, Z., Aldossary, M., Acquart, S., Cognasse, F., & Thuret, G. (2016). Global survey of corneal transplantation and eye banking. *JAMA Ophthalmology*, *134*(2), 167–173. https://doi.org/10.1001/jamaophthalmol.2015.4776

Gao, G., Schilling, A. F., Hubbell, K., Yonezawa, T., Truong, D., Hong, Y., Dai, G., & Cui, X. (2015). Improved properties of bone and cartilage tissue from 3D inkjet-bioprinted human mesenchymal stem cells by simultaneous deposition and photocrosslinking in PEG-GelMA. *Biotechnology Letters*, *37*(11), 2349–2355. https://doi.org/10.1007/S10529-015-1921-2/FIGURES/4

Gao, Qi, Xie, J., Salero, E., Nuñez del Prado, Z., Hutmacher, D. W., Ye, J., De Juan-Pardo, E. M., Sabater, A. L., & Perez, V. L. (2021). Tissue engineering of corneal stroma via melt electrowriting. *Journal of Tissue Engineering and Regenerative Medicine*, *15*(10), 841–851. https://doi.org/10.1002/TERM.3235

Gao, Qiqi, Kim, B. S., & Gao, G. (2021). Advanced Strategies for 3D Bioprinting of Tissue and Organs Analogs Using Alginate Hydrogel Bioinks. In *Marine Drugs* (Vol. 19, Issue 12). Multidisciplinary Digital Publishing Institute (MDPI). https://doi.org/10.3390/md19120708

GhavamiNejad, A., Ashammakhi, N., Wu, X. Y., & Khademhosseini, A. (2020).

Crosslinking Strategies for 3D Bioprinting of Polymeric Hydrogels. In *Small* (Vol. 16, Issue 35). https://doi.org/10.1002/smll.202002931

Ghezzi, C. E., Rnjak-Kovacina, J., & Kaplan, D. L. (2015). Corneal Tissue Engineering: Recent Advances and Future Perspectives. *Tissue Engineering - Part B: Reviews*, *21*(3), 278–287. https://doi.org/10.1089/ten.teb.2014.0397

Gibney, R., Matthyssen, S., Patterson, J., Ferraris, E., & Zakaria, N. (2017). The Human Cornea as a Model Tissue for Additive Biomanufacturing: A Review. *Procedia CIRP*, *65*, 56–63. https://doi.org/10.1016/j.procir.2017.04.040

Gillispie, G., Prim, P., Copus, J., Fisher, J., Mikos, A. G., Yoo, J. J., Atala, A., & Lee, S. J. (2020). Assessment methodologies for extrusion-based bioink printability. *Biofabrication*, *12*(2), 22003. https://doi.org/10.1088/1758-5090/ab6f0d

Giuseppe, M. Di, Law, N., Webb, B., A. Macrae, R., Liew, L. J., Sercombe, T. B., Dilley, R. J., & Doyle, B. J. (2018). Mechanical behaviour of alginate-gelatin hydrogels for 3D bioprinting. *Journal of the Mechanical Behavior of Biomedical Materials*, *79*, 150–157. https://doi.org/10.1016/J.JMBBM.2017.12.018

Gonzalez, G., Sasamoto, Y., Ksander, B. R., Frank, M. H., & Frank, N. Y. (2018). Limbal Stem Cells: Identity, Developmental Origin and Therapeutic Potential Graphical abstract HHS Public Access. *Wiley Interdiscip Rev Dev Biol*, *7*(2), 1–23. https://doi.org/10.1002/wdev.303.Limbal

Gopinathan, J., & Noh, I. (2018). Click Chemistry-Based Injectable Hydrogels and Bioprinting Inks for Tissue Engineering Applications. *Tissue Engineering and Regenerative Medicine*, *15*(5), 531. https://doi.org/10.1007/S13770-018-0152-8

Gouveia, R. M., González-Andrades, E., Cardona, J. C., González-Gallardo, C., Ionescu, A. M., Garzon, I., Alaminos, M., González-Andrades, M., & Connon, C. J. (2017). Controlling the 3D architecture of Self-Lifting Auto-generated Tissue Equivalents (SLATEs) for optimized corneal graft composition and stability. *Biomaterials*, *121*, 205–219. https://doi.org/10.1016/J.BIOMATERIALS.2016.12.023

Groll, J., Burdick, J. A., Cho, D. W., Derby, B., Gelinsky, M., Heilshorn, S. C., Jüngst, T., Malda, J., Mironov, V. A., Nakayama, K., Ovsianikov, A., Sun, W., Takeuchi, S., Yoo, J. J., & Woodfield, T. B. F. (2019). A definition of bioinks and their distinction from biomaterial inks. *Biofabrication*, *11*(1). https://doi.org/10.1088/1758-5090/aaec52

Gruene, M., Unger, C., Koch, L., Deiwick, A., & Chichkov, B. (2011). Dispensing pico to nanolitre of a natural hydrogel by laser-assisted bioprinting. *BioMedical Engineering Online*, *10*, 19. https://doi.org/10.1186/1475-925X-10-19

Gu, Z., Fu, J., Lin, H., & He, Y. (2020). Development of 3D bioprinting: From printing methods to biomedical applications. *Asian Journal of Pharmaceutical Sciences*, *15*(5), 529–557. https://doi.org/10.1016/j.ajps.2019.11.003

Gungor-Ozkerim, P. S., Inci, I., Zhang, Y. S., Khademhosseini, A., & Dokmeci, M. R. (2018). Bioinks for 3D bioprinting: An overview. *Biomaterials Science*, *6*(5), 915–946. https://doi.org/10.1039/c7bm00765e

Guo, Y., Xue, Y., Wang, P., Cui, Z., Cao, J., Liu, S., Yu, Q., Zeng, Q., Zhu, D., Xie, M., Zhang, J., Li, Z., Liu, H., Zhong, J., & Chen, J. (2020). Muse cell spheroids have therapeutic effect on corneal scarring wound in mice and tree shrews. *Science Translational Medicine*, *12*(562). https://doi.org/10.1126/SCITRANSLMED.AAW1120/SUPPL_FILE/AAW1120_SM.PDF

Gupta, Y., Kishore, A., Kumari, P., Balakrishnan, N., Lomi, N., Gupta, N., Vanathi, M., & Tandon, R. (2021). Peripheral ulcerative keratitis. *Survey of Ophthalmology*, *66*(6), 977–998. https://doi.org/10.1016/j.survophthal.2021.02.013

Gürdal, M., Ercan, G., & Zeugolis, D. I. (2020). Formation of corneal stromal-like assemblies using human corneal fibroblasts and macromolecular crowding. *Methods in Molecular Biology*, *2145*(July), 119–141. https://doi.org/10.1007/978-1-0716-0599-8_9

Guruswamy Damodaran, R., & Vermette, P. (2018). Tissue and organ decellularization in regenerative medicine. *Biotechnology Progress*, *34*(6), 1494–1505. https://doi.org/10.1002/BTPR.2699

Hauptstein, J., Böck, T., Bartolf-Kopp, M., Forster, L., Stahlhut, P., Nadernezhad, A., Blahetek, G., Zernecke-Madsen, A., Detsch, R., Jüngst, T., Groll, J., Teßmar, J., & Blunk, T. (2020). Hyaluronic Acid-Based Bioink Composition Enabling 3D Bioprinting and Improving Quality of Deposited Cartilaginous Extracellular Matrix. *Advanced Healthcare Materials*, *9*(15). https://doi.org/10.1002/adhm.202000737

Hayes, S., Lewis, P., Islam, M. M., Doutch, J., Sorensen, T., White, T., Griffith, M., & Meek, K. M. (2015). The structural and optical properties of type III human collagen biosynthetic corneal substitutes. *Acta Biomaterialia*, *25*, 121. https://doi.org/10.1016/J.ACTBIO.2015.07.009

Holland, G., Pandit, A., Sánchez-Abella, L., Haiek, A., Loinaz, I., Dupin, D., Gonzalez, M., Larra, E., Bidaguren, A., Lagali, N., Moloney, E. B., & Ritter, T. (2021). Artificial Cornea: Past, Current, and Future Directions. *Frontiers in Medicine*, *8*(November), 1–19. https://doi.org/10.3389/fmed.2021.770780

Hongisto, H., Vattulainen, M., Ilmarinen, T., Mikhailova, A., & Skottman, H. (2018). Efficient and scalable directed differentiation of clinically compatible corneal limbal epithelial stem cells from human pluripotent stem cells. *Journal of Visualized Experiments*, *2018*(140), 58279. https://doi.org/10.3791/58279

Hospodiuk, M., Dey, M., Sosnoski, D., & Ozbolat, I. T. (2017). The bioink: A comprehensive review on bioprintable materials. *Biotechnology Advances*, *35*(2), 217–239. https://doi.org/10.1016/j.biotechadv.2016.12.006

Isaacson, A., Swioklo, S., & Connon, C. J. (2018). 3D bioprinting of a corneal stroma equivalent. *Experimental Eye Research*, *173*(March), 188–193. https://doi.org/10.1016/j.exer.2018.05.010

Jester, J. V. (2008). Corneal crystallins and the development of cellular transparency. *Seminars in Cell and Developmental Biology*, *19*(2), 82–93. https://doi.org/10.1016/j.semcdb.2007.09.015

Jirsova, K., & Jones, G. L. A. (2017). Amniotic membrane in ophthalmology: properties, preparation, storage and indications for grafting—a review. *Cell and Tissue Banking*, *18*(2), 193–204. https://doi.org/10.1007/s10561-017-9618-5

Jorgensen, A. M., Chou, Z., Gillispie, G., Lee, S. J., Yoo, J. J., Soker, S., & Atala, A. (2020). Decellularized skin extracellular matrix (dsECM) improves the physical and biological properties of fibrinogen hydrogel for skin bioprinting applications. *Nanomaterials*, *10*(8), 1–10. https://doi.org/10.3390/nano10081484

Kabirian, F., & Mozafari, M. (2020). Decellularized ECM-derived bioinks: Prospects for the future. *Methods*, *171*(April 2019), 108–118. https://doi.org/10.1016/j.ymeth.2019.04.019

Kageyama, T., Osaki, T., Enomoto, J., Myasnikova, D., Nittami, T., Hozumi, T., Ito, T., & Fukuda, J. (2016). *In Situ Cross-Linkable Gelatin-CMC Hydrogels Designed for Rapid Engineering of Perfusable Vasculatures*. https://doi.org/10.1021/acsbiomaterials.6b00203

Karvinen, J., Ihalainen, T. O., Calejo, M. T., Jönkkäri, I., & Kellomäki, M. (2019). Characterization of the microstructure of hydrazone crosslinked polysaccharide-based hydrogels through rheological and diffusion studies. *Materials Science and Engineering: C*, *94*, 1056–1066. https://doi.org/10.1016/J.MSEC.2018.10.048

Kérourédan, O., Bourget, J. M., Rémy, M., Crauste-Manciet, S., Kalisky, J., Catros, S., Thébaud, N. B., & Devillard, R. (2019). Micropatterning of endothelial cells to create a capillary-like network with defined architecture by laser-assisted bioprinting. *Journal of Materials Science: Materials in Medicine*, *30*(2), 1–12. https://doi.org/10.1007/S10856-019-6230-1/FIGURES/6

Khosravimelal, S., Mobaraki, M., Eftekhari, S., Ahearne, M., Seifalian, A. M., & Gholipourmalekabadi, M. (2021). Hydrogels as Emerging Materials for Cornea Wound Healing. *Small*, *17*(30), 1–27. https://doi.org/10.1002/smll.202006335

Kilic Bektas, C., Burcu, A., Gedikoglu, G., Telek, H. H., Ornek, F., & Hasirci, V. (2019). Methacrylated gelatin hydrogels as corneal stroma substitutes: in vivo study. *Https://Doi.Org/10.1080/09205063.2019.1666236*, *30*(18), 1803–1821. https://doi.org/10.1080/09205063.2019.1666236

Kilic Bektas, C., & Hasirci, V. (2020). Cell loaded 3D bioprinted GelMA hydrogels for corneal stroma engineering. *Biomaterials Science*, *8*(1), 438–449. https://doi.org/10.1039/c9bm01236b

Kim, B. S., Das, S., Jang, J., & Cho, D. W. (2020). Decellularized Extracellular Matrix-based Bioinks for Engineering Tissue- And Organ-specific Microenvironments. *Chemical Reviews*, *120*(19), 10608–10661. https://doi.org/10.1021/acs.chemrev.9b00808

Kim, H., Park, M. N., Kim, J., Jang, J., Kim, H. K., & Cho, D. W. (2019). Characterization of cornea-specific bioink: high transparency, improved in vivo safety. *Journal of Tissue Engineering*, *10*. https://doi.org/10.1177/2041731418823382

Kim, W. J., Jang, C. H., & Kim, G. H. (2019). A Myoblast-Laden Collagen Bioink with Fully Aligned Au Nanowires for Muscle-Tissue Regeneration. *Nano Letters*, *19*(12), 8612–8620. https://doi.org/10.1021/ACS.NANOLETT.9B03182/SUPPL_FILE/NL9B03182_SI_001.PDF

Kinoshita, S., Koizumi, N., Ueno, M., Okumura, N., Imai, K., Tanaka, H., Yamamoto, Y., Nakamura, T., Inatomi, T., Bush, J., Toda, M., Hagiya, M., Yokota, I., Teramukai, S., Sotozono, C., & Hamuro, J. (2018). Injection of Cultured Cells with a ROCK Inhibitor for Bullous Keratopathy. *New England Journal of Medicine*, *378*(11), 995–1003. https://doi.org/10.1056/nejmoa1712770

Knowlton, S., Yenilmez, B., Anand, S., & Tasoglu, S. (2017). Photocrosslinking-based bioprinting: Examining crosslinking schemes. *Bioprinting*, *5*(October 2016), 10–18. https://doi.org/10.1016/j.bprint.2017.03.001

Koch, L., Deiwick, A., Schlie, S., Michael, S., Gruene, M., Coger, V., Zychlinski, D., Schambach, A., Reimers, K., Vogt, P. M., & Chichkov, B. (2012). Skin tissue generation by laser cell printing. *Biotechnology and Bioengineering*, *109*(7), 1855–1863. https://doi.org/10.1002/bit.24455

Koivusalo, L., Karvinen, J., Sorsa, E., Jönkkäri, I., Väliaho, J., Kallio, P., Ilmarinen, T., Miettinen, S., Skottman, H., & Kellomäki, M. (2018). Hydrazone crosslinked hyaluronan-based hydrogels for therapeutic delivery of adipose stem cells to treat corneal defects. *Materials Science and Engineering: C*, *85*, 68–78. https://doi.org/10.1016/J.MSEC.2017.12.013

Koivusalo, L., Kauppila, M., Samanta, S., Parihar, V. S., Ilmarinen, T., Miettinen, S., Oommen, O. P., & Skottman, H. (2019). Tissue adhesive hyaluronic acid hydrogels for sutureless stem cell delivery and regeneration of corneal epithelium and stroma. *Biomaterials*, *225*(September), 119516. https://doi.org/10.1016/j.biomaterials.2019.119516

Kolios, G., & Moodley, Y. (2013). Introduction to Stem Cells and Regenerative Medicine. *Respiration*, *85*(1), 3–10. https://doi.org/10.1159/000345615

Kumar, A., Xu, Y., Yang, E., Wang, Y., & Du, Y. (2019). Fidelity of long-term cryopreserved adipose-derived stem cells for differentiation into cells of ocular and other lineages. *Experimental Eye Research*, *189*(March), 107860. https://doi.org/10.1016/j.exer.2019.107860

Kumar, A., Yun, H., Funderburgh, M. L., & Du, Y. (2021). Regenerative therapy for the Cornea. *Progress in Retinal and Eye Research*, *September*, 101011. https://doi.org/10.1016/j.preteyeres.2021.101011

Kumar, P., Satyam, A., Fan, X., Rochev, Y., Rodriguez, B. J., Gorelov, A., Joshi, L., Raghunath, M., Pandit, A., & Zeugolis, D. I. (2015). Accelerated Development of Supramolecular Corneal Stromal-Like Assemblies from Corneal Fibroblasts in the Presence of Macromolecular Crowders. *Tissue Engineering - Part C: Methods*, *21*(7), 660–670. https://doi.org/10.1089/ten.tec.2014.0387

Kutlehria, S., Dinh, T. C., Bagde, A., Patel, N., Gebeyehu, A., & Singh, M. (2020). High-throughput 3D bioprinting of corneal stromal equivalents. *Journal of Biomedical Materials Research - Part B Applied Biomaterials*, *108*(7), 2981–2994. https://doi.org/10.1002/jbm.b.34628

Lam, T., Dehne, T., Krüger, J. P., Hondke, S., Endres, M., Thomas, A., Lauster, R., Sittinger, M., & Kloke, L. (2019). Photopolymerizable gelatin and hyaluronic acid for stereolithographic 3D bioprinting of tissue-engineered cartilage. *Journal of Biomedical Materials Research - Part B Applied Biomaterials*, *107*(8), 2649–2657. https://doi.org/10.1002/jbm.b.34354

Lee, Hyeongjin, Yang, G. H., Kim, M., Lee, J. Y., Huh, J. T., & Kim, G. H. (2018). Fabrication of micro/nanoporous collagen/dECM/silk-fibroin biocomposite scaffolds using a low temperature 3D printing process for bone tissue regeneration. *Materials Science and Engineering C*, *84*(September 2017), 140–147. https://doi.org/10.1016/j.msec.2017.11.013

Lee, Hyungseok, Han, W., Kim, H., Ha, D. H., Jang, J., Kim, B. S., & Cho, D. W. (2017). Development of Liver Decellularized Extracellular Matrix Bioink for Three-Dimensional Cell Printing-Based Liver Tissue Engineering. *Biomacromolecules*, *18*(4), 1229–1237. https://doi.org/10.1021/acs.biomac.6b01908

Lee, Shenyuan, Squelch, A., & Sun, Z. (2021). Quantitative Assessment of 3D Printed Model Accuracy in Delineating Congenital Heart Disease. *Biomolecules 2021, Vol. 11, Page 270*, *11*(2), 270. https://doi.org/10.3390/BIOM11020270

Lee, Sohyung, Shirzaei Sani, E., Spencer, A. R., Guan, Y., Weiss, A. S., Annabi, N., Lee, S., Sani, E. S., Guan, Y., Annabi, N., Spencer, A. R., & Weiss, A. S. (2020). Human-Recombinant-Elastin-Based Bioinks for 3D Bioprinting of Vascularized Soft Tissues. *Advanced Materials*, *32*(45), 2003915. https://doi.org/10.1002/ADMA.202003915

Leucht, A., Volz, A. C., Rogal, J., Borchers, K., & Kluger, P. J. (2020). Advanced gelatin-based vascularization bioinks for extrusion-based bioprinting of vascularized bone equivalents. *Scientific Reports 2020 10:1*, *10*(1), 1–15. https://doi.org/10.1038/s41598-020-62166-w

Li, H., Tan, C., & Li, L. (2018). Review of 3D printable hydrogels and constructs. *Materials and Design*, *159*, 20–38. https://doi.org/10.1016/j.matdes.2018.08.023

Li, S., Deng, Y., Tian, B., Huang, H., Zhang, H., Yang, R., Zhong, J., Wang, B., Peng, L., & Yuan, J. (2020). Healing characteristics of acellular porcine corneal stroma following therapeutic keratoplasty. *Xenotransplantation*, *27*(2), 1–8. https://doi.org/10.1111/xen.12566

Lim, K. S., Galarraga, J. H., Cui, X., Lindberg, G. C. J., Burdick, J. A., & Woodfield, T. B. F. (2020). Fundamentals and Applications of Photo-Cross-Linking in Bioprinting. *Chemical Reviews*, *120*(19), 10662–10694. https://doi.org/10.1021/acs.chemrev.9b00812

Lindroos, B., Boucher, S., Chase, L., Kuokkanen, H., Huhtala, H., Haataja, R., Vemuri, M., Suuronen, R., & Miettinen, S. (2009). Serum-free, xeno-free culture media maintain the proliferation rate and multipotentiality of adipose stem cells in vitro. In *Cytotherapy* (Vol. 11, Issue 7, pp. 958–972). https://doi.org/10.3109/14653240903233081

Liu, X., Hao, M., Chen, Z., Zhang, T., Huang, J., Dai, J., & Zhang, Z. (2021). 3D bioprinted neural tissue constructs for spinal cord injury repair. *Biomaterials*, *272*(March), 120771. https://doi.org/10.1016/j.biomaterials.2021.120771

Ljubimov, A. V, & Saghizadeh, M. (2015). Progress in corneal wound healing HHS Public Access. *Prog Retin Eye Res*, *49*(310), 17–45. https://doi.org/10.1016/j.preteyeres.2015.07.002.Progress

Lynch, A. P., & Ahearne, M. (2017). Retinoic acid enhances the differentiation of adipose-derived stem cells to keratocytes in vitro. *Translational Vision Science and Technology*, *6*(1). https://doi.org/10.1167/tvst.6.1.6

Mahdavi, S. S., Abdekhodaie, M. J., Kumar, H., Mashayekhan, S., Baradaran-Rafii, A.,

& Kim, K. (2020). Stereolithography 3D Bioprinting Method for Fabrication of Human Corneal Stroma Equivalent. *Annals of Biomedical Engineering*, *48*(7), 1955–1970. https://doi.org/10.1007/s10439-020-02537-6

Mahdavi, S. S., Abdekhodaie, M. J., Mashayekhan, S., Baradaran-Rafii, A., & Djalilian, A. R. (2020). Bioengineering Approaches for Corneal Regenerative Medicine. *Tissue Engineering and Regenerative Medicine*, *17*(5), 567–593. https://doi.org/10.1007/s13770-020-00262-8

Masaeli, E., Forster, V., Picaud, S., Karamali, F., Nasr-Esfahani, M. H., & Marquette, C. (2020). Tissue engineering of retina through high resolution 3-dimensional inkjet bioprinting. *Biofabrication*, *12*(2). https://doi.org/10.1088/1758-5090/ab4a20

Matai, I., Kaur, G., Seyedsalehi, A., McClinton, A., & Laurencin, C. T. (2020). Progress in 3D bioprinting technology for tissue/organ regenerative engineering. *Biomaterials*, *226*(October 2019), 119536. https://doi.org/10.1016/j.biomaterials.2019.119536

Matthyssen, S., Van den Bogerd, B., Dhubhghaill, S. N., Koppen, C., & Zakaria, N. (2018). Corneal regeneration: A review of stromal replacements. *Acta Biomaterialia*, *69*, 31–41. https://doi.org/10.1016/j.actbio.2018.01.023

Mazzocchi, A., Devarasetty, M., Huntwork, R., Soker, S., & Skardal, A. (2019). Optimization of collagen type I-hyaluronan hybrid bioink for 3D bioprinted liver microenvironments. *Biofabrication*, *11*(1). https://doi.org/10.1088/1758-5090/aae543

Meek, K. M., & Knupp, C. (2015). Corneal structure and transparency. *Progress in Retinal and Eye Research*, *49*, 1–16. https://doi.org/10.1016/j.preteyeres.2015.07.001

Moncal, K. K., Ozbolat, V., Datta, P., Heo, D. N., & Ozbolat, I. T. (2019). Thermally-controlled extrusion-based bioprinting of collagen. *Journal of Materials Science: Materials in Medicine*, *30*(5). https://doi.org/10.1007/s10856-019-6258-2

Montero, F. E., Rezende, R. A., da Silva, J. V. L., & Sabino, M. A. (2019). Development of a Smart Bioink for Bioprinting Applications. *Frontiers in Mechanical Engineering*, *5*(September), 1–12. https://doi.org/10.3389/fmech.2019.00056

Moshirfar, M., Moody, J. J., Barke, M. R., Martheswaran, T., Thomson, A. C., Thomson, R. J., Somani, S. N., Shmunes, K. M., Ronquillo, Y. C., & Hoopes, P. (2022). The Historical Development and an Overview of Contemporary Keratoprostheses. *Survey of Ophthalmology*. https://doi.org/10.1016/J.SURVOPHTHAL.2022.01.005

Mueller, E., Poulin, I., Bodnaryk, W. J., & Hoare, T. (2022). Click Chemistry Hydrogels for Extrusion Bioprinting: Progress, Challenges, and Opportunities. *Biomacromolecules*. https://doi.org/10.1021/acs.biomac.1c01105

Muthusamy, S., Kannan, S., Lee, M., Sanjairaj, V., Lu, W. F., Fuh, J. Y. H., Sriram, G., & Cao, T. (2021). 3D bioprinting and microscale organization of vascularized tissue constructs using collagen-based bioink. *Biotechnology and Bioengineering*, *118*(8), 3150–3163. https://doi.org/10.1002/BIT.27838

Naghieh, S., Sarker, M. D., Abelseth, E., & Chen, X. (2019). Indirect 3D bioprinting and characterization of alginate scaffolds for potential nerve tissue engineering applications. *Journal of the Mechanical Behavior of Biomedical Materials*, *93*, 183–193. https://doi.org/10.1016/J.JMBBM.2019.02.014

Nam, S. Y., & Park, S.-H. (2018). ECM Based Bioink for Tissue Mimetic 3D Bioprinting. In I. Noh (Ed.), *Biomimetic Medical Materials: From Nanotechnology to 3D Bioprinting* (pp. 335–353). Springer Singapore. https://doi.org/10.1007/978-981-13-0445-3_20

Naylor, R. W., McGhee, C. N. J., Cowan, C. A., Davidson, A. J., Holm, T. M., & Sherwin, T. (2016). Derivation of corneal keratocyte-like cells from human induced pluripotent stem cells. *PLoS ONE*, *11*(10), 1–18. https://doi.org/10.1371/journal.pone.0165464

Numa, K., Imai, K., Ueno, M., Kitazawa, K., Tanaka, H., Bush, J. D., Teramukai, S., Okumura, N., Koizumi, N., Hamuro, J., Sotozono, C., & Kinoshita, S. (2021). Five-Year Follow-up of First 11 Patients Undergoing Injection of Cultured Corneal

Endothelial Cells for Corneal Endothelial Failure. *Ophthalmology*, *128*(4), 504–514. https://doi.org/10.1016/j.ophtha.2020.09.002

Nurković, J. S., Vojinović, R., & Dolićanin, Z. (2020). Corneal Stem Cells as a Source of Regenerative Cell-Based Therapy. In *Stem Cells International* (Vol. 2020). https://doi.org/10.1155/2020/8813447

Oliva, M. S., Schottman, T., & Gulati, M. (2012). Turning the tide of corneal blindness. *Indian Journal of Ophthalmology*, *60*(5), 423. https://doi.org/10.4103/0301-4738.100540

Osei-Bempong, C., Figueiredo, F. C., & Lako, M. (2013). The limbal epithelium of the eye - A review of limbal stem cell biology, disease and treatment. *BioEssays*, *35*(3), 211–219. https://doi.org/10.1002/bies.201200086

Osidak, Egor O., Karalkin, P. A., Osidak, M. S., Parfenov, V. A., Sivogrivov, D. E., Pereira, F. D. A. S., Gryadunova, A. A., Koudan, E. V., Khesuani, Y. D., Kasyanov, V. A., Belousov, S. I., Krasheninnikov, S. V., Grigoriev, T. E., Chvalun, S. N., Bulanova, E. A., Mironov, V. A., & Domogatsky, S. P. (2019). Viscoll collagen solution as a novel bioink for direct 3D bioprinting. *Journal of Materials Science: Materials in Medicine*, *30*(3). https://doi.org/10.1007/s10856-019-6233-y

Osidak, Egor Olegovich, Kozhukhov, V. I., Osidak, M. S., & Domogatsky, S. P. (2020). Collagen as bioink for bioprinting: A comprehensive review. *International Journal of Bioprinting*, *6*(3), 1–10. https://doi.org/10.18063/IJB.V6I3.270

Ovsianikov, A., Khademhosseini, A., & Mironov, V. (2018). The Synergy of Scaffold-Based and Scaffold-Free Tissue Engineering Strategies. *Trends in Biotechnology*, *36*(4), 348–357. https://doi.org/10.1016/j.tibtech.2018.01.005

Pati, F., Jang, J., Ha, D. H., Won Kim, S., Rhie, J. W., Shim, J. H., Kim, D. H., & Cho, D. W. (2014). Printing three-dimensional tissue analogues with decellularized extracellular matrix bioink. *Nature Communications*, *5*(1), 1–11. https://doi.org/10.1038/ncomms4935

Piola, B., Sabbatini, M., Gino, S., Invernizzi, M., & Renò, F. (2022). 3D Bioprinting of Gelatin–Xanthan Gum Composite Hydrogels for Growth of Human Skin Cells. *International Journal of Molecular Sciences*, *23*(1), 539. https://doi.org/10.3390/ijms23010539

Radhakrishnan, S., Trentz, O. A., Reddy, M. S., Rela, M., Kandasamy, M., & Sellathamby, S. (2019). In vitro transdifferentiation of human adipose tissue-derived stem cells to neural lineage cells - a stage-specific incidence. *Https://Doi.Org/10.1080/21623945.2019.1607424*, *8*(1), 164–177. https://doi.org/10.1080/21623945.2019.1607424

Rajabzadeh, N., Fathi, E., & Farahzadi, R. (2019). Stem cell-based regenerative medicine. *Stem Cell Investigation*, *6*(July). https://doi.org/10.21037/sci.2019.06.04

Roversi, K., Orimi, H. E., Falchetti, M., da Rocha, E. L., Talbot, S., & Boutopoulos, C. (2021). Bioprinting of adult dorsal root ganglion (DRG) neurons using laser-induced side transfer (LIST). *Micromachines*, *12*(8), 865. https://doi.org/10.3390/mi12080865

Rueda-Gensini, L., Serna, J. A., Cifuentes, J., Cruz, J. C., & Muñoz-Camargo, C. (2021). Graphene Oxide-Embedded Extracellular Matrix-Derived Hydrogel as a Multiresponsive Platform for 3D Bioprinting Applications. *International Journal of Bioprinting*, *7*(3), 1–16. https://doi.org/10.18063/ijb.v7i3.353

Ruiz-alonso, S., Villate-beitia, I., Gallego, I., Lafuente-merchan, M., Puras, G., Saenz-del-burgo, L., & Pedraz, J. L. (2021). Current insights into 3D bioprinting: An advanced approach for eye tissue regeneration. *Pharmaceutics*, *13*(3), 1–28. https://doi.org/10.3390/pharmaceutics13030308

Salaris, F., Colosi, C., Brighi, C., Soloperto, A., de Turris, V., Benedetti, M. C., Ghirga, S., Rosito, M., Di Angelantonio, S., & Rosa, A. (2019). 3D Bioprinted Human Cortical Neural Constructs Derived from Induced Pluripotent Stem Cells. *Journal of Clinical Medicine 2019, Vol. 8, Page 1595*, *8*(10), 1595. https://doi.org/10.3390/JCM8101595

Samadian, H., Maleki, H., Allahyari, Z., & Jaymand, M. (2020). Natural polymers-based light-induced hydrogels: Promising biomaterials for biomedical applications. In *Coordination Chemistry Reviews* (Vol. 420). https://doi.org/10.1016/j.ccr.2020.213432

Sani, E. S., Kheirkhah, A., Rana, D., Sun, Z., Foulsham, W., Sheikhi, A., Khademhosseini, A., Dana, R., & Annabi, N. (2019). Sutureless repair of corneal injuries using naturally derived bioadhesive hydrogels. *Science Advances*, *5*(3). https://doi.org/10.1126/sciadv.aav1281

Schwab, A., Levato, R., D'Este, M., Piluso, S., Eglin, D., & Malda, J. (2020). Printability and Shape Fidelity of Bioinks in 3D Bioprinting. *Chemical Reviews*, *120*(19), 11028–11055. https://doi.org/10.1021/acs.chemrev.0c00084

Serban, M. A., & Skardal, A. (2019). Hyaluronan chemistries for three-dimensional matrix applications. *Matrix Biology*, *78–79*, 337–345. https://doi.org/10.1016/j.matbio.2018.02.010

Seyed-Safi, A. G., & Daniels, J. T. (2020). The limbus: Structure and function. *Experimental Eye Research*, *197*, 108074. https://doi.org/10.1016/J.EXER.2020.108074

Sharifi, S., Islam, M. M., Sharifi, H., Islam, R., Koza, D., Reyes-Ortega, F., Alba-Molina, D., Nilsson, P. H., Dohlman, C. H., Mollnes, T. E., Chodosh, J., & Gonzalez-Andrades, M. (2021). Tuning gelatin-based hydrogel towards bioadhesive ocular tissue engineering applications. *Bioactive Materials*, *6*(11), 3947. https://doi.org/10.1016/J.BIOACTMAT.2021.03.042

Shin, Y. J., Shafranek, R. T., Tsui, J. H., Walcott, J., Nelson, A., & Kim, D. H. (2021). 3D bioprinting of mechanically tuned bioinks derived from cardiac decellularized extracellular matrix. *Acta Biomaterialia*, *119*, 75–88. https://doi.org/10.1016/J.ACTBIO.2020.11.006

Singh, R., Gupta, N., Vanathi, M., & Tandon, R. (2019). Corneal transplantation in the modern era. In *Indian Journal of Medical Research* (Vol. 150, Issue 1). https://doi.org/10.4103/ijmr.IJMR_141_19

Solis, L. H., Ayala, Y., Portillo, S., Varela-Ramirez, A., Aguilera, R., & Boland, T. (2019). Thermal inkjet bioprinting triggers the activation of the VEGF pathway in human microvascular endothelial cells in vitro. *Biofabrication*, *11*(4). https://doi.org/10.1088/1758-5090/ab25f9

Soltan, N., Ning, L., Mohabatpour, F., Papagerakis, P., & Chen, X. (2019). Printability and Cell Viability in Bioprinting Alginate Dialdehyde-Gelatin Scaffolds. *ACS Biomaterials Science and Engineering*, *5*(6), 2976–2987. https://doi.org/10.1021/acsbiomaterials.9b00167

Sommer, A. C., & Blumenthal, E. Z. (2019). Implementations of 3D printing in ophthalmology. *Graefe's Archive for Clinical and Experimental Ophthalmology*, *257*(9), 1815–1822. https://doi.org/10.1007/s00417-019-04312-3

Sorkio, A., Koch, L., Koivusalo, L., Deiwick, A., Miettinen, S., Chichkov, B., & Skottman, H. (2018). Human stem cell based corneal tissue mimicking structures using laser-assisted 3D bioprinting and functional bioinks. *Biomaterials*, *171*, 57–71. https://doi.org/10.1016/j.biomaterials.2018.04.034

Sridhar, M. S. (2018). *Review Article for Residents Anatomy of cornea and ocular surface*. https://doi.org/10.4103/ijo.IJO_646_17

Suman, S., Domingues, A., Ratajczak, J., & Ratajczak, M. Z. (2019). Potential clinical applications of stem cells in regenerative medicine. In *Advances in Experimental Medicine and Biology* (Vol. 1201, pp. 1–22). Springer. https://doi.org/10.1007/978-3-030-31206-0_1

Syed-Picard, F. N., Du, Y., Hertsenberg, A. J., Palchesko, R., Funderburgh, M. L., Feinberg, A. W., & Funderburgh, J. L. (2018). Scaffold-free tissue engineering of functional corneal stromal tissue. *Journal of Tissue Engineering and Regenerative Medicine*, *12*(1), 59–69. https://doi.org/10.1002/term.2363

Takahashi, K., Tanabe, K., Ohnuki, M., Narita, M., Ichisaka, T., Tomoda, K., &

Yamanaka, S. (2007). Induction of Pluripotent Stem Cells from Adult Human Fibroblasts by Defined Factors. *Cell*, *131*(5), 861–872. https://doi.org/10.1016/J.CELL.2007.11.019

Tan, D. T. H., Dart, J. K. G., Holland, E. J., & Kinoshita, S. (2012). Corneal transplantation. In *The Lancet* (Vol. 379, Issue 9827, pp. 1749–1761). Elsevier. https://doi.org/10.1016/S0140-6736(12)60437-1

Taylor, H. R., Burton, M. J., Haddad, D., West, S., & Wright, H. (2014). Trachoma. *The Lancet*, *384*(9960), 2142–2152. https://doi.org/10.1016/S0140-6736(13)62182-0

Thomson, J. A., Itskovitz-Eldor, J., Shapiro, S. S., Waknitz, M. A., Swiergiel, J. J., Marshall, V. S., & Jones, J. M. (1998). Embryonic Stem Cell Lines Derived from Human Blastocysts. *Science*, *282*(5391), 1145–1147. https://doi.org/10.1126/SCIENCE.282.5391.1145

Tirkkonen, L., Haimi, S., Huttunen, S., Wolff, J., Pirhonen, E., Sándor, G., & Miettinen, S. (2013). Osteogenic medium is superior to growth factors in differentiation of human adipose stem cells towards bone-forming cells in 3D culture. *European Cells and Materials*, *25*, 144–158. https://doi.org/10.22203/ecm.v025a10

Tran, T. M., Duong, H., Bonnet, C., Kashanchi, A., Buckshey, A., & Aldave, A. J. (2020). Corneal Blindness in Asia: A Systematic Review and Meta-Analysis to Identify Challenges and Opportunities. *Cornea*, *39*(9), 1196–1205. https://doi.org/10.1097/ICO.0000000000002374

Tse, C., Whiteley, R., Yu, T., Stringer, J., MacNeil, S., Haycock, J. W., & Smith, P. J. (2016). Inkjet printing Schwann cells and neuronal analogue NG108-15 cells. *Biofabrication*, *8*(1). https://doi.org/10.1088/1758-5090/8/1/015017

Tytgat, L., Van Damme, L., Ortega Arevalo, M. del P., Declercq, H., Thienpont, H., Otteveare, H., Blondeel, P., Dubruel, P., & Van Vlierberghe, S. (2019). Extrusion-based 3D printing of photo-crosslinkable gelatin and κ-carrageenan hydrogel blends for adipose tissue regeneration. *International Journal of Biological Macromolecules*, *140*, 929–938. https://doi.org/10.1016/J.IJBIOMAC.2019.08.124

Urtaza, U. ; ;, Zubiarrain-Laserna, A. ;, Alonso-Varona, A. ;, Zaldua, A. M. A., Sarasua, J.-R., Vega, J. F., Gorroñogoitia, I., Urtaza, U., Zubiarrain-Laserna, A., Alonso-Varona, A., & Miren Zaldua, A. (2022). A Study of the Printability of Alginate-Based Bioinks by 3D Bioprinting for Articular Cartilage Tissue Engineering. *Polymers 2022, Vol. 14, Page 354*, *14*(2), 354. https://doi.org/10.3390/POLYM14020354

Vaidyanathan, U., Hopping, G. C., Liu, H. Y., Somani, A. N., Ronquillo, Y. C., Hoopes, P. C., & Moshirfar, M. (2019). Persistent Corneal Epithelial Defects: A Review Article. *Medical Hypothesis, Discovery & Innovation Ophthalmology Journal*, *8*(3), 163–176. http://www.ncbi.nlm.nih.gov/pubmed/31598519%0Ahttp://www.pubmedcentral.nih.gov/articlerender.fcgi?artid=PMC6778469

Van Hoorick, J., Tytgat, L., Dobos, A., Ottevaere, H., Van Erps, J., Thienpont, H., Ovsianikov, A., Dubruel, P., & Van Vlierberghe, S. (2019). (Photo-)crosslinkable gelatin derivatives for biofabrication applications. *Acta Biomaterialia*, *97*, 46–73. https://doi.org/10.1016/j.actbio.2019.07.035

Vattulainen, M., Ilmarinen, T., Koivusalo, L., Viiri, K., Hongisto, H., & Skottman, H. (2019). Modulation of Wnt/BMP pathways during corneal differentiation of hPSC maintains ABCG2-positive LSC population that demonstrates increased regenerative potential. *Stem Cell Research and Therapy*, *10*(1). https://doi.org/10.1186/s13287-019-1354-2

Vijayavenkataraman, S., Yan, W. C., Lu, W. F., Wang, C. H., & Fuh, J. Y. H. (2018). 3D bioprinting of tissues and organs for regenerative medicine. *Advanced Drug Delivery Reviews*, *132*, 296–332. https://doi.org/10.1016/j.addr.2018.07.004

Visscher, D. O., Lee, H., van Zuijlen, P. P. M., Helder, M. N., Atala, A., Yoo, J. J., & Lee, S. J. (2021). A photo-crosslinkable cartilage-derived extracellular matrix (ECM) bioink for auricular cartilage tissue engineering. *Acta Biomaterialia*, *121*, 193. https://doi.org/10.1016/J.ACTBIO.2020.11.029

Wang, L. L., Highley, C. B., Yeh, Y. C., Galarraga, J. H., Uman, S., & Burdick, J. A. (2018). Three-dimensional extrusion bioprinting of single- and double-network hydrogels containing dynamic covalent crosslinks. *Journal of Biomedical Materials Research - Part A*, *106*(4), 865–875. https://doi.org/10.1002/jbm.a.36323

Wang, X., Ao, Q., Tian, X., Fan, J., Tong, H., Hou, W., & Bai, S. (2017). Gelatin-Based Hydrogels for Organ 3D Bioprinting. *Polymers 2017, Vol. 9, Page 401*, *9*(9), 401. https://doi.org/10.3390/POLYM9090401

West-Mays, J. A., & Dwivedi, D. J. (2006). The keratocyte: Corneal stromal cell with variable repair phenotypes. *International Journal of Biochemistry and Cell Biology*, *38*(10), 1625–1631. https://doi.org/10.1016/j.biocel.2006.03.010

Whitcher, J. P., Srinivasan, M., & Upadhyay, M. P. (2001). Corneal blindness: A global perspective. *Bulletin of the World Health Organization*, *79*(3), 214–221. https://doi.org/10.1590/S0042-96862001000300009

Wilson, S. E. (2020). Bowman's layer in the cornea– structure and function and regeneration. *Experimental Eye Research*, *195*, 108033. https://doi.org/10.1016/J.EXER.2020.108033

Wong, K. H., Kam, K. W., Chen, L. J., & Young, A. L. (2017). Corneal blindness and current major treatment concern-graft scarcity. *International Journal of Ophthalmology*, *10*(7), 1154. https://doi.org/10.18240/IJO.2017.07.21

Wu, Z., Su, X., Xu, Y., Kong, B., Sun, W., & Mi, S. (2016). Bioprinting three-dimensional cell-laden tissue constructs with controllable degradation. *Scientific Reports*, *6*(September 2015), 1–10. https://doi.org/10.1038/srep24474

Xeroudaki, M., Thangavelu, M., Lennikov, A., Ratnayake, A., Bisevac, J., Petrovski, G., Fagerholm, P., Rafat, M., & Lagali, N. (2020). A porous collagen-based hydrogel and implantation method for corneal stromal regeneration and sustained local drug delivery. *Scientific Reports*, *10*(1). https://doi.org/10.1038/S41598-020-73730-9

Xia, X., Atkins, M., Dalal, R., Kuzmenko, O., Chang, K. C., Sun, C. B., Benatti, C. A., Rak, D. J., Nahmou, M., Kunzevitzky, N. J., & Goldberg, J. L. (2019). Magnetic Human Corneal Endothelial Cell Transplant: Delivery, Retention, and Short-Term Efficacy. *Investigative Ophthalmology & Visual Science*, *60*(7), 2438–2448. https://doi.org/10.1167/IOVS.18-26001

Yam, G. H. F., Riau, A. K., Funderburgh, M. L., Mehta, J. S., & Jhanji, V. (2020). Keratocyte biology. *Experimental Eye Research*, *196*(March), 108062. https://doi.org/10.1016/j.exer.2020.108062

Yang, X., Lu, Z., Wu, H., Li, W., Zheng, L., & Zhao, J. (2018). Collagen-alginate as bioink for three-dimensional (3D) cell printing based cartilage tissue engineering. *Materials Science and Engineering: C*, *83*, 195–201. https://doi.org/10.1016/J.MSEC.2017.09.002

Yazdanpanah, G., Jabbehdari, S., & Djalilian, A. R. (2017). Limbal and corneal epithelial homeostasis. *Current Opinion in Ophthalmology*, *28*(4), 348. https://doi.org/10.1097/ICU.0000000000000378

Yazdanpanah, G., Jiang, Y., Rabiee, B., Omidi, M., Rosenblatt, M. I., Shokuhfar, T., Pan, Y., Naba, A., & Djalilian, A. R. (2021). Fabrication, Rheological, and Compositional Characterization of Thermoresponsive Hydrogel from Cornea. *Tissue Engineering - Part C: Methods*, *27*(5), 307–321. https://doi.org/10.1089/TEN.TEC.2021.0011/ASSET/IMAGES/LARGE/TEN.TEC.2021.0011_FIGURE7.JPEG

Yokoi, T., Seko, Y., Yokoi, T., Makino, H., Hatou, S., Yamada, M., Kiyono, T., Umezawa, A., Nishina, H., & Azuma, N. (2012). Establishment of functioning human corneal endothelial cell line with high growth potential. *PLoS ONE*, *7*(1), 1–8. https://doi.org/10.1371/journal.pone.0029677

Yusoff, N. Z. B. M., Riau, A. K., Yam, G. H. F., Binte Halim, N. S. H., & Mehta, J. S. (2022). Isolation and Propagation of Human Corneal Stromal Keratocytes for Tissue Engineering and Cell Therapy. *Cells 2022, Vol. 11, Page 178*, *11*(1), 178. https://doi.org/10.3390/CELLS11010178

Zhang, B., Xue, Q., Hu, H. yi, Yu, M. fei, Gao, L., Luo, Y. chen, Li, Y., Li, J. tao, Ma, L., Yao, Y. feng, & Yang, H. yong. (2019). Integrated 3D bioprinting-based geometry-control strategy for fabricating corneal substitutes. *Journal of Zhejiang University: Science B*, *20*(12), 945–959. https://doi.org/10.1631/jzus.B1900190

Zhang, B., Xue, Q., Li, J., Ma, L., Yao, Y., Ye, H., Cui, Z., & Yang, H. (2019). 3D bioprinting for artificial cornea: Challenges and perspectives. *Medical Engineering and Physics*, *71*, 68–78. https://doi.org/10.1016/j.medengphy.2019.05.002

Zhang, S., Espandar, L., Imhof, K. M. P., & Bunnell, B. A. (2013). Differentiation of Human Adipose-derived Stem Cells along the Keratocyte Lineage In vitro. *Journal of Clinical & Experimental Ophthalmology*, *4*(270). https://doi.org/10.4172/2155-9570.1000270

Zhang, Wei, Yang, W., Liu, X., Zhang, L., Huang, W., & Zhang, Y. (2014). Rapidly constructed scaffold-free embryonic stem cell sheets for ocular surface reconstruction. *Scanning*, *36*(3), 286–292. https://doi.org/10.1002/SCA.21103

Zhang, Wenhui, Du, A., Liu, S., Lv, M., & Chen, S. (2021). Research progress in decellularized extracellular matrix-derived hydrogels. *Regenerative Therapy*, *18*, 88–96. https://doi.org/10.1016/j.reth.2021.04.002

8. APPENDICES

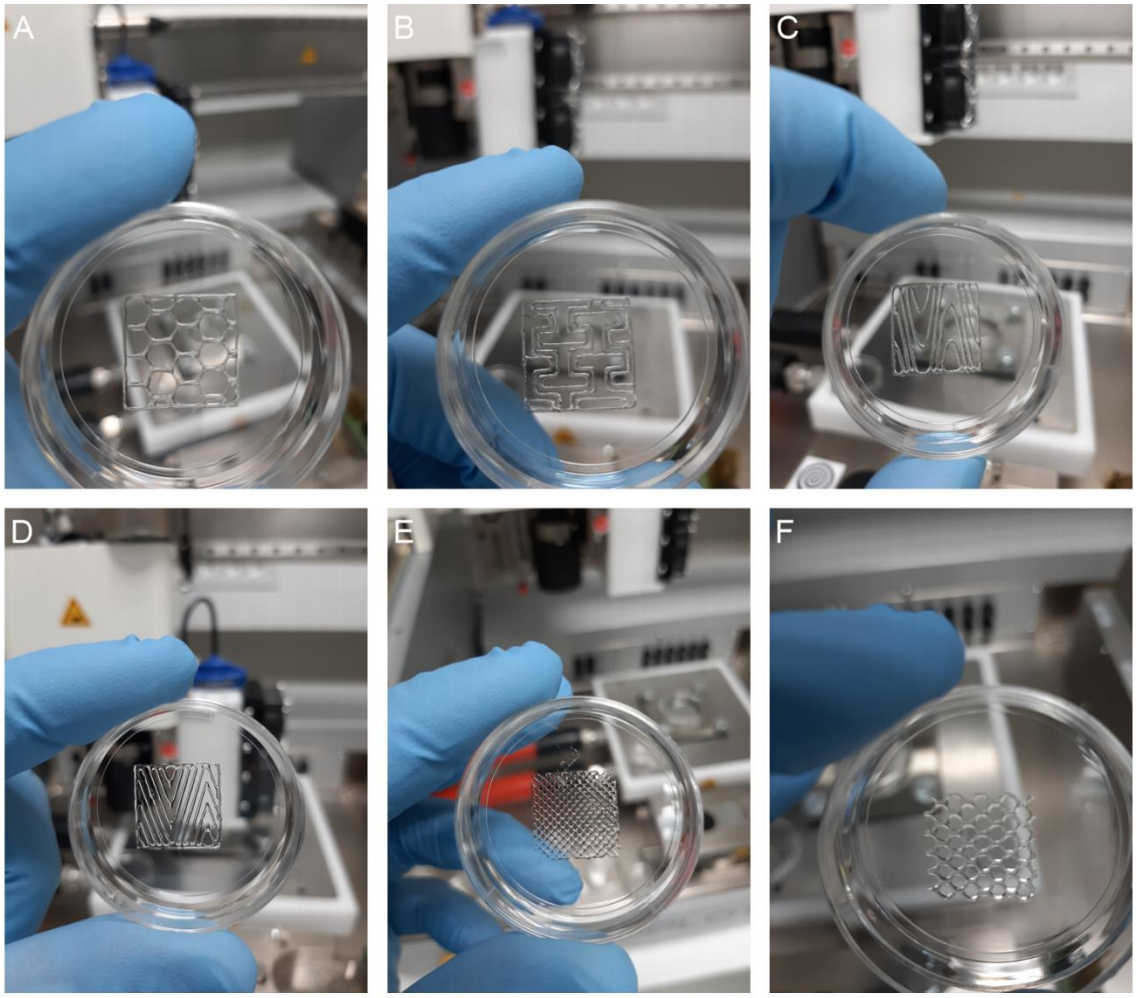

Appendix 1: *Various structures bioprinted with Co-dCDM to demonstrate its versatility. (A) Honeycomb, (B) Space, (C) Waves, (D) Zig Zag, (E) Dense pores and (F) Honeycomb with higher density.*